Technische Universität München

Fakultät für Medizin

Mechanisms leading to radioresistance in pancreatic cancer

Lily Thuy Duong Nguyen

Vollständiger Abdruck der von der Fakultät für Medizin der Technischen Universität München zur Erlangung des akademischen Grades eines Doktors der Naturwissenschaften (Dr. rer. nat.) genehmigten Dissertation.

Vorsitzender: Prof. Dr. Wolfgang Weber

Prüfende der Dissertation:

1. Prof. Dr. Stephanie E. Combs

2. apl. Prof. Dr. Michael W. Pfaffl

Die Dissertation wurde am 11.05.2020 bei der Technischen Universität München eingereicht und durch die Fakultät für Medizin am 06.10.2020 angenommen.

Table of contents

Abstract

The worldwide incidence and mortality rate of pancreatic cancer is continuously increasing, thus constituting one of the most serious global burdens. Radioresistance in pancreatic cancer patients is still a critical challenge that remains to be met. Understanding the molecular mechanisms underlying radioresistance and targeting the respective pathways may lead to a better response to radiotherapy and, thus, a better treatment outcome. In this study, two radioresistant pancreatic cancer cell lines were generated by fractionated radiation. The acquired radioresistance was validated *in vitro* and *in vivo*. The cell lines were further investigated with regard to proliferation, radiation-induced apoptosis, cell cycle distribution, repair of DNA damage, generation of reactive oxygen species, and migration and invasion capacity. The results of this study showed that radioresistant pancreatic cancer cell lines revealed a greater DNA repair efficiency and lower levels of basal and radiation-induced reactive oxygen species. Therefore, an increased DNA repair capacity and an enhanced antioxidant response might constitute potential mechanisms involved in the acquired radioresistance. In addition, the migration and invasion capacity of the cell lines was differentially affected through the acquired radioresistance. Furthermore, RNA and small RNA sequencing revealed specific mRNAs and miRNAs associated with radioresistance or migration and invasion capacity. In conclusion, this thesis provides new insights into the radioresistance of pancreatic cancer and identifies potential biomarkers and treatment targets for personalized therapy.

Zusammenfassung

Die weltweite Inzidenz und Sterblichkeitsrate von Pankreaskarzinomen nimmt ständig zu und stellt damit eine der schwerwiegendsten globalen Belastungen dar. Die Radioresistenz bei Patienten mit Pankreaskarzinom ist nach wie vor eine kritische Herausforderung, die es zu bewältigen gilt. Das Aufklären der molekularen Mechanismen, die der Radioresistenz zugrunde liegen, kann zu einem besseren Ansprechen auf die Strahlentherapie und damit zu einem besseren Behandlungsergebnis führen. In dieser Studie wurden zwei strahlenresistente Pankreaskarzinom-Zelllinien durch fraktionierte Bestrahlung generiert. Die erworbene Strahlenresistenz wurde *in vitro* und *in vivo* validiert. Die Zelllinien wurden im Hinblick auf die Proliferation, die strahleninduzierte Apoptose, die Zellzyklusverteilung, die Reparatur von DNA-Schäden, die Erzeugung reaktiver Sauerstoffspezies sowie die Migrations- und Invasionskapazität untersucht. Die Ergebnisse dieser Studie zeigten, dass strahlenresistente Pankreaskarzinomzelllinien eine höhere DNA-Reparatur-Effizienz und niedrigere Mengen an basalen und strahleninduzierten reaktiven Sauerstoffspezies aufweisen. Mögliche Mechanismen, die an der erworbenen Strahlenresistenz beteiligt sind, sind daher eine erhöhte DNA-Reparaturkapazität und eine verbesserte antioxidative Antwort. Darüber hinaus wurde die Migrations- und Invasionskapazität der strahlenresistenten Zelllinien durch die erworbene Strahlenresistenz unterschiedlich beeinflusst. Des Weiteren ergab die Analyse der mRNA- und miRNA-Sequenzierung spezifische mRNA- sowie miRNA-Profile, die mit der Strahlenresistenz und Migrations- und Invasionskapazität assoziiert sind. Zusammenfassend liefert diese Studie damit neue Erkenntnisse über die Strahlenresistenz von Pankreaskarzinomen und identifiziert potenzielle Biomarker und Zielstrukturen für eine personalisierte Therapie.

List of abbreviations

ABCC3	ATP binding cassette subfamily C member 3
ACTB	Actin beta
AHR	Aryl hydrocarbon receptor
ANXA1	Annexin A1
ATM	Ataxia telangiectasia mutated
ATR	Ataxia telangiectasia and Rad3-related
B2M	Beta-2-microglobulin
BCL2L1	Bcl-2-like 1
BER	Base excision repair
BSA	Bovine serum albumin
CA 19-9	Carbohydrate antigen 19-9
CBCT	Cone beam computed tomography
CCL5	Chemokine (C-C motif) ligand 5
CDKN2A	Cyclin dependent kinase inhibitor 2A
CFA	Colony formation assay
CHK1	Checkpoint kinase 1
CSC	Cancer stem cell
CT	Computed tomography
DNA	Deoxyribonucleic acid
DNA-PKcs	DNA-dependent protein kinase catalytic subunit
DSB	Double-strand break
DSMZ	Deutsche Sammlung von Mikroorganismen und Zellkulturen
DT	Doubling time
EMT	Epithelial-mesenchymal transition
ESPAC-1	European Study Group for Pancreatic Cancer 1 Trial
FCS	Fetal calf serum
GAPDH	Glyceraldehyde-3-phosphate dehydrogenase
GCLC	Glutamate-cysteine ligase catalytic subunit

Gy	Gray
HIPK2	Homeodomain interacting protein kinase 2
HPRT1	Hypoxanthine phosphoribosyltransferase 1
HR	Homologous recombination
IPA	Ingenuity pathway analysis
KRAS	KRAS proto-oncogene, GTPase
LIF	Leukemia inhibitory factor
LQM	Linear quadratic model
MB	Myoglobin
MFI	Mean fluorescence intensity
miRNA	MicroRNA
mRNA	Messenger RNA
MRI	Magnetic resonance imaging
NDRG1	N-Myc Downstream Regulated 1
NHEJ	Non-homologous end-joining
NRF2	Nuclear factor erythroid 2 related factor 2
PanIn	Pancreatic intraepithelial neoplasia
PARP	Poly (ADP-ribose) polymerases
PCA	Principal component analysis
PDAC	Pancreatic ductal adenocarcinoma
PE	Plating efficiency
PFA	Paraformaldehyde
RIN	RNA integrity number
RISC	RNA-induced silencing complex
RLP0	Ribosomal protein large P0
RNA	Ribonucleic acid
RNAi	RNA-mediated interference
ROS	Reactive oxygen species
RR	Radioresistant
s.c.	Subcutaneous
SCARA3	Scavenger Receptor Class A Member 3
SF	Survival fraction

SHH	Sonic hedgehog signaling molecule
SMAD4	SMAD family member 4
SOD	superoxide dismutase
SSB	Single-strand break
TP53	tumor protein p53
TRX	Thioredoxin
TXNRD	Thioredoxin reductase 1

1. Introduction

1.1 Pancreatic cancer

The worldwide incidence and mortality rate of pancreatic cancer is rising, making it one of the most serious global health burdens [1, 2]. Although it is only the 14th most common type of cancer, pancreatic cancer accounts for the 7th highest cancer mortality rate in the world, with nearly as many deaths (n = 432,000) as cases (n = 459,000) in 2018 [3, 4]. Despite extensive research, numerous insights, and advances in diagnosis, the 5-year survival is still below 10 % (2014: 6 % and 2018: 9 %), with only 1/4 of all patients surviving the first year after diagnosis [5]. Between 1990 and 2017, the number of incidence and deaths due to pancreatic cancer more than doubled, and it is even expected to be the 2nd leading cause of cancer-related death after lung cancer by 2030 [1, 6, 7]. These increases, mainly seen in the western countries (Europe, North America, Australia, and New Zealand) with higher human development index and gross domestic product per capita are likely due to the aging population and particular lifestyle factors [1, 2, 4]. Aside from family history and genetic factors, risk factors include tobacco smoking, diabetes mellitus, obesity, and alcohol consumption [8, 9].

There are different tumor types in the pancreas, all with distinct clinical presentation and genetic mutations. Pancreatic ductal adenocarcinoma (PDAC) is the most common pancreatic malignancy, accounting for 90 % of all pancreas neoplasms [10, 11]. In order to advance from a minimally dysplastic epithelium to invasive carcinoma, several mutations are necessary, including the four major driver mutations of pancreatic cancer: *KRAS, p16/CDKN2A, TP53,* and *SMAD4* [12, 13] (Figure 1.1).

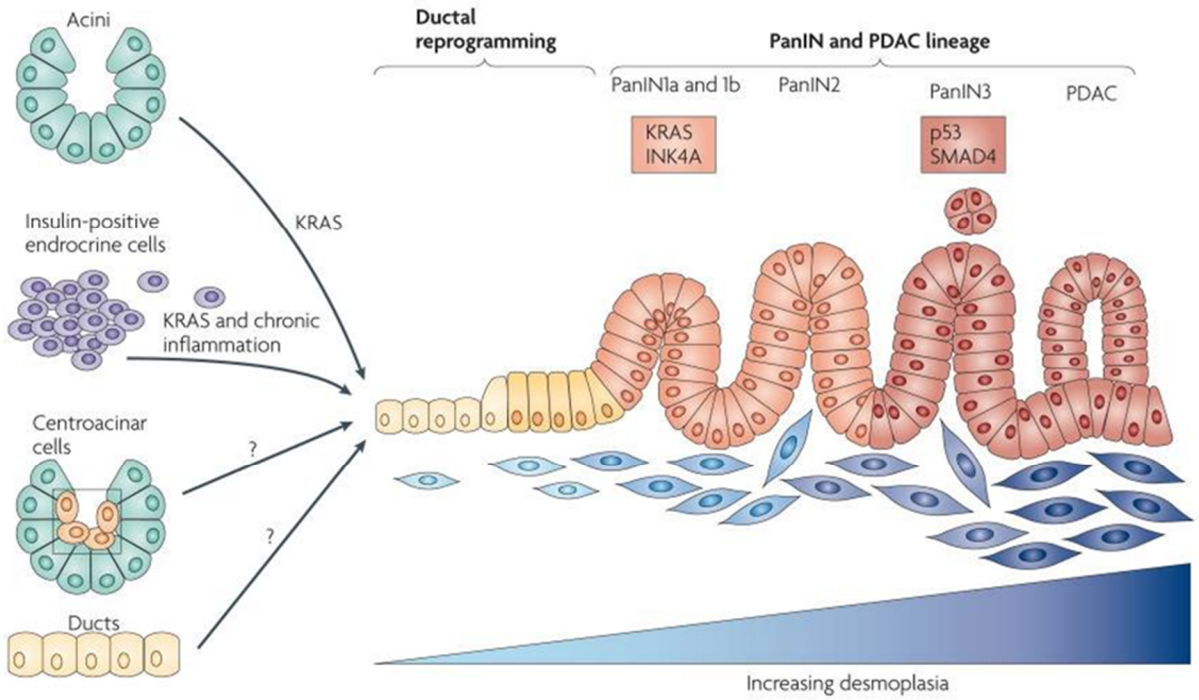

Figure 1.1. Progression model for pancreatic cancer. Pancreatic intraepithelial neoplasia (PanIN), a precursor lesion, can progress to pancreatic cancer after a serial accumulation of mutations. Figure reprinted from [14].

Pancreatic cancer can be divided into four clinical staging groups. In stage I (resectable), the cancer shows no spread and has grown to 2-4 cm. In stage II (borderline resectable), the tumor is greater than 4 cm and can present with spreading to nearby lymph nodes. Further expansion to blood vessels or nerves is characteristic for stage III (unresectable/locally advanced). When the cancer has spread to distant organs, it is referred to as stage IV (metastatic) [5]. 80-90 % of all patients are in an advanced stage when diagnosed, rendering the tumor non-resectable. Approximately 50 % of patients who have undergone surgery and adjuvant therapy tend to develop liver metastases within two years [15]. It is assumed that 90 % of all pancreatic cancer deaths are attributed to metastases [16, 17].

Unspecific symptoms considerably complicate an early diagnosis, which in turn impairs the prognosis for pancreatic cancer patients. These symptoms, which may also have other causes, include weight loss, nausea, indigestion, stomach or back pain, and fatigue [18, 19].

For the diagnosis of pancreatic cancer, several imaging modalities are used. Imaging has become a crucial and decisive factor in the detection and assessment of pancreatic cancer [20]. Imaging modalities include abdominal ultrasonography, tri-phasic pancreatic protocol computed tomography (CT), magnetic resonance imaging (MRI), and endoscopic ultrasound-guided fine-needle aspiration [5, 21, 22]. The most commonly used serological marker is the glycoprotein Carbohydrate antigen 19-9 (CA 19-9). However, CA 19-9 shows variable sensitivity (69 – 98 %) and specificity (46 – 98 %), and only 65 % of patients in stage I present with elevated levels [20]. Nonetheless, higher CA 19-9 levels were demonstrated to be associated with poorer treatment outcomes in patients with locally advanced pancreatic cancer receiving chemoradiation [23].

Pancreatic cancer treatment involves multidisciplinary therapy, including surgery, chemotherapy, radiotherapy, chemoradiotherapy, and palliative therapy. Treatment is primarily based on the stage of the disease at the time of diagnosis (Figure 1.2).

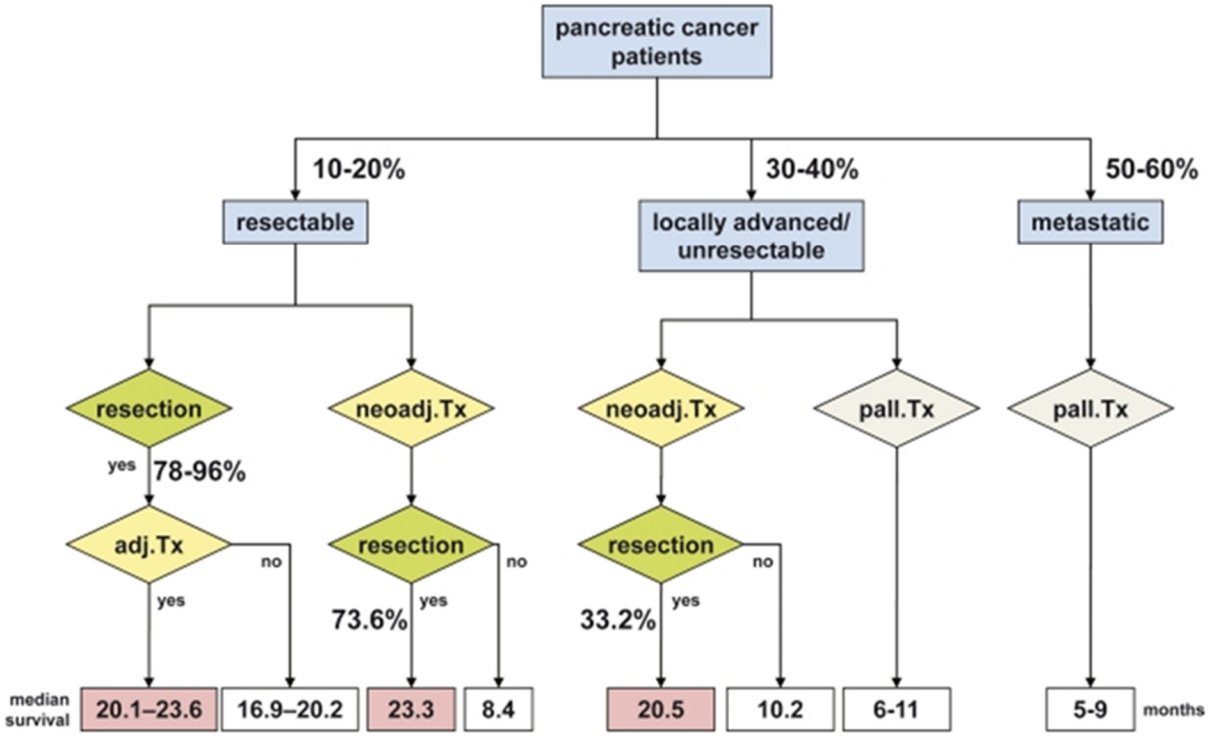

Figure 1.2. Overview of pancreatic cancer disease stages and treatment course. Shown are the survival and resection percentages of different groups of patients with pancreatic cancer. The borderline resectable tumors are included in the locally advanced/unresectable group. Figure reprinted from [24].

The only treatment cure for pancreatic cancer is surgical resection, which has shown significant improvement in overall survival [25]. Since many patients suffer a recurrence after surgical resection [15], adjuvant therapy, a treatment administered after surgery, is generally considered. While there is supporting evidence for a combined chemoradiotherapy treatment in comparison to chemotherapy alone as an adjuvant treatment [26-29], it was also shown that only patients receiving adjuvant chemotherapy after surgery have a significantly improved survival rate compared to patients in the chemoradiotherapy arm. Furthermore, chemoradiotherapy seemed to worsen the prognosis for the patients [30, 31]. However, this ESPAC-1 trial was criticized for several aspects, including the absence of radiation quality control, heterogeneous treatment fields, and low radiation dose [32]. Adjuvant chemoradiotherapy remains controversial, as evidenced by the fact that it is not used in Europe, while in Northern America, patients continue to receive chemotherapy in combination with radiotherapy because a specific subpopulation of patients can benefit from it [19, 33].

However, at the time of diagnosis, 80 % of patients are no longer in the primary resectable stage. Those patients either present with distant metastasis or without metastasis but with locally advanced pancreatic cancer, thus surgery is no longer a therapeutic option. For patients presenting with metastatic disease, chemoradiotherapy, e.g., the FOLFIRINOX (folinic acid, fluorouracil, irinotecan, and oxaliplatin) regimen, is recommended [32]. For patients without metastasis but non-resectable or borderline resectable pancreatic cancer, neoadjuvant therapy in the sense of chemotherapy in combination with radiotherapy offers the possibility of downstaging borderline resectable and locally advanced tumors, thus improving not only the resection rate but also overall survival [34, 35]. It was not only shown that patients with locally advanced pancreatic cancer undergoing chemoradiotherapy had an overall survival rate similar to patients with primary resectable tumors [36, 37] but moreover, patients with tumor recurrence can be treated safely with chemoradiotherapy for successive surgery [38]. However, the advantage of a combination treatment with chemoradiotherapy compared to chemotherapy alone is still inconsistent and widely discussed in the literature [39-41]. This may be due to the heterogeneous nature of pancreatic cancer and the inherent radioresistance, thus

limiting the efficacy [42, 43]. Only one-third of patients show a response to radiation therapy in most clinical studies [44-47]. However, the underlying mechanisms that lead to treatment failure in ~70 % of pancreatic cancer patients receiving radiotherapy are still unclear. Therefore, it is crucial to investigate mechanisms leading to radioresistance in pancreatic cancer and to thereby gain new insights for potential individualized radiotherapy [37].

1.2 Radiotherapy

In addition to surgery, chemotherapy, and palliative care, radiotherapy is an integral treatment option in the field of cancer [48]. The clinical application of x-rays was first reported in the late 19th century, shortly after the discovery by Roentgen in 1895 [48-50]. In the clinical setting, ionizing radiation, i.e., x-rays and γ-rays, is commonly used for the treatment of cancer, in order to achieve loco-regional disease control, tumor downsizing, prevention of tumor cell dissemination and invasion while sparing the normal tissue. About half of all cancer patients are treated with radiotherapy over the course of their disease [48, 51, 52]. In order to spare the normal tissue, thus diminishing normal cell toxicity, patients receive multiple fractions of radiotherapy over several weeks. While the external beam radiotherapy involves the use of a device to administer the radiation from outside, brachytherapy involves the introduction of a radioactive material into the body in the vicinity of the cancerous tissue [48].

The primary target of radiation is the DNA, where the high-energy deposition causes damage. Besides the direct effect of irradiation on the DNA, 60 – 70 % of the DNA damage is produced indirectly by free radicals, i.e., reactive oxygen species (ROS) [53, 54], the products from the radiolysis of water (Figure 1.3). The radiation dose is measured in units gray (Gy), one Gy of irradiation induces 2000 base modifications, 1000 DNA single-strand breaks (SSBs), and about 35 DNA double-strand breaks (DSBs) per cell [55]. When two SSBs are in close proximity, DSBs are likely to arise. Since DSBs are much more complicated to repair, they are viewed as fatal damage to the cell, with unpaired DSBs leading to cell death [42].

The vast majority of radiation-induced damages are caused by ROS. The radiolysis of water due to irradiation leads immediately (< 1 second) to the formation of free radicals, including hydroperoxyl radical, hydrogen radical, and hydroxyl radical [56]. ROS are important for cell signaling and homeostasis; therefore, free radicals are continuously generated in the environment of a cell. Under physiological conditions, the accumulation of ROS, leading to oxidative stress, is prevented by scavenging systems, including glutathione, thioredoxin, dismutase, peroxidase, and catalase [57, 58].

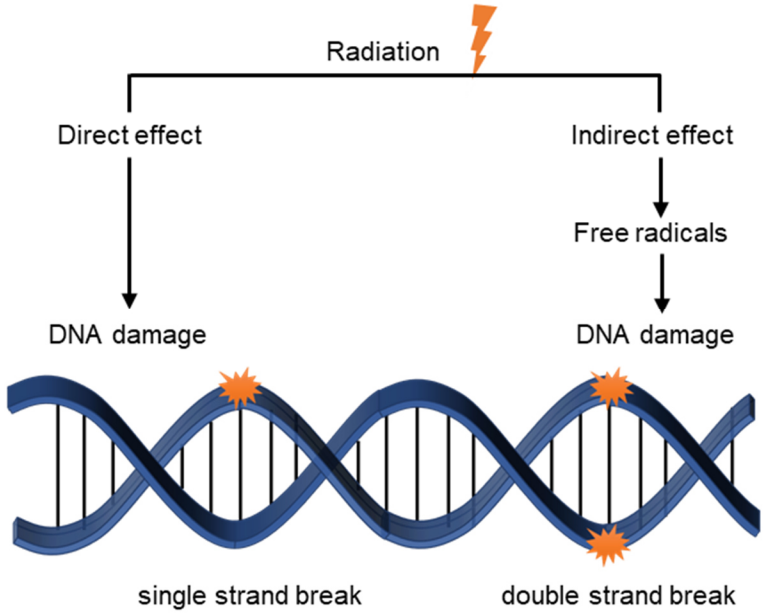

Figure 1.3. Direct and indirect DNA damage. Ionizing radiation can cause DNA damage in two ways. Figure adapted from [48].

Radiation can trigger several cell responses, including senescence, apoptosis, necrosis, or autophagy. For cells to survive radiation-induced damage, DNA damage response and DNA repair are of crucial importance. SSBs are recognized by members of the Poly(ADP-ribose) polymerase (PARP) family, which recruit the base excision repair (BER) machinery in order to repair the lesion [42] (Figure 1.4).

Ataxia-telangiectasia mutated (ATM), ataxia-telangiectasia, and Rad3-related (ATR) and DNA-dependent protein kinase catalytic subunit (DNA-PKcs) are activated after the induction of DSBs [59]. These kinases then phosphorylate the histone H2AX at the

site of the DNA damage in order to induce DNA repair. Following the formation of γH2AX, DNA damage repair pathways are initiated, mainly homologous recombination (HR) and non-homologous end-joining (NHEJ) [60]. HR is considered to be an error-free mechanism, as it requires a homologous DNA sequence provided by the sister chromatid [61]. In contrast, during NHEJ DSBs are repaired through the ligation of the broken DNA ends, possibly resulting in more errors due to the loss or modification of genetic information [61]. NHEJ is the more dominant repair mechanism for DSBs.

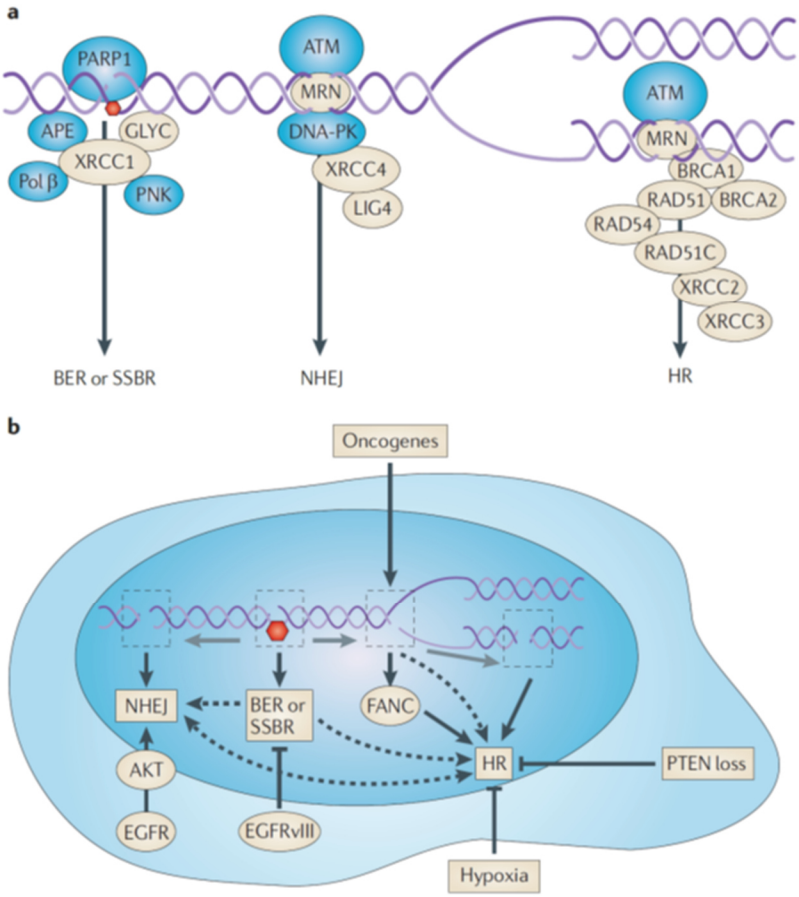

Figure 1.4. Radiation-induced DNA damage repair. A. Several DNA repair pathways for the different DNA lesions are shown. B. The influence of the tumor-associated cellular processes on DNA damage is shown. APE, AP endonuclease; ATM, ataxia telangiectasia mutated; BER, base excision repair; DNA-PK, DNA-dependent protein kinase; EGFR, epidermal growth factor receptor; FANC, Fanconi anaemia pathway; GLYC, glycosylase; HR, homologous recombination; LIG4, DNA ligase IV; MRN, MRE11–RAD50–nibrin complex; NHEJ, non-homologous end joining. Figure reprinted from [52].

In theory, any success of radiotherapy can be achieved by two main mechanisms: 1) increasing the amount of radiation-induced DNA damage within the tumor or 2) decreasing the efficiency of DNA repair within tumor cells [62]. Cells that can efficiently repair the radiation damage are radioresistant, a characteristic enabling the cells to survive and replicate. Radioresistant tumor cells are the limiting factor for the efficacy of radiotherapy and remain the most critical obstacle to overcome. Radioresistance is the main cause of radiotherapy failure and leads to a poor prognosis in cancer patients due to possible tumor relapse or metastasis spread [63]. Concerning radioresistance, cancer stem cells (CSCs) moved into the focus since they are more resistant to radio- and chemotherapy and therefore considered as the leading cause of tumor recurrence [64]. Due to their superior DNA repair capacity and ROS defense as well as their self-renewal capacity, CSCs are associated with radioresistance compared to non-CSCs [63].
However, the exact mechanisms that contribute to radioresistance in pancreatic cancer are still largely unknown. Targeting the pathways that play a role in the radioresistance of pancreatic cancer represents a promising strategy for improving the poor treatment outcome in the future.

1.3 Invasion

About half of all pancreatic cancer patients present with metastasis at the time of diagnosis [24]. Since it is assumed that 90 % of all deaths from pancreatic cancer are due to metastases [16, 17], therefore, elucidating the mechanisms involved is of critical clinical importance. The complex processes underlying invasion and metastasis, where tumor cells leave the primary tumor, invade adjacent tissue, and circulate to distant organs forming new colonies, are mostly unknown [17]. The spread of cancer cells from the primary tumor to anatomically distant organs entails a multi-step process. During the first step, invasion, cells invade the extracellular matrix to leave their niche. Following the entering of the blood and lymphatic vessels, termed intravasation, cells must survive the systemic circulation (systemic transport). In order

to enter the distant tissue, cells have to leave the blood vessels, known as extravasation. The last step, metastatic colonization, involves the survival in the new microenvironment and the subsequent forming of metastases [65-67]. The epithelial-mesenchymal transition (EMT), a prominent and significant feature of pancreatic cancer, is of crucial importance for a metastatic progression [15]. During EMT, the expression of adhesion molecules is changed, epithelial markers are downregulated and instead, a mesenchymal cytoskeleton is produced [15, 68]. EMT in pancreatic cancer is associated with drug resistance and increased invasiveness [69].

There are two models postulated for the metastatic progression, the Darwinian linear model and the parallel model. In the linear model, the progression to metastatic disease is viewed as a stepwise process, from the tumor initiation through mutations in driver genes to the last step, the formation of distant metastasis. In contrast, the parallel model hypothesized that tumor cell dissemination occurs early during tumorigenesis before the primary tumor is even detectable in the clinic, and the metastases develop in parallel to the primary tumor [15, 68].

1.4 MicroRNAs

MicroRNAs (miRNAs) were first discovered by Lee et al. in 1993 and are non-coding, single-stranded RNAs with a length of ~ 22 nucleotides [70, 71]. As a new class of gene regulators, miRNAs that bind to target mRNA lead to either translational repression or degradation of the target mRNA, depending on the degree of complementarity between the miRNA and its target mRNA [71]. With perfect complementarity to the target mRNA, miRNAs induce the RNA-mediated interference (RNAi) pathway with the subsequent degradation of the target mRNA (Figure 1.5). However, in eukaryotic cells miRNA mediated translational repression is the more common mechanism of gene regulation, in which not entirely complementary mRNA are bound, leading to translational repression of the target mRNA instead of mRNA cleavage [71]. miRNAs are transcribed by RNA polymerase II to a longer precursor

pri-miRNA transcript in the nucleus. After further processing by the ribonuclease complex Drosha-Pasha to the hairpin-shaped pre-miRNA, transporter proteins export the pre-miRNA to the cytoplasm. There, the pre-miRNA is further processed and incorporated into the RNA-induced silencing complex (RISC). For the negative regulation of gene expression, the mature miRNA can then bind to complementary sites in the target mRNA [71, 72].

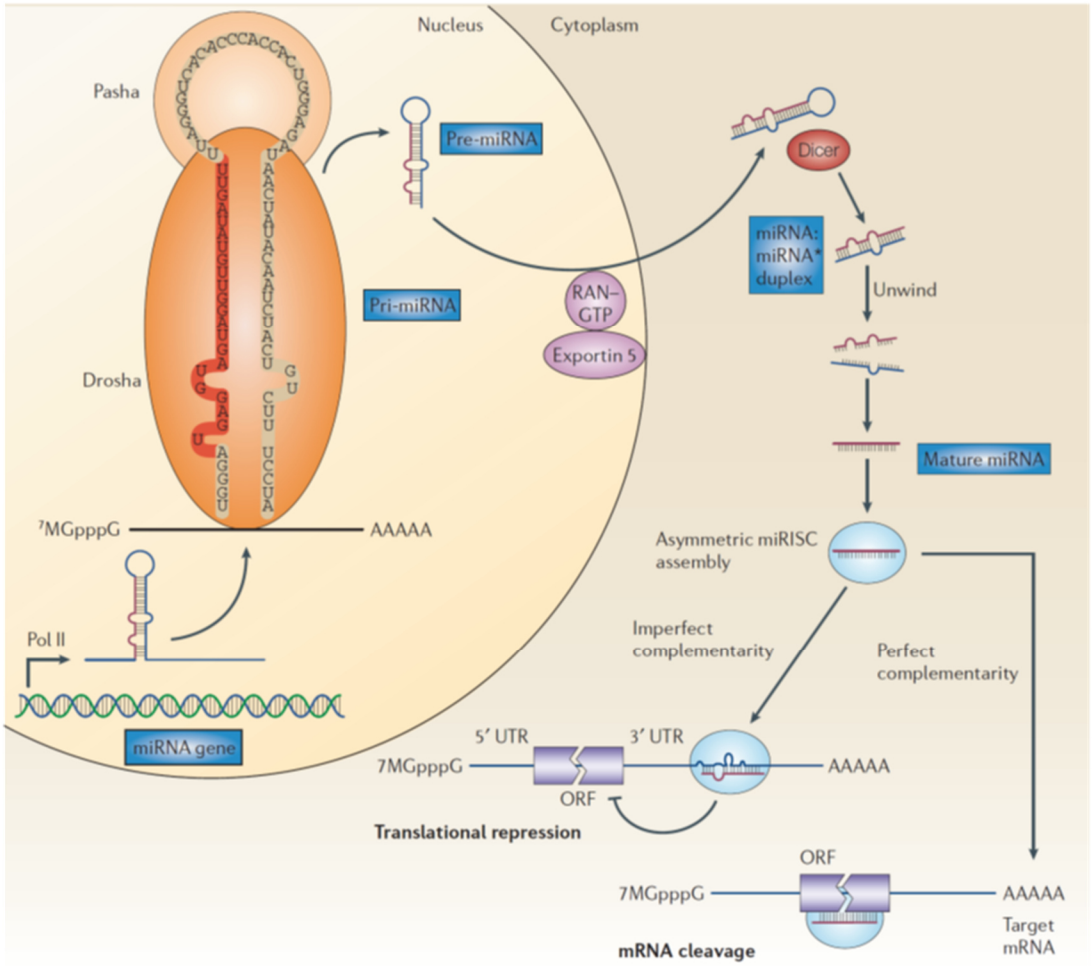

Figure 1.5. The biogenesis of microRNAs. microRNAs (miRNAs) are transcribed by RNA polymerase II in the nucleus to pri-miRNA. This precursor is further processed to pre-mRNA, which is then transported into the cytoplasm. After several processing steps, the mature miRNA is incorporated in the RNA-induced silencing complex (RISC), subsequently leading to post-transcriptional repression of target mRNAs by mature miRNAs. Figure reprinted from [71].

Due to their role in a plethora of biological signaling pathways, e.g., cell growth, differentiation, and apoptosis, it has been proposed that deregulation of miRNA expression could be involved in tumorigenesis. Calin et al. were the first to describe an association between deregulated miRNAs and cancer [73]. Since then, several

studies have shown that miRNAs are deregulated in many tumor entities, including pancreatic cancer, where miRNAs possess either oncogenic or tumor suppressor functions and thus are involved in the development and progression of cancer [74-77].

Most patients with pancreatic cancer are diagnosed at a late stage when the curative option of surgery is no longer feasible, leading to a dismal prognosis. Therefore, biomarkers detecting the disease at an early stage are urgently needed. There is growing evidence that miRNAs might serve as diagnostic biomarkers in pancreatic cancer [78, 79]. In addition, their high stability in body fluids such as serum and plasma make them attractive candidates for non-invasive biomarkers. Several studies have shown that pancreatic cancer patients can be distinguished from healthy donors based on different miRNAs detectable in plasma, serum, or whole blood [78, 79]. Furthermore, in combination with the serum marker CA-19-9, the diagnostic value was significantly improved [80, 81].

Apart from the potential diagnostic value of miRNAs, several studies have shown an association between the expression of miRNAs and survival in pancreatic cancer patients. High expression of some miRNAs was found to predict poorer overall outcome and survival, distinguish long from short-term survivors, or correlate with distant metastasis [82-85].

Furthermore, miRNAs are associated with radioresistance in pancreatic cancer. Several miRNAs were shown to regulate the response to radiation, either rendering the cells radioresistance or radiosensitive [86-89]. Therefore, there is a growing interest in the investigation of miRNAs as potential biomarkers for the prediction of radiation response. For pancreatic cancer patients in an advanced stage, radiotherapy in combination with chemotherapy offers an opportunity to downstage the tumor and thus improve overall survival. Nonetheless, only ~ 30 % of pancreatic cancer patients show a response to radiation therapy [44-47]. A miRNA panel that can predict the response to radiotherapy could help to identify those patients who would benefit from a treatment, ultimately leading to personalized radiotherapy.

1.5 Aim of the study

The goal of the study was to investigate the mechanisms leading to radioresistance in pancreatic cancer and further evaluate miRNAs as predictive biomarkers of radiation response. Therefore, isogenic radioresistant (RR) pancreatic cancer cell lines were generated, and the mechanisms leading to radioresistance were identified. The migratory and invasive properties of the radioresistant cell lines were subsequently examined. Furthermore, miRNAs associated with radioresistance were investigated *in vitro* and *in vivo*.

2. Material and Methods

2.1 Cell culture

Established human pancreatic cancer cell lines were obtained from the University Hospital of Heidelberg, American Type Culture Collection (ATCC, LGC Standards GmbH) and German Collection of Microorganisms and Cell Cultures (DSMZ GmbH). Cell line authentication was performed by Eurofins Genomics, Germany. Panc-1 and MIA PaCa-2 were cultivated in DMEM High Glucose (#D6429, Sigma) supplemented with 10 % fetal calf serum (#F7524, Sigma) (FCS) and 1 % penicillin/streptomycin (#P0781, Sigma) (P/S). AsPC-1, BxPC-3, T3M-4 and SU.86.86 were maintained in RPMI-1640 (#R8758, Sigma) supplemented with 10 % FCS (#F7524, Sigma) and 1 % P/S. All cells were grown as monolayer culture and kept at 37 °C in a controlled atmosphere with 5% CO2 and 95% humidity. Cells were routinely checked and determined as negative for mycoplasma contamination (#LT07-318, Lonza).

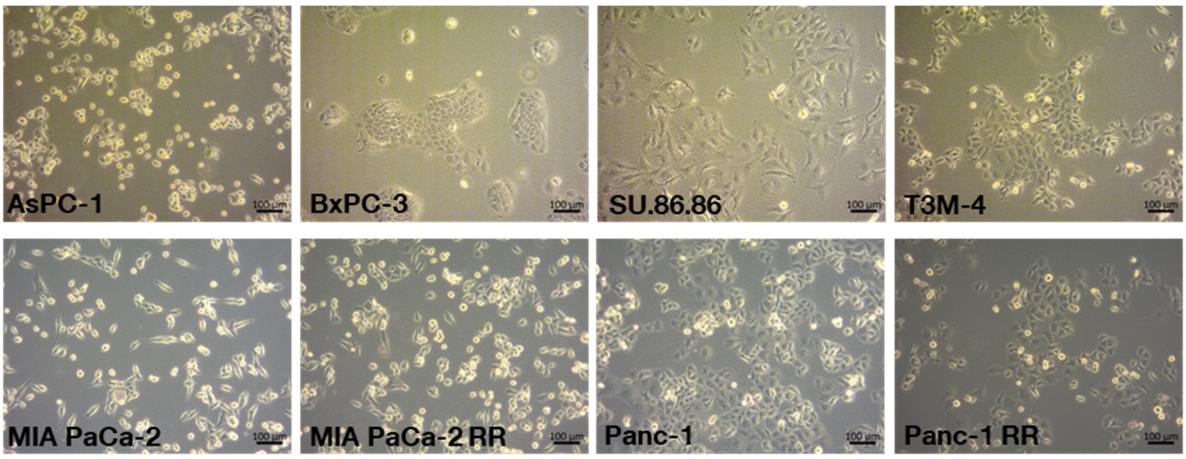

Figure 2.1: Established human pancreatic cancer cell lines and generated radioresistant cell lines.

Table 2.1: Characteristics of established pancreatic cancer cell lines. Source: Deer et al. [90] and https://web.expasy.org/cellosaurus/

Cell line	Age	Gender	Derivation	Metastasis	Differentiation
AsPC-1	62	Female	Ascites	Yes	Poor
BxPC-3	61	Female	Primary tumor	No	Moderate to poor
MIA PaCa-2	65	Male	Primary tumor	unknown	Poor
Panc-1	56	Female	Primary tumor	Yes	Poor
Su.86.86	57	Female	Liver metastasis	Yes	Moderate to poor
T3M-4	64	Male	Lymph node metastasis	yes	unknown

Table 2.2: Molecular alterations of *KRAS*, *TP53*, *p16*, and *SMAD4* in established pancreatic cancer cell lines. Source: Deer et al. [90], Moore et al. [91] and https://web.expasy.org/cellosaurus/

Cell line	KRAS	TP53	p16/CDKN2A	SMAD4/DPC4
AsPC-1	mutated	mutated	Wildtype/deleted	Wildtype/deleted
BxPC-3	wildtype	Mutated	Wildtype/deleted	Deleted
MIA PaCa-2	Mutated	Mutated	Deleted	Wildtype
Panc-1	Mutated	Mutated	Deleted	Wildtype
Su.86.86	Mutated	Mutated	Deleted	Wildtype
T3M-4	Wildtype	Mutated	Deleted	wildtype

2.2 Cell irradiation

X-ray irradiation was performed using the RS225A irradiation device (Gulmay/Xstrahl, UK), at a dose rate of 1 Gy/min (15 mA, 200 kV).

2.3 Functional analysis

2.3.1 Colony formation assay

Cells were seeded in 12-well plates and 24 hours later irradiated with a single dose of radiation ranging from 0 to 8 Gy. After 8 – 15 days, colonies were fixed with ice-cold methanol, stained with 0.1 % crystal violet and counted. Colonies were imaged with GelCount™ (Oxford optronics). Colonies consisting of more than 50 single cells were

counted as one colony, counting was performed manually. The plating efficiency (PE) was determined as the ratio between formed colonies and the number of cells seeded at 0 Gy, with the following formula:

$$PE = \frac{number\ of\ colonies}{seeded\ cells} \cdot 100$$

The survival fraction (SF) is represented by the following formula:

$$SF = \frac{number\ of\ colonies}{(seeded\ cells\ \cdot PE)}$$

Survival curves were fitted according to the linear-quadratic model (LQM) using GraphPad Prism (GraphPad Software Inc., San Diego, USA). The formula for the LQM is the following:

$$SF = -\alpha \cdot D - \beta \cdot D^2$$

2.3.2 Generation of radioresistant pancreatic cancer cells

For the generation of RR cell lines, two approaches were used. First, Panc-1 and MIA PaCa-2 cells were exposed to 10 fractions of 2 Gy per day for 2 weeks, excluding weekends, in T75 flasks, as previously described [92]. After each irradiation procedure, media was exchanged, and cells were washed with PBS. Cells were passaged after five fractions of 2 Gy. Second, Panc-1 and MIA PaCa-2 cells were irradiated after a previously described protocol with minor modifications [86]. Briefly, cells were seeded in T75 flasks in complete medium. Upon reaching ~ 70 %, confluency cells were irradiated with 2 Gy using the RS225A irradiation device (Gulmay/Xstrahl, Camberley, UK) at a dose rate of 1 Gy/min (15 mA, 200 kV). At a confluency of 80 – 90 % cells were then subcultured into new flasks. Whenever cells

reached 70 % confluency, cells where serially irradiated with increasing doses (4, 6, and 8 Gy) and an additional six cycles of 10 Gy radiation. The cumulative dose was 80 Gy. In both procedures, the surviving cells were allowed to recover and expanded for at least one month before further experiments were conducted.

2.3.3 Cell growth

Cells were seeded in 12-well plates and incubated at 37 °C. Cells were trypsinized and counted 24, 48, 72, and 96 hours after seeding. Cell doubling time (DT) was determined using the following equation:

$$DT\ (h) = T\ \cdot \frac{\ln(2)}{\ln(\frac{X_e}{X_b})}$$

where T is the time in hours; X_e cell number at the end of incubation time; X_b the initial cell number.

2.3.4 γH2AX foci assay

24 hours prior to irradiation, cells were seeded in chamber slides with removable wells and allowed to attach at 37 °C in a humidified incubator. 24 hours after irradiation cells were washed with PBS and fixed with 2 % paraformaldehyde (PFA) for 15 minutes. Cells were then washed with PBS and permeabilized with three washing steps in PBS + 0.15 % Triton X-100, each step for 5 minutes. Blocking of unspecific binding was carried out with a blocking buffer consisting of PBS, 0.15 % Glycine, and 1 % Bovine Serum Albumin (BSA). Cells were washed with the blocking buffer three times for 10 minutes. After the blocking steps, cells were incubated with the primary antibody H2AX clone JBW301 (#05-636, Millipore), diluted 1:350 in blocking buffer, overnight at 4 °C. Afterward, cells were washed with PBS for 5 minutes, incubated with PBS and 0.15 % Triton X-100 for 10 minutes, washed with PBS, and

subsequently blocking buffer was added for 7 minutes. The secondary antibody, Alexa Fluor 488 goat-anti-mouse (#A11029, Invitrogen) was diluted 1:500 in blocking buffer and incubated for one hour at room temperature. Cells were then washed twice with PBS and 0.15 % Triton X-100 for 10 minutes and with PBS for 10 minutes. The remaining liquids were removed to mount cells with one drop of Vectashield with Dapi (#H-1200, Vectorlabs). Foci from at least 100 cells were counted manually for each cell line (Zeiss Imager Z1 microscope).

2.3.5 γH2AX flow cytometry

Cells were seeded in T25 flasks 24 hours prior to irradiation and allowed to attach at 37 °C in a humidified incubator. Cells were trypsinized and fixed 30 minutes after irradiation with 1 % PFA for 15 minutes at 4 °. Cells were then resuspended in 70 % cold (-20 °C) Ethanol and stored at -20 °C for at least 2 hours. After a washing step with PBS, cells were resuspended in 1 % BSA in PBS and incubated with the primary antibody H2AX clone JBW301 (#05-636, Millipore), diluted 1:500, for 2 hours at room temperature. Cells were washed with 1 % BSA in PBS and incubated with the secondary antibody, Alexa Fluor 488 goat-anti-mouse (#A11029, Invitrogen), diluted 1:400, for 30 min at room temperature in the dark. After washing cells with 1 % BSA in PBS, cells were finally incubated with propidium iodide (PI) staining solution (0.02 mg/ml PI (#537059, Calbiochem) + 0.1% Triton X-100 (#T8787, Sigma) + 0.2 mg/ml DNase free RNase A (#R4875, Sigma) in PBS) for 30 min at room temperature. The analysis was performed using the FACSCalibur (Becton Dickinson, USA). The CellQuest software was used to determine the mean fluorescence intensity of the γH2AX signal in the cell cycle phases G1, S, and G2/M.

2.3.6 Cell cycle distribution

Cells were seeded in T25 flasks 24 hours prior to irradiation and allowed to attach at 37 °C in a humidified incubator. 24 hours after irradiation, cells were trypsinized, centrifuged, resuspended in cold PBS, and transferred dropwise to ice-cold ethanol

(70 %). Cells were fixed at -20 °C for at least 2 hours. Afterward, cells were stained with PI staining solution (see γH2AX flow cytometry) and analyzed using the FACSCalibur (Becton Dickinson, USA). The cell cycle distribution was calculated using Modfit software (Verity Software House Inc, Topsham, USA).

2.3.7 Caspase 3/7 flow cytometry

The levels of apoptotic cells were determined using CellEvent™ Caspase-3/7 Green Flow Cytometry Assay Kit (#C10427, Invitrogen) and flow cytometry. Cells were seeded in T25 flasks 24 hours prior to irradiation and allowed to attach at 37 °C in a humidified incubator. 48 hours after irradiation, cells were trypsinized, centrifuged, and resuspended in PBS with 10 % FCS. 0.5 µl Caspase-3/7 Green Detection Reagent was added to the cells, and cell samples were incubated for 30 minutes at 37°C, protected from light. Afterward, 0.5 µl of the 1 mM SYTOX® AADvanced dead cell stain solution in DMSO was added to the cells and cell samples were incubated for a further 5 minutes at 37°C. Samples were evaluated by flow cytometry using FACSCalibur (Becton Dickinson, USA). The data analysis was performed using CellQuest software with Caspase 3/7 positive and Sytox negative cells.

2.3.8 Measurement of intracellular reactive oxygen species

Cells were collected by trypsinization and incubated in PBS containing 10 µM CM-H2DCFDA (#C6827, Thermo Fisher), an indicator for ROS, for 30 minutes at 37 °C. Cells were then treated with radiation and immediately placed on ice. Cells were measured with the FACSCalibur flow cytometer. The data analysis was performed using CellQuest software.

2.3.9 Migration and invasion assay

For the migration assay, 8 µm pore sized control inserts (#354578, Corning) and for invasion matrigel coated invasion inserts (#354480, Corning) were used. Cells were

seeded in T25 flasks 24 hours prior to irradiation and allowed to attach at 37 °C in a humidified incubator. 24 hours after irradiation cells were trypsinized, centrifuged, and resuspended in medium containing 0.5 % serum. Meanwhile, inserts were thawed for 15 minutes at room temperature and afterward rehydrated for 2 hours at 37 °C with medium containing 0.5 % serum, filled in the upper and lower chamber of the insert. The rehydration medium was removed from the insert and the insert transferred to a new plate. Medium containing 10 % FCS (chemoattractant) was filled into the lower chamber, whereas the cell suspension (20,000 cells/well for Panc-1 and 40,000 cells/well for MIA PaCa-2 cells) was added to the upper chamber. Cells were allowed to migrate for 24 hours at 37 °C in a humidified incubator. Afterward, non-migrated cells were removed from the upper side of the chamber using a cotton tip. Migrated cells (on the lower side) were fixed with ice-cold methanol and stained with 0.1% crystal violet. Membranes were cut out of the insert and fixed with Eukitt R Quick-hardening mounting medium (#03989, Sigma) on a glass slide. Zeiss Imager Z1 microscope at 10x magnification was used to acquire six independent microscope fields of each membrane for counting. Cells were automatically counted using ImageJ.

2.4 Molecular biology

2.4.1 RNA Extraction

About 50 mg of tumor tissue was homogenized using the dismembrator (Mikro-Dismembrator, Sartorius) and lysed with 700 µl Qiazol Lysis Reagent (#79306, Qiagen) and one stainless steel bead (#69989, Qiagen) in a cryogenic vial (#5000-0012, Nalgene). 48 hours after cell seeding, cells were trypsinized, centrifuged, resuspended in Qiazol Lysis Reagent, and stored at -80 °C. RNA extraction of *in vitro* cultivated cells and xenograft tumor material frozen in RNALater was performed using the miRNeasy Mini Kit (#217004, Qiagen). For blood plasma, the miRNeasy Serum/Plasma Kit (#217184, Qiagen) was used following the

manufacturer's protocol. RNA quantity and quality were assessed using the Nanophotometer P-Class (Implen).

2.4.2 RT² Profiler PCR Assay – oxidative stress

RT² Profiler 96 well-plates with 84 genes related to oxidative stress (#330231, Qiagen) were used. cDNA synthesis was performed using the RT2 First Strand Kit according to the manufacturers' instructions. Briefly, 500 ng of total RNA from each sample was used for reverse transcription. The fold changes of genes on the array were calculated using the $2^{-\Delta\Delta Ct}$ method with actin beta (*ACTB*), beta-2-microglobulin (*B2M*), glyceraldehyde-3-phosphate dehydrogenase (*GAPDH*), hypoxanthine phosphoribosyltransferase 1 (*HPRT1*) and ribosomal protein large P0 (*RLP0*) used as endogenous controls. The mean value of their ct-value was substracted from the sample ct-values.

2.5 Western blot analysis

In cooperation with the Institute of Radiation Biology (ISB) at the Helmholtz Centre Munich, western blot analysis was performed. 48 hours after cell seeding, cells were trypsinized and centrifuged. The supernatant was removed and cell pellets were frozen at -20 °C.

The cells were lysed using RIPA lysis buffer (ThermoFisher) and the protein concentrations were measured in triplicate by the Bradford assay (Sigma Aldrich) according to the manufacturer´s recommendations.

Cellular protein lysates (10 µg) were separated by gradient 4 – 12 % SDS-PAGE and were transferred to nitrocellulose membranes (GE Healthcare) using a Trans-Blot Turbo™ system (Bio-Rad) according to the manufacturer´s recommendations. The membranes were blocked using 3 % BSA in TBS, pH 7.4, for 1 h at room temperature, washed three times in 10 mM Tris-HCl, pH 7.4, 150 mM NaCl for 5 min and incubated overnight at 4 °C with primary antibodies using dilutions recommended by the

manufacturer. Immunoblot analysis was performed using anti-phospho-Nrf2 (phospho S40) (#ab76026, Abcam), anti-Nrf2 (#ab62352, Abcam), anti-SOD2/ MnSOD (#ab13533, abcam), anti-SOD1 (#ab13498, abcam), anti-TRX (#ab133524, abcam), and anti-GAPDH (#5174, cell signalling). After washing three times, the blots were incubated with the alkaline phosphatase-conjugated anti-mouse, anti-rabbit or anti-goat secondary antibody (Santa Cruz Biotechnology) for 2 h at room temperature and developed using 1-stepTM NBT/BCIP method (ThermoFisher) following standard procedures. GAPDH was used as the loading control. Image J software was applied to quantify the bands. Therefore, the background was subtracted, then values were normalized to the loading control, GAPDH.

2.6 *In vivo* xenografts

All animal experiments were approved by the government of Upper Bavaria, Germany (ROB-55.2Vet-2532.Vet_02-17-111) and conducted according to the German animal protection guidelines.

2.6.1 Subcutaneous tumor injection

For the subcutaneous (s.c.) implantation of tumor cells, cells were grown to confluency in growth medium. Afterward, cells were trypsinized, counted, and centrifuged. Cells were resuspended in an adequate volume of PBS (#D8537, Sigma). Mice were anesthetized with 2 – 3 % isoflurane. 4 x 10^6 cells suspended in 30 µl PBS were subcutaneously injected into the right flank of 7-8-week-old female athymic CD1-Foxn1 nude mice (crl:CD1-Foxn1^{nu}, Charles River Laboratories) using a 1 ml syringe with a 27-gauge needle.

2.6.2 Measurement of tumor volumes

Tumor growth was measured three times weekly with a digital caliper and two times weekly using an ultrasound imaging system (Logiq C5, GE). Tumor volume was calculated with the digital caliper measurement using the following formula:

$$tumor\ volume\ (mm^3) = lenght\ (mm) \cdot\ width\ (mm)^2\ \cdot \frac{\pi}{6}$$

Measurements with the ultrasound were conducted in three dimensions and the following formula was used to calculate tumor volume:

$$tumor\ volume\ (mm^3) = lenght\ (mm) \cdot\ width\ (mm)\ \cdot\ depth\ (mm)\ \cdot \frac{\pi}{6}$$

2.6.3 Irradiation

When tumors reached a size of 60 – 100 mm³, mice were randomized into groups (0, 5, or 10 Gy) and treatment was initiated. High-precision irradiation was performed with either a single dose of 5 or 10 Gy using the Small animal radiation research platform (SARRP, XStrahl). Mice were anesthetized with 2 – 3 % isoflurane during the procedure of imaging, treatment planning, and high-precision irradiation. A cone-beam computed tomography (CBCT) was performed on each mouse to calculate the dosimetry and to determine the radiation beam arrangement. For CBCT imaging, the X-ray source of SARRP was operated at a voltage of 60 kV and a current of 0.8 mA. The Muriplan (Xstrahl) preclinical treatment planning software for SARRP was used for treatment planning. Radiation was delivered at 220 kV and 13 mA. Irradiation was performed using a 10 × 10 mm² collimator and two beams in order to achieve a uniform dose distribution inside the tumor and with minimum doses in healthy tissues surrounding the tumor. Control mice were subjected to the same treatment except for the irradiation step.

2.6.4 Tumor growth delay

To assess the tumor growth delay after irradiation, tumors were measured with a caliper and ultrasound as described above. Tumor volume was normalized to the volume on the day of irradiation. The tumor growth over time t after treatment was fitted to an exponential function, $V(t) = V_0 e^{\alpha t}$, with parameters V_0 and α. The time when the tumor reached four times its volume at treatment was denoted as $t = T_4$ and was calculated using $T_4 = \ln(4)/\alpha$. The tumor growth delay was defined as the T4 difference between control and irradiated animals. A tumor > 1 cm in any dimension was considered as a terminal endpoint and mice were sacrificed.

2.6.5 Molecular analysis

For further molecular analysis (i.e., sequencing), mice were irradiated when tumors reached a size of 60 – 100 mm^3. Mice were randomized and treated with 0, 5, or 10 Gy. 24 hours after irradiation, mice were sacrificed. Blood from mice was taken by cardiac puncture and collected in EDTA tubes (#20.1341.100, Sarstedt) with a 24-gauge needle rinsed with 0.5 M EDTA (#AM9260G, Thermo Fisher). The tubes were centrifuged at 300 g for 15 minutes at 4 °C. The clear supernatant was transferred to a new tube and centrifuged at 16,000 g for 10 min at 4 °C and plasma was collected and stored at -80 °C. In addition, tumor samples were collected and frozen in RNALater RNA stabilization reagent (#76106, Qiagen) and snap-frozen in liquid nitrogen. Samples were stored at -80 °C.

2.7 Next Generation Sequencing

2.7.1 mRNA Sequencing

In cooperation with the Division of Animal Physiology and Immunology at the Technical University of Munich, mRNA sequencing was performed. 1000 ng total RNA was used for the library preparation with the NEBNext Ultra RNA Library Prep Kit for Illumina (#E7530S, New England Biolabs) according to the manufacturer's protocol. RNA integrity number (RIN) and yield were assessed using an RNA 6000 Nano Kit (#5067-1512, Agilent). Only samples with RIN > 8.8 were used for downstream cDNA synthesis and library preparation. After cDNA synthesis, each sample was subjected to 12 cycles of PCR amplification. After PCR amplification of the fragmented libraries, the samples were purified with Agencourt AMPure XP beads (#A63881, Beckman Coulter) and eluted in 20 µl of molecular-grade water. The Agilent High Sensitivity DNA Kit (#5067-4626, Agilent) was used to evaluate and to determine the concentration of the resulting library. The samples were sequenced on Illumina HiSeq 2500 system with the following conditions: rapid run, 100-bp single-end reads, and dual-indexed sequencing. Clustering and sequencing were performed using the HiSeq SR Rapid Cluster Kit v2 (#GD-402-4002, Illumina) and HiSeq Rapid SBS Kit v2 (#FC-402-4022, Illumina). Five independent biological replicates were analyzed for each cell line.

Sequencing data for mRNA were processed using the snakemake pipeline bulkSeqPipe (v0.5) (https://gitlab.lrz.de/ImmunoPhysio/bulkSeqPipe) [93]. The quality of sequencing data was assessed using fastqc (v.1.2) prior to clipping adaptor sequences using trimmomatic (v.0.36) [94]. STAR (v.2.7.1a) [95] was used to align reads to the human genome build 38 with annotation 95. Mapped reads were counted using htseq (v.0.9.1) [96]. Differential expression analysis was performed using R (v.3.6.1) and the Bioconductor package DESeq2 (v.1.24.0) with the included median ratios of mean expression-based normalization and false discovery correction according to Benjamini-Hochberg. Read counts were modeled as a negative binomial distribution with estimated mean values and gene-specific dispersion parameters. Thresholds of log2 fold change ≥ |1|, adjusted p-value ≤ 0.05, and baseMean ≥ 50

were set to identify significantly regulated transcripts. Visualization of gene expression, principal component analysis, and venn diagrams were carried out in R using the packages gplots [97], genefilter [98], ggfortify [99], RColorBrewer [100], EnhancedVolcano [101], and VennDiagram [102].

2.7.2 Small RNA Sequencing

In cooperation with the Division of Animal Physiology and Immunology at the Technical University of Munich, small RNA sequencing was performed. Small RNA library preparation was done with the NEBNext Multiplex Small RNA Library Prep Kit from Illumina (#E7560S, New England Biolabs), as described in Buschmann et al. [103]. 200 ng total RNA of cells and tumor material and entire RNA isolated from 100 µl plasma was used for small RNA library preparation, respectively. Quality and quantity of RNA were analyzed using Nanophotometer P300 (Implen), RNA 6000 Nano Kit (#5067-1512, Agilent) and RNA 6000 Pico Kit (#5067-1513, Agilent). To compensate for the low RNA input, all adaptors and primers were diluted 1:3 in nuclease-free water. 3′ and 5′ adapters were sequentially ligated to the ends of small RNAs and reverse transcribed to generate cDNA.

Following adaptor ligation and cDNA synthesis, cDNA was amplified using a primer complementary to the 3’ adaptor and a primer containing 1 of 48 index sequences with 15 cycles of PCR. Libraries were size selected for a 130-150 bp fragment on high-resolution 4% agarose gel electrophoresis and purified using the Monarch PCR Cleanup Kit (#T1030L, New England Biolabs). After purification of the library pools, the quality and molarity of small RNA libraries were validated using Agilent High Sensitivity DNA Kit (#5067 4626, Agilent). The samples were sequenced on Illumina HiSeq 2500 system with the following conditions: rapid run, 50-bp single-end reads sequencing. Clustering and sequencing were performed using the HiSeq SR Rapid Cluster Kit v2 (#GD-402-4002, Illumina) and HiSeq Rapid SBS Kit v2 (#FC-402-4022, Illumina). At least four independent biological replicates were analyzed for each cell line. For tumor and plasma material, at least four mice from each treatment group were sequenced.

Sequencing data were processed as described previously [104]. For the quality

assessment of sequence length distribution FastQC (v0.10.1) was used. The remaining reads were filtered for low-quality reads, contaminating 5′ adapters, homopolymers, trimmed for 3′ adapters, and aligned to human miRNA sequences in the most recent version of miRbase (v22). Differential gene expression analysis was subsequently performed via the Bioconductor Package DESeq2 (v1.8.1) [105]. Significant miRNAs were selected based on a log2 fold change ≥ |0.7| (for cells) or log2 fold change ≥ |1| (for tumor tissue and plasma) and an adjusted p-value of ≤ 0.05. Only transcripts with a baseMean ≥ 50 were included in the analysis. Visualization of gene expression and principal component analysis were carried out in R using the packages gplots [97], ggfortify [99], RColorBrewer [100], and EnhancedVolcano [101]. An online tool (http://bioinformatics.psb.ugent.be/webtools/Venn) was used to create Venn diagrams.

2.8 Ingenuity pathway analysis

Pathway analysis on deregulated mRNAs was performed by the software tool IPA (QIAGEN Inc., https://www.qiagenbioinformatics.com/products/ingenuitypathway-Analysis) [106] in cooperation with the Institute of Radiation Biology (ISB) from the Helmholtz Zentrum Munich.

2.9 Statistics

Statistical analysis was performed using GraphPad Prism software (v8.2.1, GraphPad Software Inc., San Diego, USA). Statistical significance between parental and radioresistant cell lines was determined using two-way ANOVA. The Student's t-test was used to evaluate significant differences between two groups. A p-value of ≤ 0.05 was considered to be statistically significant.

3. Results

3.1 Radiosensitivity of established human pancreatic cancer cell lines

In order to determine the radiosensitivity of six established human pancreatic cancer cell lines, colony formation assay (CFA) was performed. Cells were exposed to 0, 2, 4, 6, and 8 Gy of X-ray irradiation. The survival after irradiation was cell line dependent, an indication for the heterogeneity in the pancreatic cancer cells. The cell lines MIA Paca-2 and Panc-1 were more sensitive to irradiation than cell lines BxPC-3, T3M-4, and AsPC-1 with an intermediate radiosensitivity. The cell line SU.86.86 demonstrated the highest radioresistance (Figure 3.1).

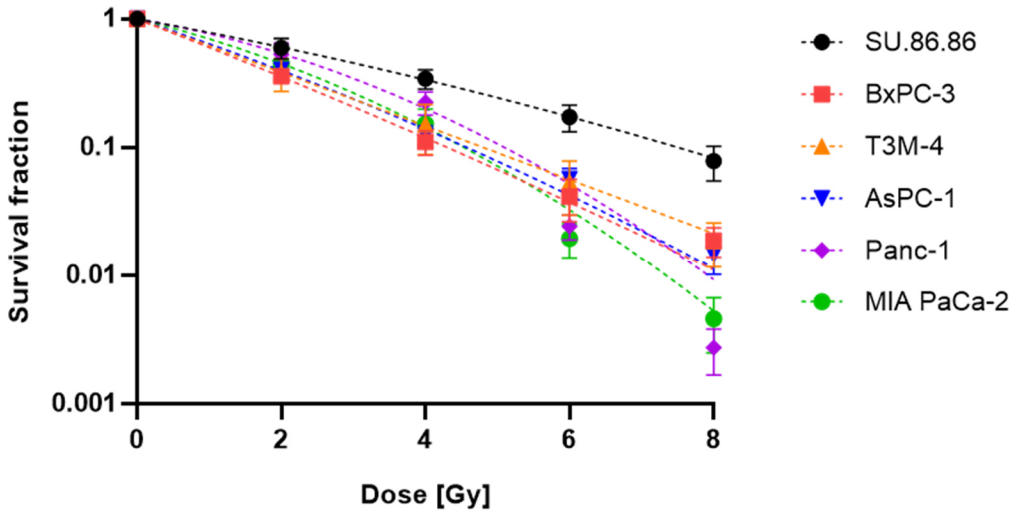

Figure 3.1. Colony formation assay of the established human pancreatic cancer cell lines. Shown are the survival curves fitted to the linear-quadratic model. Error bars represent SD (n > 3).

The linear-quadratic coefficients, α and β, were determined for each cell line (Table 3.1).

Table 3.1. Calculated linear-quadratic parameters of the dose-response cell survival curve for human established pancreatic cancer cell lines.

Cell line	α [Gy^{-1}] [a]	β [Gy^{-2}] [a]
Su.86.86	0.23 ± 0.12	0.01 ± 0.02
BxPC-3	0.49 ± 0.10	0.01 ± 0.03
T3M-4	0.48 ± 0.19	0.00 ± 0.03
AsPC-1	0.42 ± 0.09	0.02 ± 0.02
Panc-1	0.21 ± 0.16	0.05 ± 0.03
MIA PaCa-2	0.31 ± 0.09	0.05 ± 0.01

[a] α and β values were derived from the linear-quadratic equation $SF = \exp[-\alpha \times D - \beta \times D2]$.

3.2 Generation of radioresistant pancreatic cancer cell lines

As MIA PaCa-2 and Panc-1 were the most radiosensitive human pancreatic cancer cell lines investigated during this study, these two cell lines were subjected to multiple fractions of X-ray irradiation in order to generate isogenic radioresistant (RR) cell lines. Therefore, two different approaches were used. First, cells were subjected to 10 fractions of 2 Gy over a time period of 2 weeks. Second, cells underwent fractionated irradiation with increasing doses (2, 4, 6, and 8 Gy) and additional six cycles with 10 Gy, thereby receiving a cumulative dose of 80 Gy. Afterward, surviving cells were expanded for further experiments (Figure 3.2).

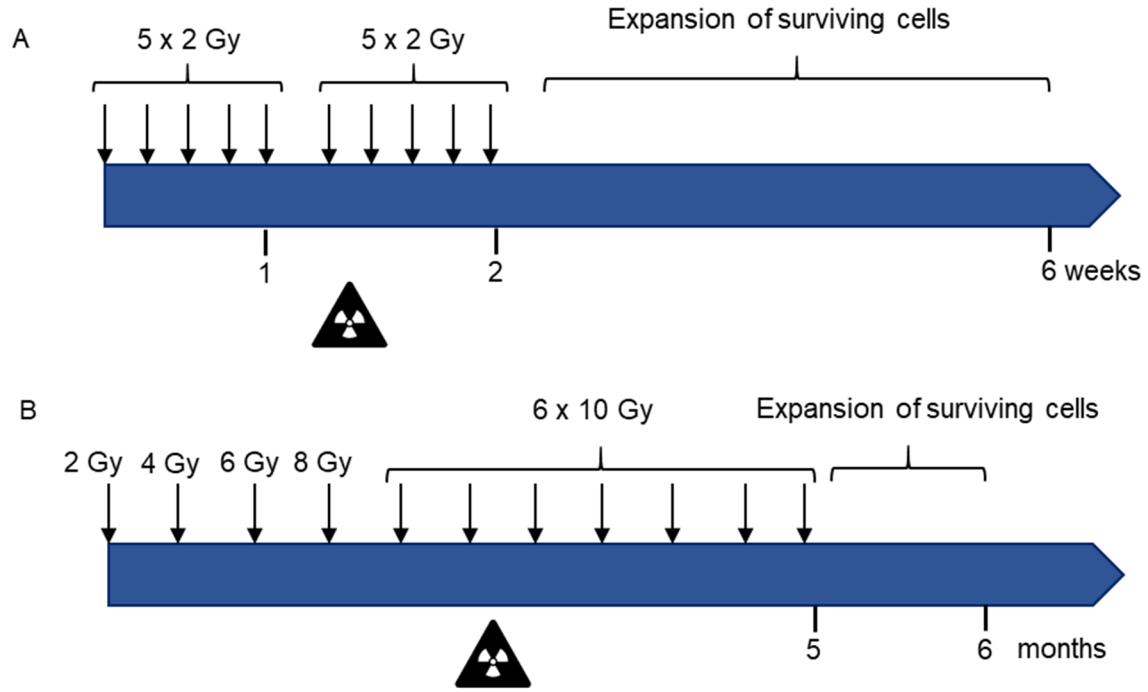

Figure 3.2. Scheme for the generation of radioresistant cell lines. MIA PaCa-2 and Panc-1 pancreatic cancer cell lines were subjected to multiple fractions of x-Ray. (A) Cells were irradiated with 10 fractions of 2 Gy over a time period of 2 weeks. (B) Cells were irradiated with increasing doses for several months. Afterward, surviving cells were expanded for one month before further experiments were conducted.

3.3 Characterization of radioresistant pancreatic cancer cell lines *in vitro* and *in vivo*

3.3.1 Comparison of two methods for generating radioresistant cell lines

CFA were performed with the radioresistant subclones in order to validate the radioresistance. The corresponding parental cell lines were used as a control. First, cells that received a cumulative dose of 20 Gy (see Figure 3.2A) were investigated regarding their radiosensitivity. Figure 3.3 shows that Panc-1 RR (20 Gy) cells exhibited higher radioresistance for the doses 6 and 8 Gy, whereas a significant difference was only seen at 8 Gy for MIA PaCa-2 RR (20 Gy). Furthermore, the calculated D_{10} and D_{50} values, the dose to reduce survival fraction to 10 % and 50 %, respectively, as well as a two-way ANOVA for both cell lines in comparison to the parental cells, revealed no significant differences (Table 3.2).

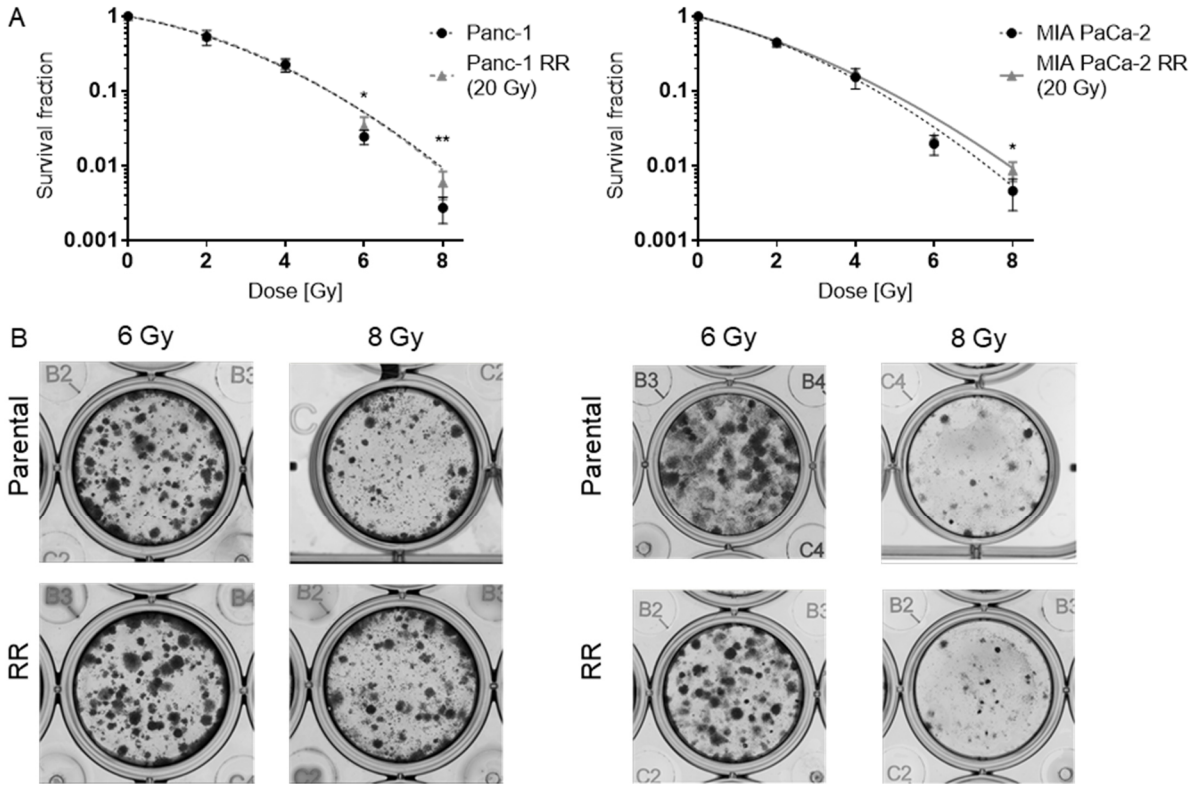

Figure 3.3. Colony formation assay of established pancreatic cancer cell lines Panc-1 and MIA PaCa-2 and cells treated with 20 Gy. (A) Cells indicated as RR were prior irradiated with 20 Gy (see Figure 3.2A). Shown are the survival curves fitted to the linear-quadratic model. Error bars represent SD ($n > 3$). Two-tailed t-test was applied to calculate significances.*: $p \leq 0.05$; **: $p \leq 0.01$. (B) Exemplary images of CFA for doses 6 and 8 Gy.

Table 3.2. Calculated linear-quadratic parameters of the dose-response cell survival curve for parental and cells exposed to 20 Gy.

Cell line	D10 [Gy] [a]	D50 [Gy] [b]	α[Gy-1] [c]	β[Gy-2] [c]
Panc-1	4.94 ± 0.31	2.19 ± 0.45	0.21 ± 0.16	0.05 ± 0.03
Panc-1 RR (20 Gy)	5.09 ± 0.30	2.25 ± 0.03	0.20 ± 0.07	0.05 ± 0.01
MIA PaCa-2	4.50 ± 0.44	1.80 ± 0.27	0.31 ± 0.09	0.05 ± 0.01
MIA PaCa-2 RR (20 Gy)	4.80 ± 0.15	1.82 ± 0.11	0.32 ± 0.04	0.03 ± 0.01

Mean values ± SD are shown.
[a] D10, dose [Gy] to reduce survival fraction to 10%.
[b] D50, dose [Gy] to reduce survival fraction to 50%.
[c] α and β values were derived from the linear-quadratic equation $SF = \exp[-\alpha \times D - \beta \times D2]$.

Second, CFAs with the cells receiving a cumulative dose of 80 Gy (Figure 3.2B) were performed. Both MIA PaCa-2 RR (80 Gy) and Panc-1 RR (80 Gy) cell lines showed a significant increase in their radioresistance as compared to the parental cell lines

(two-way ANOVA p<0.001; Figure 3.4). This acquired radioresistance is also reflected in the increased D_{10} and D_{50} value in the two RR cell lines (Table 3.3).

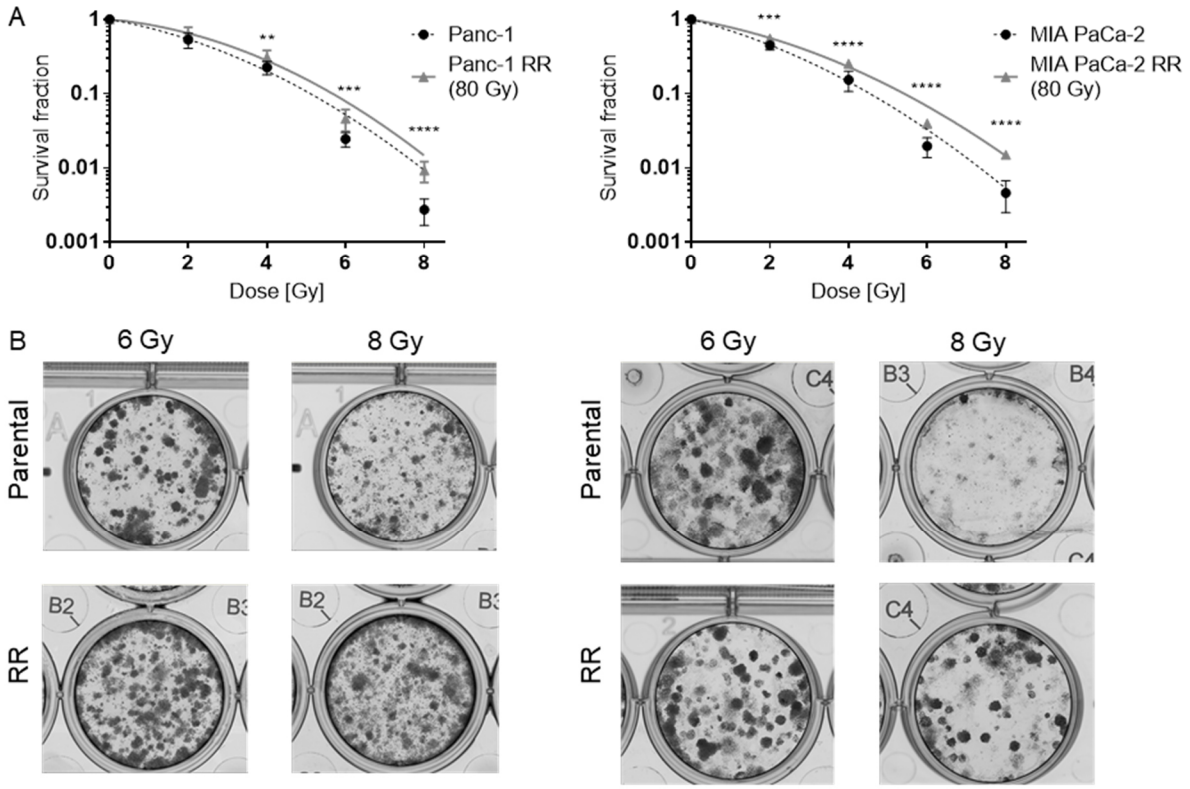

Figure 3.4. CFA of parental and radioresistant (RR) pancreatic cancer cell lines Panc-1 and MIA PaCa-2. (A) Cells indicated with RR were treated with 80 Gy beforehand (see Figure 3.2B). Shown are the survival curves fitted to the linear-quadratic model. Error bars represent SD (n > 3). Two-tailed t-test was applied to calculate significances.**: p≤0.01; ***: p ≤ 0.001; ****: p ≤ 0.000. Figure reprinted from [107]. (B) Exemplary images of CFA for doses 6 and 8 Gy.

Table 3.3. Calculated linear-quadratic parameters of the dose-response cell survival curve for parental and radioresistant (RR) pancreatic cancer cell lines Panc-1 and MIA PaCa-2. Table reprinted from [107].

Cell line	D_{10} [Gy] [a]	D_{50} [Gy] [b]	α[Gy^{-1}] [c]	β[Gy^{-2}] [c]
Panc-1	4.94 ± 0.31	2.19 ± 0.45	0.21 ± 0.16	0.05 ± 0.03
Panc-1 RR (80 Gy)	5.63 ± 0.45***	2.67 ± 0.46*	0.11 ± 0.17	0.05 ± 0.04
MIA PaCa-2	4.50 ± 0.44	1.80 ± 0.27	0.31 ± 0.09	0.05 ± 0.01
MIA PaCa-2 RR (80 Gy)	5.40 ± 0.16****	2.30 ± 0.26****	0.21 ± 0.08	0.04 ± 0.02

Mean values ± SD are shown. Significant differences between parental and RR cells are indicated *: p ≤ 0.05; **: p ≤ 0.01; ***: p ≤ 0.001; ****: p ≤ 0.0001.
[a] D10, dose [Gy] to reduce survival fraction to 10%.
[b] D50, dose [Gy] to reduce survival fraction to 50%.
[c] α and β values were derived from the linear-quadratic equation SF = exp [−α × D −β × D2].

Compared to the respective parental cell line, the cells receiving a cumulative dose of 80 Gy showed a higher radioresistance than the cells receiving a cumulative dose of 20 Gy. Therefore, further experiments were only conducted with MIA PaCa-2 RR (80 Gy) and Panc-1 RR (80 Gy). All the following cell lines termed with RR are derived from the cell population exposed to a cumulative dose of 80 Gy.

3.3.2 Doubling time

The doubling times of the two established RR cell lines and the respective parental cell lines was determined. Therefore, cells were counted every 24 hours for four consecutive days. The doubling time of the MIA PaCa-2 RR and Panc-1 RR cells was not significantly different from the parental cell lines (Table 3.4).

Table 3.4. Doubling times of parental and radioresistant (RR) pancreatic cancer cell lines Panc-1 and MIA PaCa-2. Table reprinted from [107].

Cell line	DT [h]
Panc-1	25.97 ± 2.06
Panc-1 RR	31.13 ± 4.93
MIA PaCa-2	23.67 ± 0.26
MIA PaCa-2 RR	24.21 ± 0.96

Cells were counted at 24, 48, 72, and 96 h after seeding. Doubling Time (DT) values are the mean ± SD of three independent experiments each performed in triplicate.

3.3.3 Tumor growth delay

The generated RR cell line MIA PaCa-2 RR was further investigated *in vivo*. Therefore, MIA PaCa-2 RR, as well as the parental cell line MIA PaCa-2, were subcutaneously injected into the right flank of immunodeficient nude mice. For the tumor growth delay experiments, mice were stratified into one of three groups, a control group (0 Gy) and two irradiation groups receiving single fractions of either 5 or 10 Gy. The tumor size was measured with a digital caliper or an ultrasound system. Figure 3.5 shows exemplary images of the tumors measured by the ultrasound device on the day of irradiation (0 Gy) and when the terminal endpoint was reached.

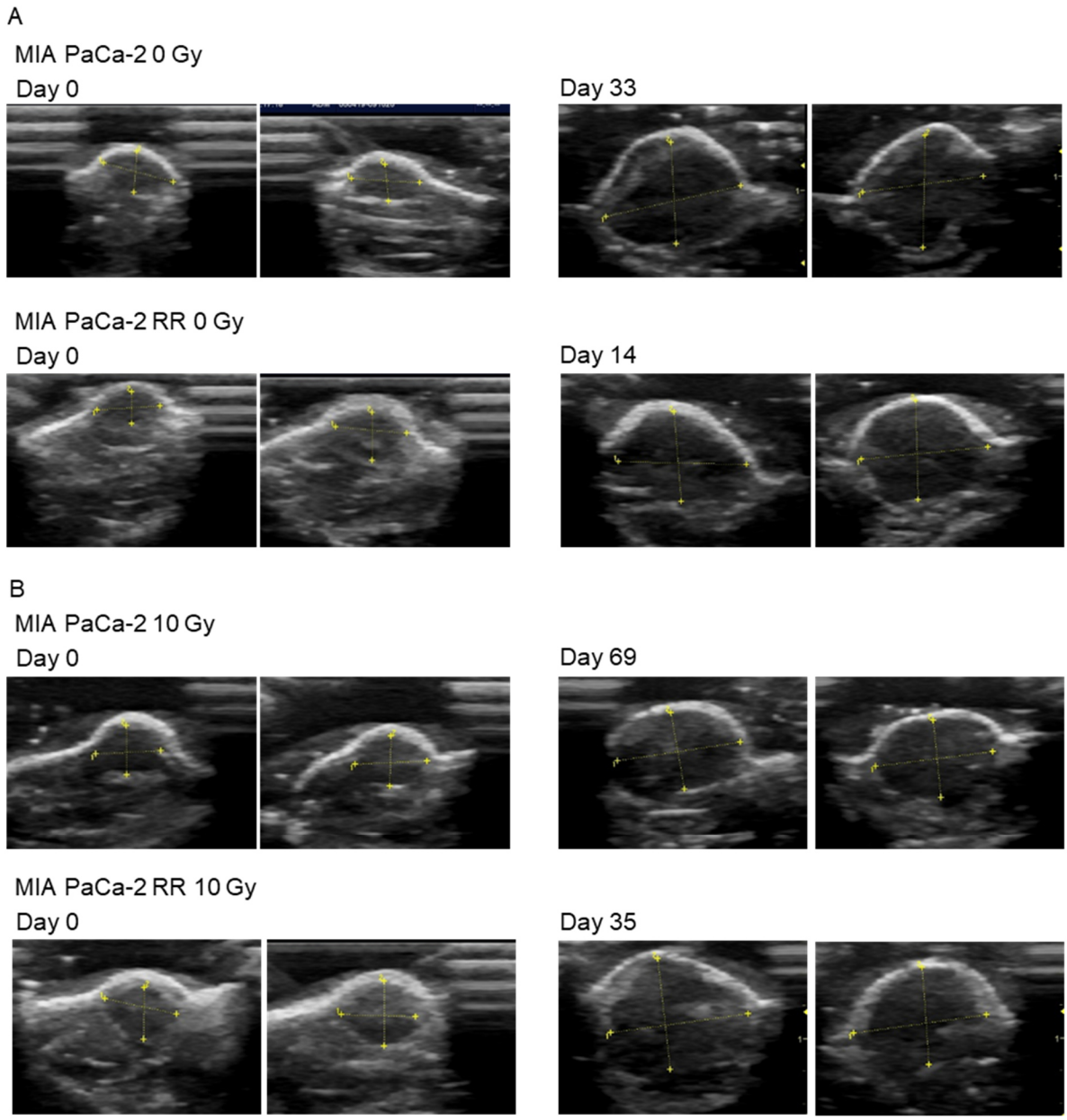

Figure 3.5. Exemplary images of the tumors. Shown are the control (A) and irradiated (B) tumors on the day of irradiation (Day 0) and when the terminal endpoint was reached.

Two conclusions were drawn from these experiments. First, MIA PaCa-2 RR cells exhibited a significantly faster growth *in vivo* than the parental cells (Figure 3.6 and Table 3.5). Non-irradiated MIA PaCa-2 RR tumors showed a significant decrease in the time to reach 4-fold volume compared to non-irradiated MIA PaCa-2 tumors. Measurements with the digital caliper and ultrasound system rendered similar results for the analysis of the tumors to reach a 4-fold volume.

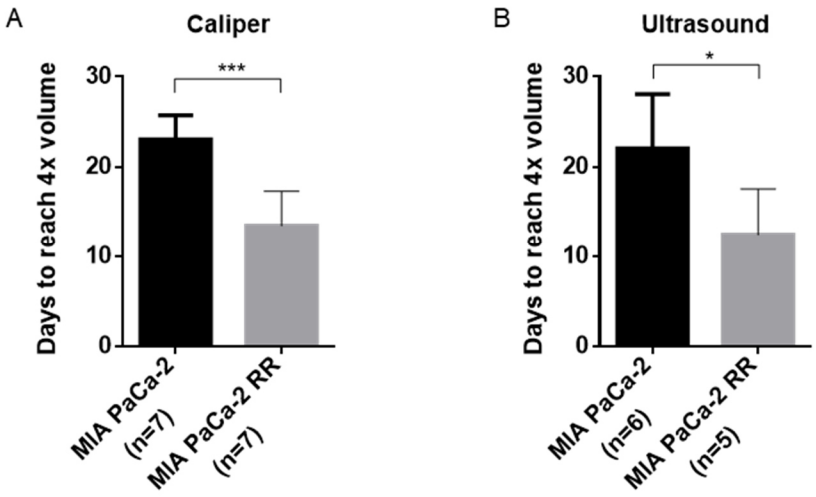

Figure 3.6. Tumor growth of parental and radioresistant (RR) pancreatic cancer cell lines MIA PaCa-2 *in vivo*. Tumor size was measured with either (A) a digital caliper or (B) an ultrasound system. Shown are the days for the tumors to reach the 4-fold volume. Error bars represent SD. *: $p \leq 0.05$; ***: $p \leq 0.001$. Figure (A) adapted from [107].

Table 3.5. Growth of unirradiated tumors. Tumor size was either measured with a digital caliper or an ultrasound system. Shown are the days for the tumors to reach the 4-fold volume.

	MIA PaCa-2	MIA PaCa-2 RR
Caliper	23.03 ± 2.67	13.49 ± 3.83
Ultrasound	22.06 ± 6.00	12.44 ± 5.10

Second, after irradiation and a monitoring time of several weeks, MIA PaCa-2 RR cells demonstrated a shorter growth delay compared to the tumors derived from the parental cell line (Figure 3.7). After 5 Gy irradiation, parental MIA PaCa-2 cells exhibited a longer growth delay than RR cells, suggesting that irradiation had a greater effect on these cells. For 5 Gy, measurements with the caliper suggested a faster growth than measurement with the ultrasound device.

Whereas the tumors of the RR cells demonstrated a growth delay of approximately 28 days after irradiation with 10 Gy, the observed delay for the parental cells was near twice as long (Table 3.6). However, the difference in tumor growth delay between parental and RR derived tumors was only significant for the measurements with the digital caliper.

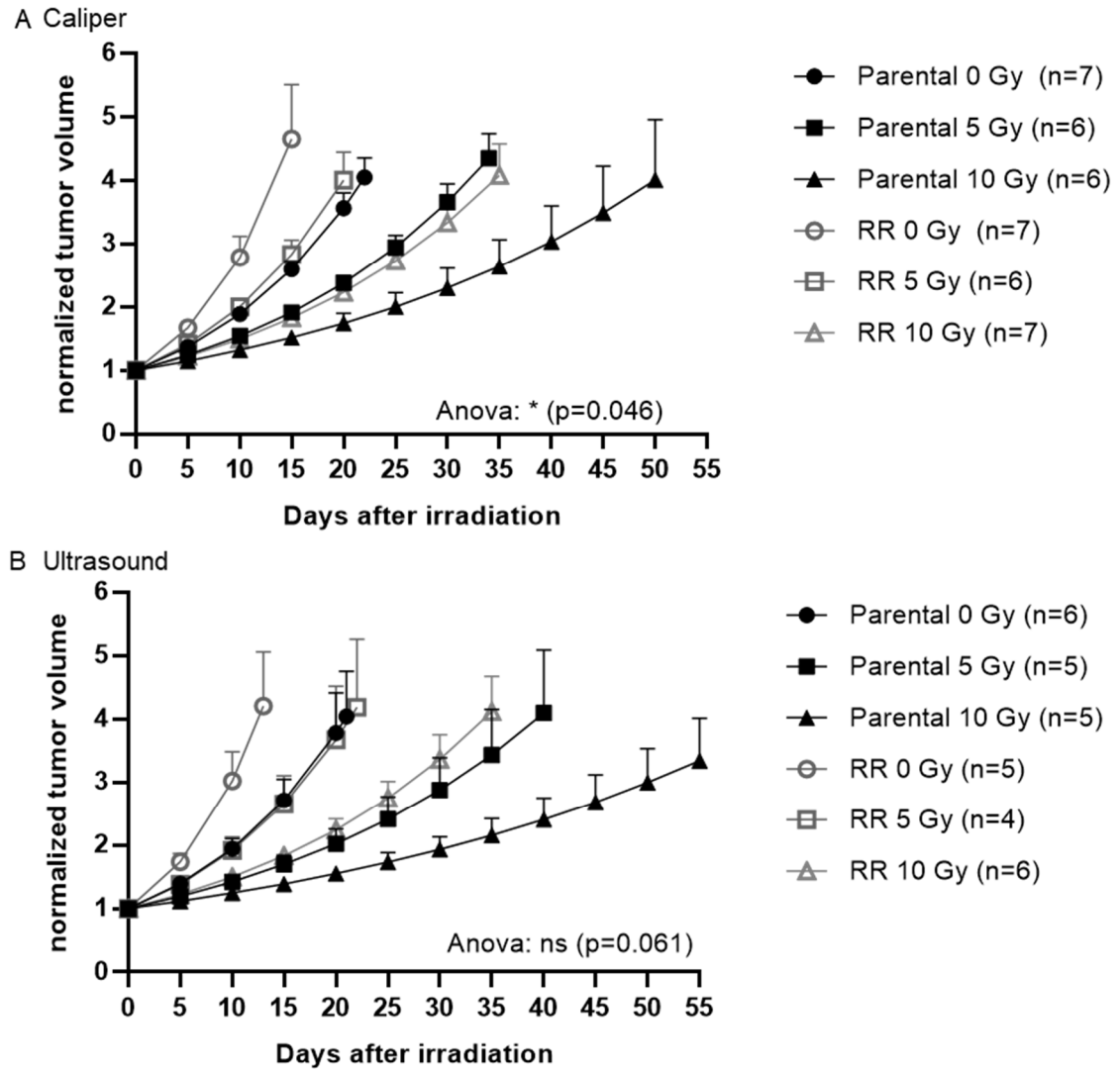

Figure 3.7. Relative tumor growth of parental and radioresistant (RR) MIA PaCa-2 cell lines *in vivo* after irradiation. Tumor volume was normalized to the volume on the day of irradiation. The normalized tumor volumes were plotted against the number of days. Tumor size was measured with either (A) a digital caliper or (B) an ultrasound system. Ns = not significant. Figure (A) adapted from [107].

Table 3.6. Tumor growth delay characteristics.

	Caliper		Ultrasound	
	Parental [days]	RR [days]	Parental [days]	RR [days]
0 Gy to 5 Gy	9.53 ± 2.89	6.73 ± 2.94	25.67 ±9.98	15.90 ± 10.77
0 Gy to 10 Gy	55.82 ± 16.24	27.40 ± 5.11	69.33 ± 20.55	29.07 ± 6.92

These findings are in accordance with the results from the colony formation assay, suggesting that the generated RR cells not only exhibit higher radioresistance *in vitro* but additionally *in vivo.*

3.4 Investigation of mechanisms involved in radioresistance

3.4.1 Cell cycle distribution

Cell cycle distribution was analyzed in Panc-1 RR and MIA PaCa-2 RR and the respective parental cell lines 24 hours after irradiation (Figure 3.8). Both Panc-1 RR and MIA PaCa-2 RR exhibited a significantly higher cell population in the G2/M phase when compared to the respective parental cell line. All four cell lines showed a G2/M arrest after irradiation with 8 Gy. Whereas in Panc-1 RR significantly fewer cells were in the G2/M phase compared to Panc-1, no difference in the G2/M phase for MIA PaCa-2 and MIA PaCa-2 RR after 8 Gy irradiation was observed.

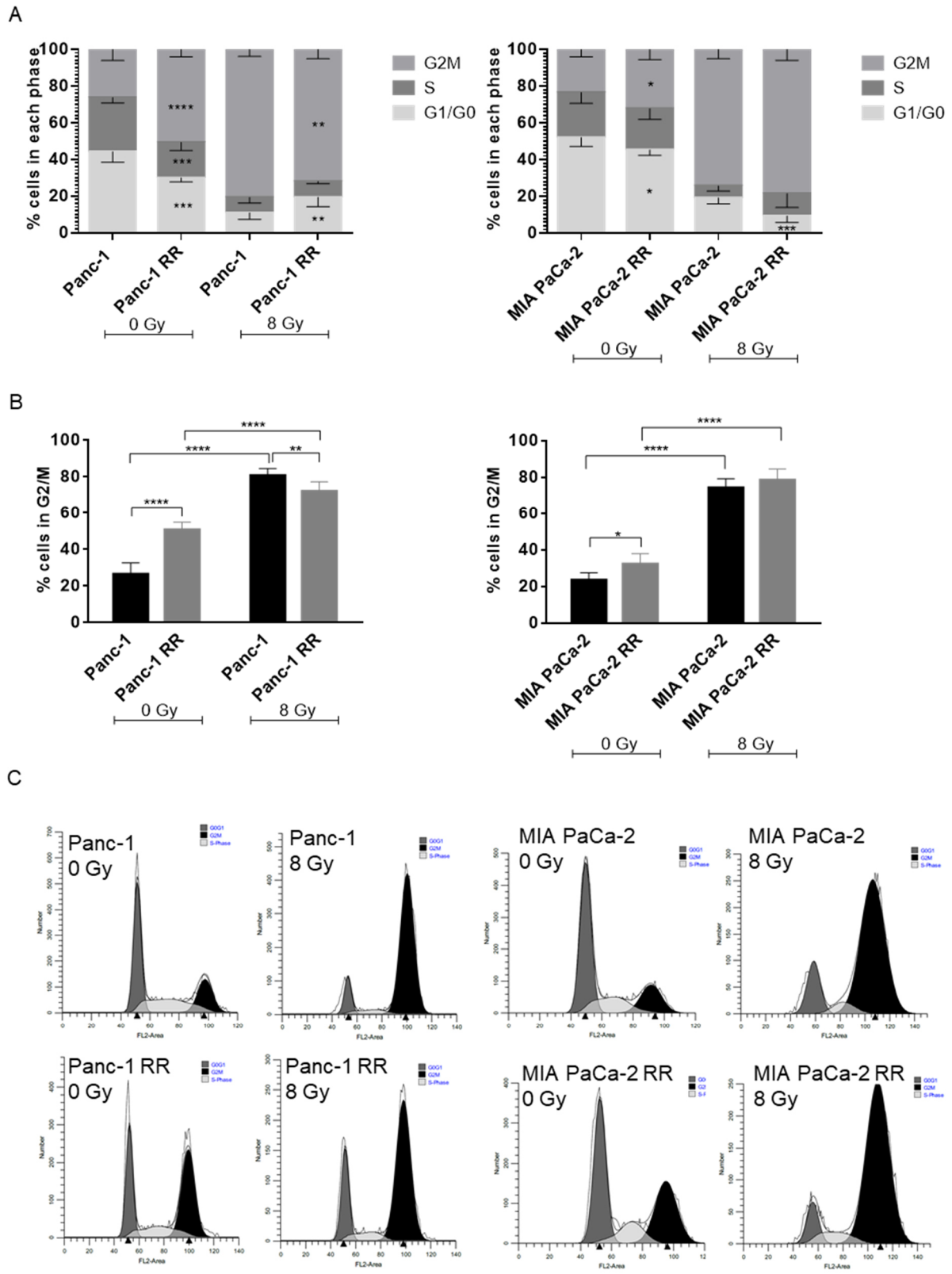

Figure 3.8. Cell cycle distribution of parental and radioresistant (RR) pancreatic cancer cell lines Panc-1 and MIA PaCa-2. (A) Shown are the cell cycle distribution with (8 Gy) and without (0 Gy) irradiation. (B) Quantification of cells in the G2/M phase is shown. Data are expressed as mean ± SD ($n > 3$). *: $p \leq 0.05$; **: $p \leq 0.01$; ***: $p \leq 0.001$; ****: $p \leq 0.0001$. (C) Representative flow cytometry histograms for Panc-1, Panc-1 RR, MIA PaCa-2, and MIA PaCa-2 RR with 0 and 8 Gy irradiation are shown. Figure reprinted from [107].

3.4.2 Radiation-induced apoptosis

In order to investigate apoptosis induction in RR and parental cells after irradiation, the activation of caspase 3/7 was measured using flow cytometry. Figure 3.9 shows the percentage of apoptotic cells 48 hours post-irradiation. MIA PaCa-2 and MIA PaCa-2 RR demonstrated a significant increase in apoptotic cells after irradiation with 8 Gy. However, MIA PaCa-2 RR showed comparable induction of apoptosis after irradiation with 8 Gy when compared to the parental cell line. For Panc-1 RR, no difference was observed in comparison to Panc-1, neither without irradiation nor after 8 Gy.

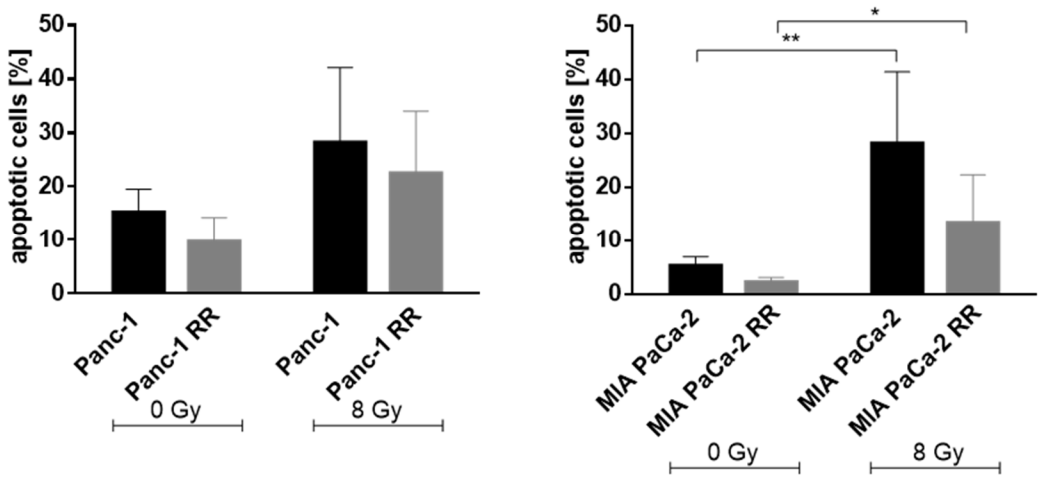

Figure 3.9. Apoptotic cells in parental and radioresistant (RR) pancreatic cancer cell lines Panc-1 and MIA PaCa-2 after irradiation. Shown are Caspase 3/7 positive (=apoptotic cells) 48 hours after irradiation with 0 and 8 Gy. Data are expressed as mean ± SD ($n > 3$). *: $p \leq 0.05$; **: $p \leq 0.01$. Figure reprinted from [107].

3.4.3 DNA damage repair

To analyze the induction of DNA double strand breaks (DSBs) in the RR cell lines and the respective parental cells, γH2AX FACS were performed to measure the mean fluorescence intensity (MFI) of the γH2AX signal 30 min after irradiation with 8 Gy X-rays. Figure 3.10 reveals that Panc-1 RR cells had an initial (without irradiation) lower γH2AX signal than the parental cell line. For MIA PaCa-2 and MIA PaCa-2 RR

cells, no difference was observed. The γH2AX signal increased significantly in all four cell lines after irradiation; however, the increase was lower in both RR cell lines and significant for Panc-1 RR cells.

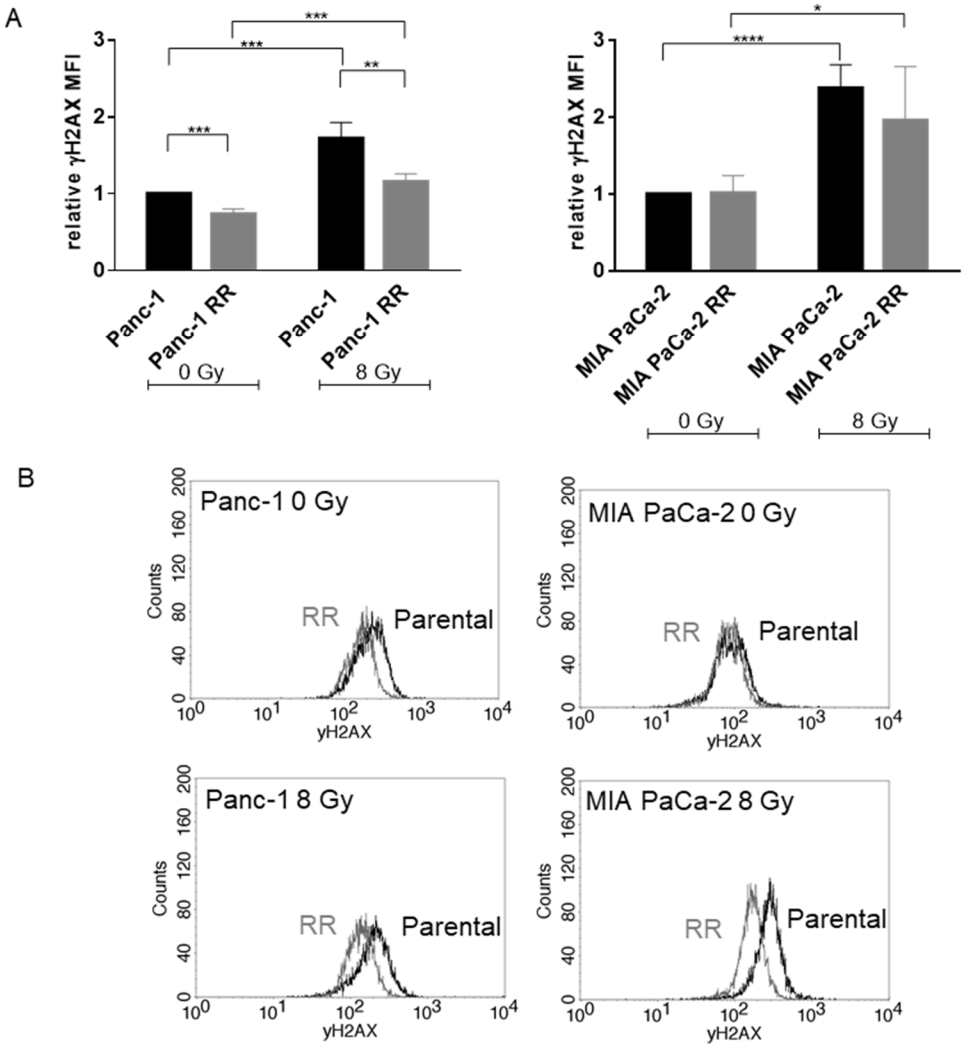

Figure 3.10. γH2AX FACS of parental and radioresistant (RR) pancreatic cancer cell lines Panc-1 and MIA PaCa-2 after irradiation with 0 and 8 Gy. (A) Shown are relative MFI of X-ray irradiation-induced γH2AX. Values were normalized to 0 Gy of the respective parental cell line, which was set as one. Error bars represent SD (n > 3). *: p ≤ 0.05; **: p ≤ 0.01; ***: p ≤ 0.001; ****: p ≤ 0.0001. (B) Representative flow cytometry histograms for Panc-1, Panc-1 RR, MIA PaCa-2, and MIA PaCa-2 RR after 0 and 8 Gy irradiation are shown. Figure reprinted from [107].

To compare the repair efficiency by analyzing residual DSBs 24 hours after irradiation, γH2AX foci were counted (Figure 3.11). The background damage of sham irradiated (= 0 Gy) cells was comparable for all cell lines. After 8 Gy irradiation, the number of foci was significantly increased in all four cell lines. Nonetheless, both RR cell lines

demonstrated a significantly lower number of unrepaired foci than the respective parental cell lines.

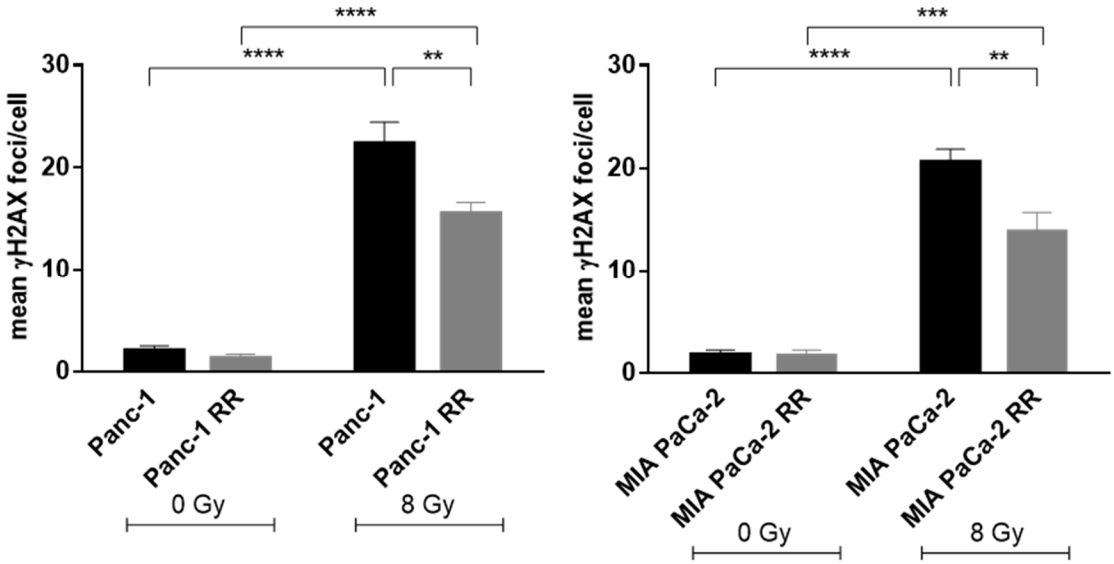

Figure 3.11. γH2AX Foci of parental and radioresistant (RR) pancreatic cancer cell lines Panc-1 and MIA PaC-2. Shown are the residual γH2AX foci, 24 hours after irradiation. Error bars represent SD (n = 3). **: $p \leq 0.01$; ***: $p \leq 0.001$; ****: $p \leq 0.0001$. Figure reprinted from [107].

In summary, the RR cell lines showed lower radiation-induced DNA damage and greater efficiency to repair DNA DSBs.

3.4.4 Oxidative stress

Reactive oxygen species (ROS) are one of the mediators contributing to DNA damage and DNA damage response. Therefore, intracellular ROS levels were measured with CM-H_2DCFDA and flow cytometry. Sham-irradiated Panc-1 RR and MIA PaCa-2 RR cells demonstrated significantly lower basal ROS levels than the respective parental cell lines (Figure 3.12). Irradiation-induced increase in ROS levels was observed in all cell lines; however, the levels in Panc-1 RR and MIA PaCa-2 RR were significantly lower when compared to the respective parental cell lines.

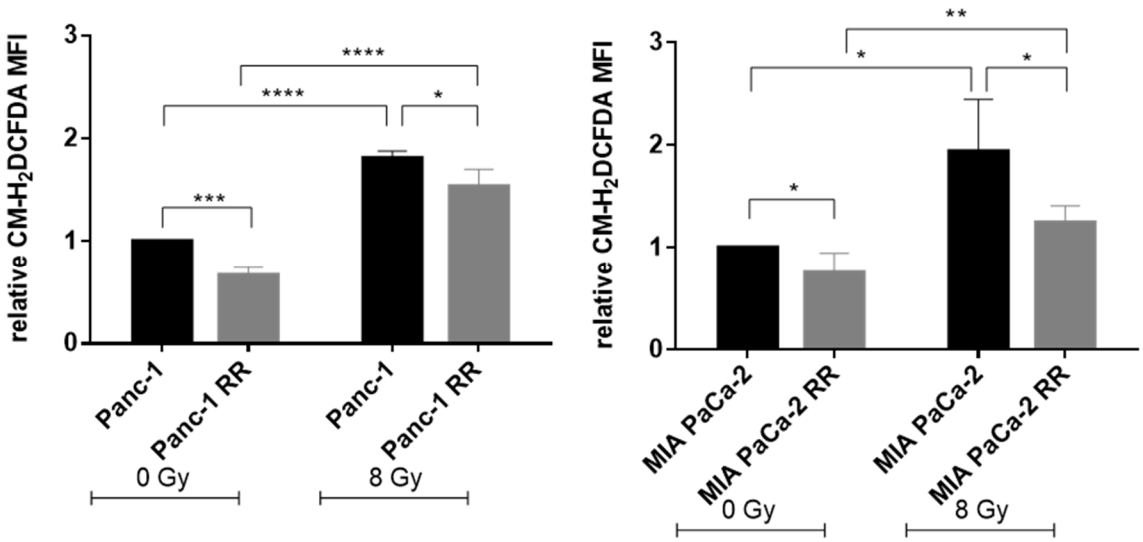

Figure 3.12. Reactive oxygen species levels in parental and radioresistant (RR) pancreatic cancer cell lines Panc-1 and MIA PaCa-2. Intracellular reactive oxygen species were measured by CM-H2DCFDA and flow cytometry immediately after irradiation with 8 Gy. MFI values for each cell line were normalized to the MFI obtained for the respective unirradiated parental cell line. Error bars represent SD ($n > 3$). *: $p \leq 0.05$; **: $p \leq 0.01$; ***: $p \leq 0.001$; ****: $p \leq 0.0001$. Figure reprinted from [107].

These results suggest that lower ROS levels are involved in the radioresistance of Panc-1 RR and MIA PaCa-2 RR cells.

To identify genes involved in the oxidative stress pathway in RR cell lines, an mRNA profiler was applied. This array screens for the expression of 84 genes critical for the oxidative stress pathway. Fold changes were calculated by normalizing C_t values to all endogenous controls (*ACTB, B2M, GAPDH, HPRT1,* and *RPLP0*) provided. Fold changes > 2 or < 0.5 were considered to be deregulated. Gene expression levels of RR cells were normalized to the respective parental cell line (Appendix 1). 22 and 7 genes were found to be upregulated in Panc-1 RR and MIA-PaCa-2 RR, respectively (Figure 3.13 and Table 3.7). Merely 5 and 4 genes were downregulated in Panc-1 RR and MIA PaCa-2 RR when compared to the parental cells, respectively. Only *chemokine (C-C motif) ligand 5* (*CCL5)* and *myoglobin (MB)* were upregulated in both Panc-1 RR and MIA PaCa-2 RR, whereas *superoxide dismutase 3* (*SOD3)* was downregulated in the two RR cell lines.

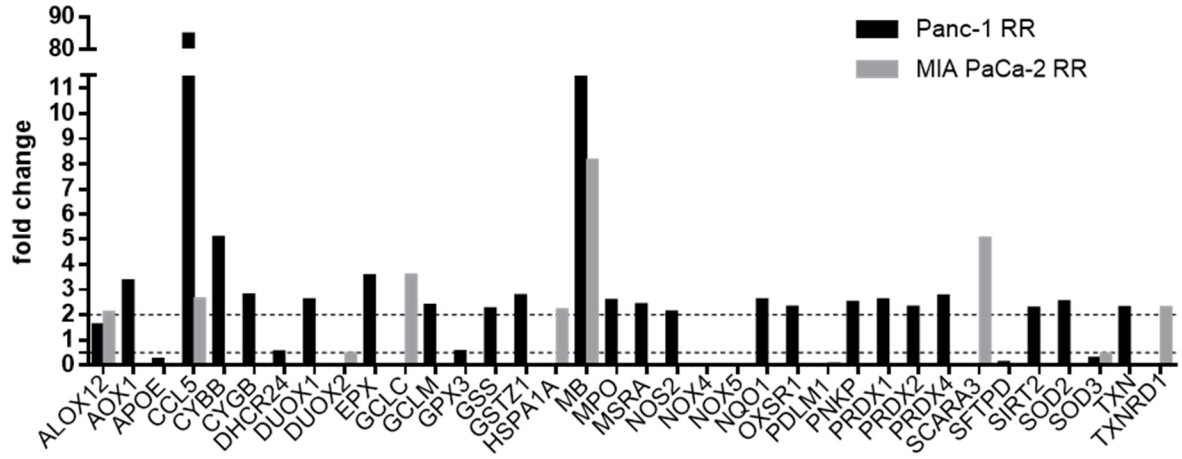

Figure 3.13. Profiler on genes relevant for oxidative stress. Shown are the expression fold changes for radioresistant (RR) Panc-1 RR and MIA Paca-2 RR cells relative to the respective parental cell line. Fold changes were filtered for either > 2 (upregulation) or < 0.5 (downregulation).

Table 3.7. List of expression fold changes of the oxidative stress profiler. Shown are the expression fold changes for radioresistant (RR) cell lines Panc-1 RR and MIA Paca-2 RR relative to the respective parental cell line. Fold changes in parenthesis do not fit the filtering criteria (> 2 or < 0.5) but were included, as the filtering criteria were achieved in the other cell line. nd = not detected (Cp > 35).

Gene	Panc-1 RR	MIA Paca-2 RR
ALOX12	(1.56)	2.06
AOX1	3.29	nd
APOE	0.20	(0.55)
CCL5	84.45	2.58
CYBB	5.03	nd
CYGB	2.75	nd
DHCR24	0.49	(1.78)
DUOX1	2.55	(0.53)
DUOX2	nd	0.42
EPX	3.51	(1.42)
GCLC	(1.97)	3.53
GCLM	2.33	(1.43)
GPX3	0.50	(1.14)
GSS	2.19	(0.54)
GSTZ1	2.71	(1.10)
HSPA1A	(1.68)	2.16
MB	11.96	8.11
MPO	2.53	(0.96)
MSRA	2.36	(0.98)
NOS2	2.07	(1.73)
NQO1	2.55	(1.11)
OXSR1	2.27	(1.15)
PDLM1	(1.20)	0.04
PNKP	2.45	(0.84)
PRDX1	2.55	(1.20)
PRDX2	2.27	(0.76)
PRDX4	2.69	(1.24)
SCARA3	(1.56)	4.99
SFTPD	0.08	nd
SIRT2	2.22	(0.55)
SOD2	2.48	(0.98)
SOD3	0.24	0.41
TXN/TRX	2.23	(0.81)
TXNRD1	(1.24)	2.23

In order to analyze the level of expression of proteins involved in the oxidative stress pathway, western blot analysis of the whole-cell lysates of Panc-1 RR and MIA PaCa-2 RR along with the parental counterparts was performed. The significantly enhanced protein expression of superoxide dismutase 2 (SOD2) in Panc-1 RR confirmed the increased expression relative to the parental cells seen on the gene expression level (2.48-fold change, Table 3.7 and Figure 3.14). Furthermore, Panc-1 RR cells also exhibited a significant increase of nuclear factor erythroid 2-related factor 2 (NRF2), phosphorylated NRF2 (p-NRF2), and thioredoxin (TRX) protein levels. The upregulation of TRX protein in Panc-1 RR cells is consistent with the observed increased mRNA level (2.23-fold change, Table 3.7). In contrast, no significant changes were seen in MIA PaCa-2 RR cells for SOD2 and TRX protein expression levels, reflecting the results on the gene expression level. NRF2 and p-NRF2 protein expression were unchanged in MIA PaCa-2 RR. The protein expression level of superoxide dismutase 1 (SOD1) protein remained unchanged in both RR cell lines as compared to the parental cells.

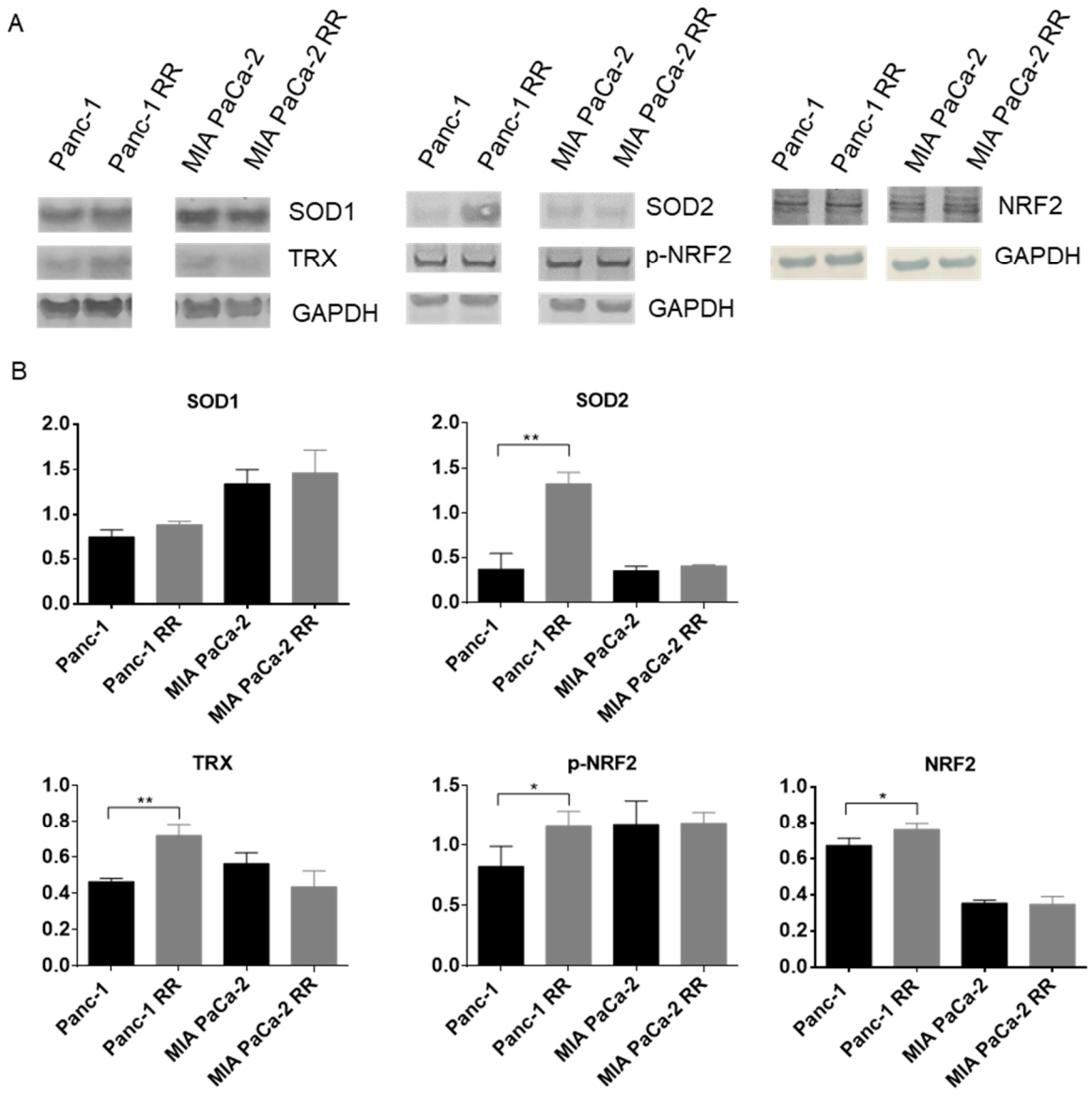

Figure 3.14. Analysis of the expression of selected proteins involved in the oxidative stress pathway in parental and radioresistant (RR) pancreatic cancer cell lines Panc-1 and MIA PaCa-2. (A) Exemplary western blot images. (B) Quantification of western blot analysis. The graph represents the quantification of proteins relative to GAPDH. Error bars represent SD (n = 3). *: $p < 0.05$; **: $p < 0.01$.

3.5 mRNA profile of radioresistant pancreatic cancer cell lines

The changes on the mRNA expression level in the generated RR and respective parental cell lines were investigated by mRNA sequencing. Several mRNAs were significantly altered through the acquired radioresistance, and 121 genes were shared between both RR cell lines when compared to the parental cell line (Figure 3.15A and Table 3.8), with 76 genes showing deregulation in the same direction. A total of 528 and 574 mRNAs were up- and downregulated in Panc-1 RR, respectively. MIA PaCa-2 RR cells exhibited 408 upregulated and 201 downregulated genes. Principal component analysis of mRNA expression clearly distinguished RR cells from parental cell lines (Figure 3.15B). Furthermore, limiting the input for the principal component analysis to the 500 mRNAs with the highest variance improved the separation (Figure 3.15C).

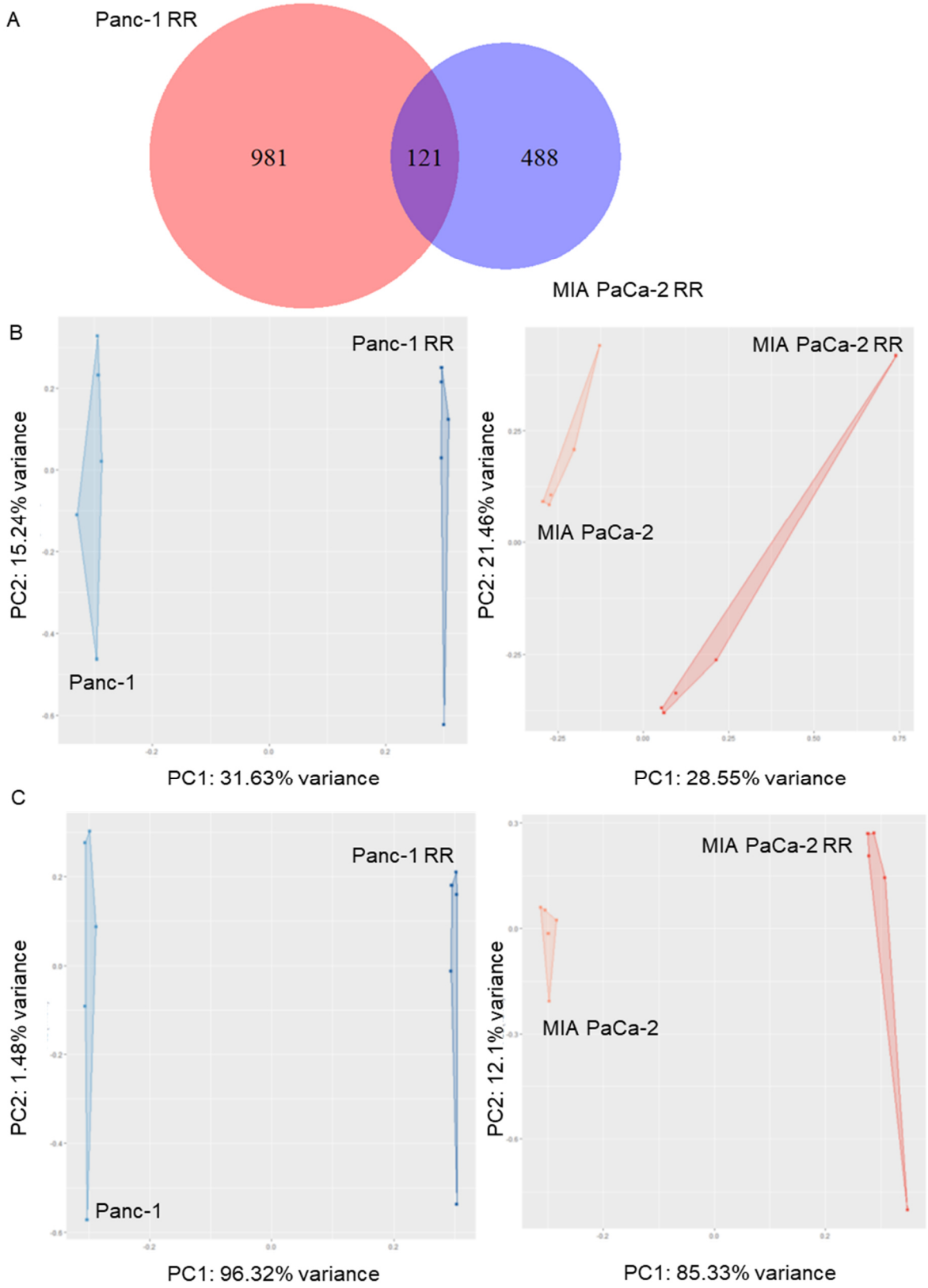

Figure 3.15. mRNA profile of parental and radioresistant (RR) pancreatic cancer cell lines Panc-1 and MIA PaCa-2. (A) Venn diagram of deregulated mRNAs in Panc-1 RR and MIA PaCa-2 RR cells relative to the respective parental cell lines and the overlap of deregulated genes. (B) Principal component analysis of mRNA expression in Panc-1 and MIA PaCa-2 as well as the RR cells. (C) Principal component analysis of the top 500 highest variance mRNA expression in Panc-1 and MIA PaCa-2 as well as the RR cells. Analysis of top 500 highest variance mRNAs in the dataset separated RR from parental cells (PC1) and PC2 showed intra-cell line variability.

Table 3.8. Commonly deregulated mRNAs in radioresistant (RR) cell lines Panc-1 RR and MIA PaCa-2 RR. Positive log2 fold changes indicate mRNAs upregulated in RR cells compared to parental cells, whereas negative log2 fold changes indicate mRNAs downregulated in RR cells.

Gene	ID	Panc-1 RR log2FC	MIA PaCa-2 RR log2FC
AATK	ENSG00000181409	-1.50	1.07
ABCC3	ENSG00000108846	1.01	3.76
AC012513.3	ENSG00000279348	-1.05	-1.25
ADGRG1	ENSG00000205336	2.62	1.98
ADORA1	ENSG00000163485	2.21	1.15
AHR	ENSG00000106546	2.06	9.80
AIF1L	ENSG00000126878	-1.32	-1.44
AK4	ENSG00000162433	-2.22	1.03
AMPD3	ENSG00000133805	1.00	1.63
ANK2	ENSG00000145362	-3.04	1.05
ANKRD18B	ENSG00000230453	-2.38	3.36
ANO1	ENSG00000131620	2.62	-1.44
ANXA1	ENSG00000135046	1.20	-1.84
APOL6	ENSG00000221963	2.96	2.11
ARFGEF3	ENSG00000112379	-2.13	4.04
ARHGAP31	ENSG00000031081	1.55	3.37
B3GNT5	ENSG00000176597	1.21	3.48
B4GALNT3	ENSG00000139044	-1.43	1.06
BCAT1	ENSG00000060982	-3.72	3.44
BCL2L1	ENSG00000171552	1.09	-1.36
BCL3	ENSG00000069399	1.74	1.15
BICDL1	ENSG00000135127	-1.15	2.27
BMP1	ENSG00000168487	1.26	1.10
C12orf56	ENSG00000185306	-1.08	-1.49
CAMKK1	ENSG00000004660	1.10	1.00
CCDC88C	ENSG00000015133	1.09	-1.01
CDKN1A	ENSG00000124762	1.17	2.16
CDON	ENSG00000064309	-1.45	1.26
CKAP4	ENSG00000136026	1.10	1.29
CLDN1	ENSG00000163347	1.54	1.54
COL13A1	ENSG00000197467	2.54	1.23
CSF1	ENSG00000184371	1.83	1.67
CX3CL1	ENSG00000006210	4.88	9.69
CYP1B1	ENSG00000138061	1.83	1.46

DDX60L	ENSG00000181381	1.56	3.05
DSG2	ENSG00000046604	-2.91	1.43
ERAP2	ENSG00000164308	1.55	1.29
F11R	ENSG00000158769	-1.15	1.04
F2R	ENSG00000181104	-1.29	-2.80
F2RL1	ENSG00000164251	-1.74	-8.73
FAM102A	ENSG00000167106	1.37	1.34
FAM107B	ENSG00000065809	2.59	-1.75
FAM71D	ENSG00000172717	-1.01	2.90
FHL1	ENSG00000022267	1.19	2.09
FOXQ1	ENSG00000164379	-3.54	3.21
FRMPD3	ENSG00000147234	-3.29	5.39
GADD45A	ENSG00000116717	1.34	1.79
GCH1	ENSG00000131979	-1.27	2.67
GEM	ENSG00000164949	1.03	3.22
HECW2	ENSG00000138411	1.81	3.01
HIPK2	ENSG00000064393	1.35	4.46
HLA-B	ENSG00000234745	1.16	2.67
IL15RA	ENSG00000134470	1.24	1.36
IRF1	ENSG00000125347	1.30	1.05
ISG20	ENSG00000172183	1.85	1.85
ITPKB	ENSG00000143772	1.26	3.24
JAG1	ENSG00000101384	1.59	-5.72
JDP2	ENSG00000140044	-1.28	1.28
JMY	ENSG00000152409	-2.57	-1.25
KCNQ2	ENSG00000075043	-2.69	-1.12
KIF1A	ENSG00000130294	-2.30	2.63
KRT15	ENSG00000171346	-2.38	1.12
LFNG	ENSG00000106003	1.01	1.62
LGALS3BP	ENSG00000108679	2.03	2.42
LIF	ENSG00000128342	1.08	1.19
LIMS2	ENSG00000072163	2.66	-1.44
LINC01963	ENSG00000260804	-1.16	-1.07
LIPG	ENSG00000101670	1.34	2.57
LOXL2	ENSG00000134013	1.34	1.95
LPAR3	ENSG00000171517	-1.73	-1.14
MISP	ENSG00000099812	1.53	1.21
MRC2	ENSG00000011028	1.47	2.16

MT1A	ENSG00000205362	-3.17	-1.10
MYL9	ENSG00000101335	1.85	-1.38
NAV2	ENSG00000166833	1.20	1.75
NDRG1	ENSG00000104419	-1.31	1.28
NEBL	ENSG00000078114	-1.38	1.02
NIPAL2	ENSG00000104361	2.17	1.09
NLRC5	ENSG00000140853	1.21	2.23
NPTX1	ENSG00000171246	1.78	1.47
NUPR1	ENSG00000176046	-1.08	4.58
OSBPL10	ENSG00000144645	-1.95	2.64
OSMR	ENSG00000145623	1.00	1.44
PALLD	ENSG00000129116	1.17	4.36
PARP10	ENSG00000178685	1.76	3.13
PEG10	ENSG00000242265	2.23	-4.23
PHGDH	ENSG00000092621	-2.07	1.64
PHLDA3	ENSG00000174307	-1.38	1.26
PIK3R1	ENSG00000145675	-1.01	-2.30
PLXNA3	ENSG00000130827	-1.08	1.05
PPM1H	ENSG00000111110	-1.29	2.21
PPM1K	ENSG00000163644	1.16	3.21
PROS1	ENSG00000184500	-1.08	1.21
PSMB8	ENSG00000204264	1.63	5.21
PTX3	ENSG00000163661	3.41	-1.45
RAB11FIP4	ENSG00000131242	-1.93	1.15
RAB36	ENSG00000100228	1.47	1.42
RAI14	ENSG00000039560	-1.59	2.44
RNF128	ENSG00000133135	-1.85	2.14
S100A3	ENSG00000188015	1.47	2.45
SEL1L3	ENSG00000091490	-5.05	2.15
SH3RF1	ENSG00000154447	1.15	2.15
SHH	ENSG00000164690	1.47	3.48
SOCS2	ENSG00000120833	1.63	2.45
SRGN	ENSG00000122862	1.35	-1.35
SSPN	ENSG00000123096	1.05	1.24
ST6GAL1	ENSG00000073849	1.43	-1.56
STAP2	ENSG00000178078	1.63	1.64
STEAP3	ENSG00000115107	1.35	1.04
STMN3	ENSG00000197457	1.29	-1.12

SYP	ENSG00000102003	-2.15	-1.40
TAP1	ENSG00000168394	1.44	1.70
TAPBPL	ENSG00000139192	1.63	1.20
TET1	ENSG00000138336	-1.20	-1.16
THSD4	ENSG00000187720	1.83	2.52
TIFA	ENSG00000145365	1.08	1.13
TMEM184A	ENSG00000164855	1.40	1.65
TRIM16L	ENSG00000108448	1.29	1.07
TTC39C	ENSG00000168234	1.35	4.38
WT1	ENSG00000184937	2.13	2.20
ZNF516	ENSG00000101493	-2.31	1.31

To identify the mechanisms underlying the acquired radioresistance, the 121 genes commonly deregulated in Panc-1 RR and MIA PaCa-2 RR were further analyzed by the Ingenuity Pathway Analysis (IPA) software. As illustrated in Figure 3.16, IPA predicted increased cell viability in both RR cell lines. A total of 18 genes that are involved in cell viability were found, indicating molecular changes that promote the survival of RR cells.

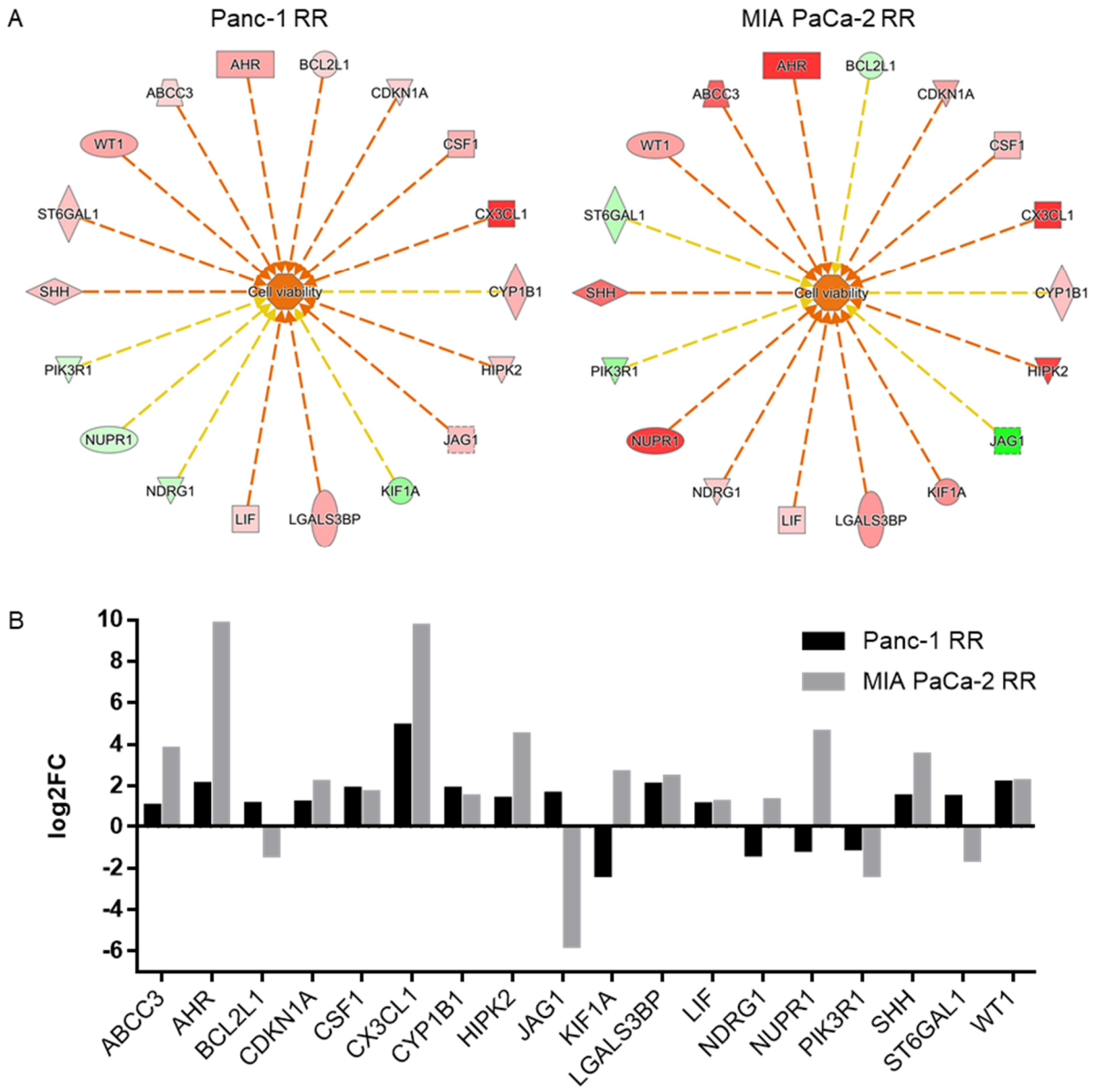

Figure 3.16. Ingenuity Pathway Analysis of commonly deregulated mRNAs in radioresistant (RR) cell lines Panc-1 RR and MIA PaCa-2 RR. (A) IPA prediction of activation of cell viability based on the shared deregulated mRNAs in Panc-1 RR and MIA PaCa-2 RR. The upregulated genes are marked in red and downregulated in green. The orange line indicates the mRNAs expression leading to the activation of the node, respectively. Inconsistent findings are shown with the yellow line. The orange color of the node (cell viability) indicates activation. Figure reprinted from [107]. (B) Shown are the genes involved in the predicted activation of cell viability. Positive log2 fold changes indicate mRNAs upregulated in RR cells compared to parental cells, whereas negative log2 fold changes indicate mRNAs downregulated in RR cells.

As an mRNA profiler of MIA PaCa-2 RR and Panc-1 RR cells in comparison to the respective parental cell lines was also performed (see paragraph 3.4.4), further investigations were conducted to determine whether any genes from the oxidative stress profiler were also deregulated in the mRNA sequencing data. While in Panc-1 RR cells the upregulation of *CCL5, CYGB, MB* and *SOD2* were confirmed in the RNA sequencing data (Table 3.9), the upregulation of *glutamate-cysteine ligase catalytic subunit* (*GCLC), Scavenger Receptor Class A Member 3 (SCARA3)* and *Thioredoxin reductase 1* (*TXNRD)* were additionally observed in MIA PaCa-2 RR cells. (Table 3.10).

Table 3.9. List of genes deregulated in oxidative stress pathway derived from mRNA sequencing. Shown are the expression fold changes (from oxidative stress profiler) and log2 foldchanges (from mRNA sequencing) for radioresistant (RR) cell line Panc-1 RR relative to the parental cell line. Expression fold changes > 2 and < 0.5 indicate upregulation and downregulation in the RR cells, respectively. Positive log2 fold changes indicate mRNAs upregulated in RR cells compared to parental cells, whereas negative log2 fold changes indicate mRNAs downregulated in RR cells.

Gene	Panc-1 RR	
	Expression fold changes	Log2 fold changes
APOE	0.20	-2.07
CCL5	84.45	5.27
CYGB	2.75	1.01
GPX3	0.50	-1.49
MB	11.96	3.46
SOD2	2.48	1.15

Table 3.10. List of genes deregulated in oxidative stress pathway derived from mRNA sequencing. Shown are the expression fold changes (from oxidative stress profiler) and log2 foldchanges (from mRNA sequencing) for radioresistant (RR) cell line MIA PaCa-2 RR relative to the parental cell line. Expression fold changes > 2 and < 0.5 indicate upregulation and downregulation in the RR cells, respectively. Positive log2 fold changes indicate mRNAs upregulated in RR cells compared to parental cells, whereas negative log2 fold changes indicate mRNAs downregulated in RR cells.

Gene	MIA PaCa-2 RR	
	Expression fold changes	Log2 fold changes
GCLC	3.53	1.34
PDLIM1	0.04	-3.41
SCARA3	4.99	1.86
TXNRD	2.23	1.03

3.6 Migration and invasion capacity of radioresistant pancreatic cancer cell lines

Apart from the predicted enhanced cell viability of Panc-1 RR and MIA PaCa-2 RR, IPA additionally showed predictions regarding the migration and invasion capacity of those cell lines. Whereas Panc-1 RR cells were predicted to have an enhanced migration and invasion, MIA PaCa-2 RR cells were projected to show a decrease in both characteristics (Figure 3.17A and B). These estimations are mainly based on the deregulation of the following genes: *Annexin A1* (*ANXA1*), *Bcl-2-like 1* (*BCL2L1*), and *N-Myc Downstream Regulated 1* (*NDRG1*).

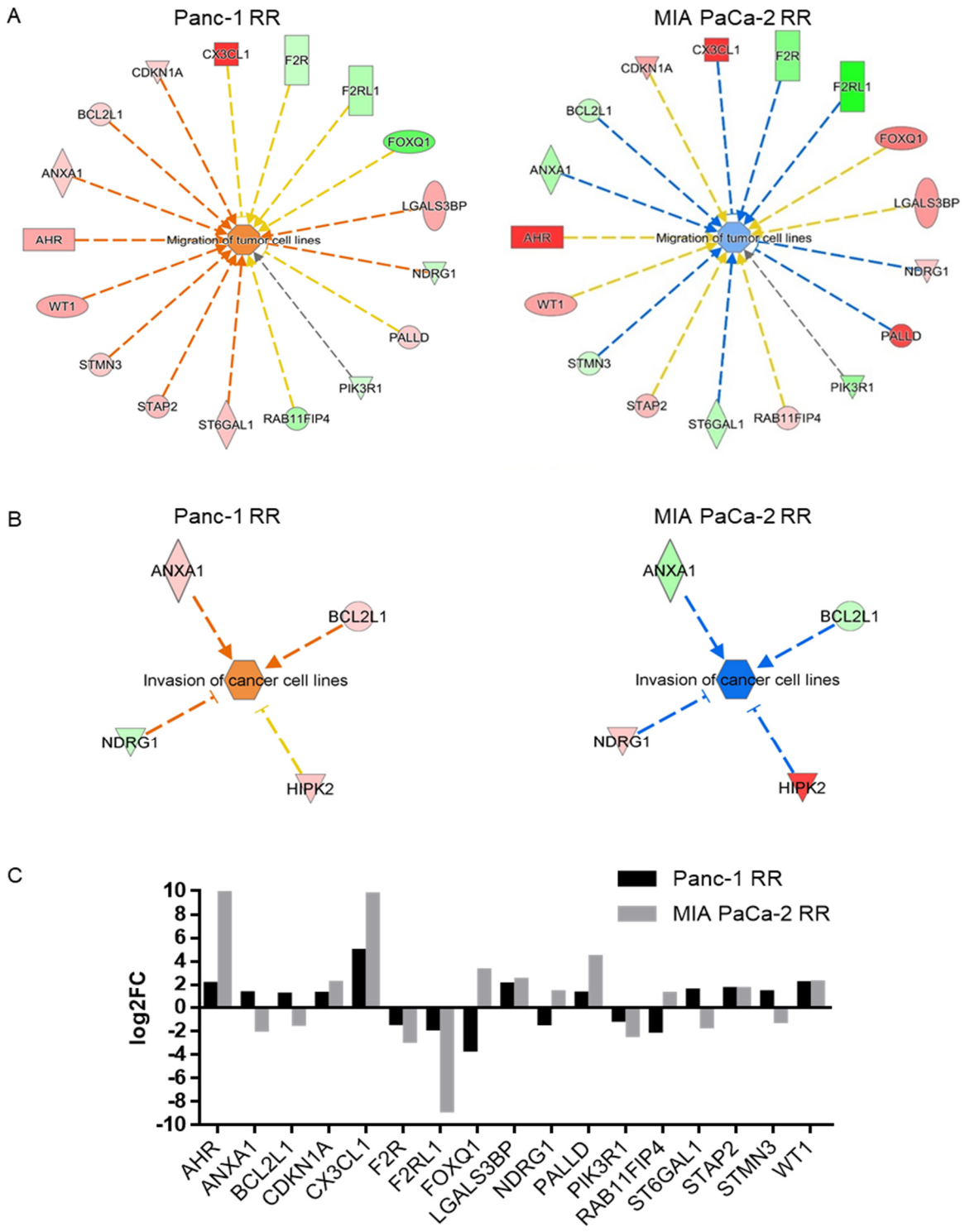

Figure 3.17. Ingenuity Pathway Analysis of commonly deregulated mRNAs in radioresistant (RR) cell lines Panc-1 RR and MIA PaCa-2 RR. (A) IPA prediction of activation and inactivation of migration based on the shared deregulated mRNAs in Panc-1 RR and MIA PaCa-2 RR. (B) IPA prediction of activation and inactivation of invasion based on the shared deregulated mRNAs in Panc-1 RR and MIA PaCa-2 RR. The upregulated genes are marked in red and downregulated in green. The orange and blue lines indicate the mRNAs expression leading to the activation and inactivation of the node, respectively. Inconsistent findings are shown with the yellow line. The orange color of the node indicates activation, whereas the blue node indicates inactivation. Figures (A) and (B) reprinted from [107]. (C) Shown are the genes involved in the predicted activation/inactivation of migration and invasion. Positive log2 fold changes indicate mRNAs upregulated in RR cells compared to parental cells.

In order to validate the prediction from IPA on the migratory and invasive potential, transwell migration and invasion assays with the generated RR cells as well as the parental cell lines were performed. Panc-1 RR cells showed a significantly higher migration as well as an increased invasion rate as compared to the parental cells (Figure 3.18). In contrast, MIA PaCa-2 RR cells demonstrated a decrease in their migratory and invasive potential. These functional data confirm the IPA prediction and indicate that the radiation-induced changes in RR cells differentially affect the invasion and migration capacity.

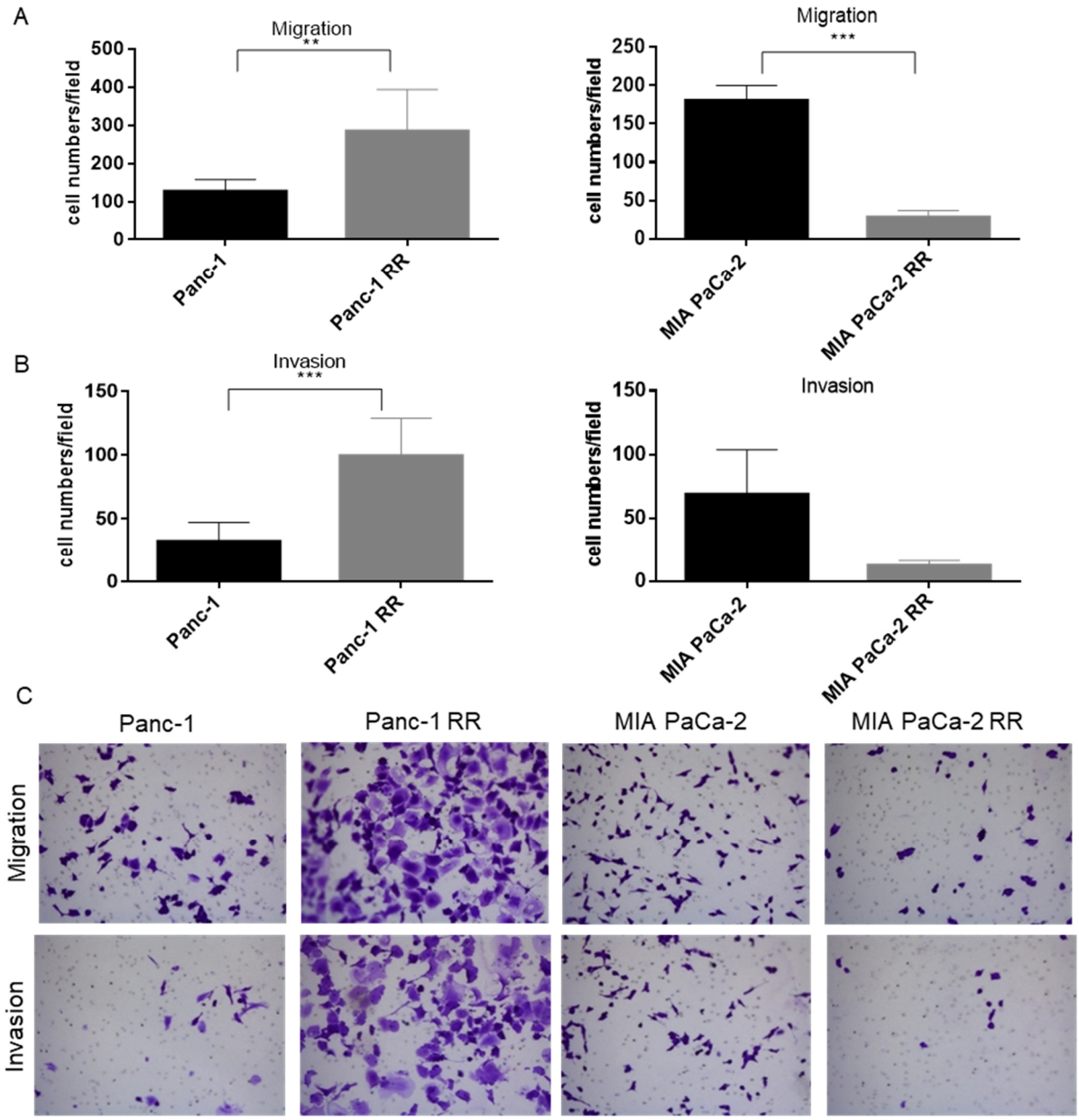

Figure 3.18. Basal migration and invasion capacity of parental and radioresistant (RR) pancreatic cancer cell lines Panc-1 and MIA PaCa-2. (A) Migration and (B) invasion capacity were measured using transwell assays. Error bars represent SD ($n \geq 3$). **: $p \leq 0.01$; ***: $p \leq 0.001$. (C) Representative images of transwell migration and invasion assays. Figure reprinted from [107].

Additionally, the influence of irradiation on the migratory and invasive potential of the RR and parental cells was investigated. The migratory and invasive capacity of irradiated cells was calculated in relation to the unirradiated control for each cell line. As shown in Figure 3.19, irradiation with 2 and 8 Gy significantly increased the migration of Panc-1 cells, whereas in Panc-1 RR cells the migration was not affected by irradiation. These results are additionally reflected in the invasion capacity, where Panc-1 cells exhibited an increase after irradiation, while Panc-1 RR cells were not affected. Apart from this, MIA PaCa-2 and MIA PaCa-2 RR cells demonstrated a decrease in their migratory potential after irradiation, which was significant at 8 Gy irradiation. Likewise, a lower invasive capacity was observed after irradiation, but this was only significant for MIA PaCa-2 RR cells.

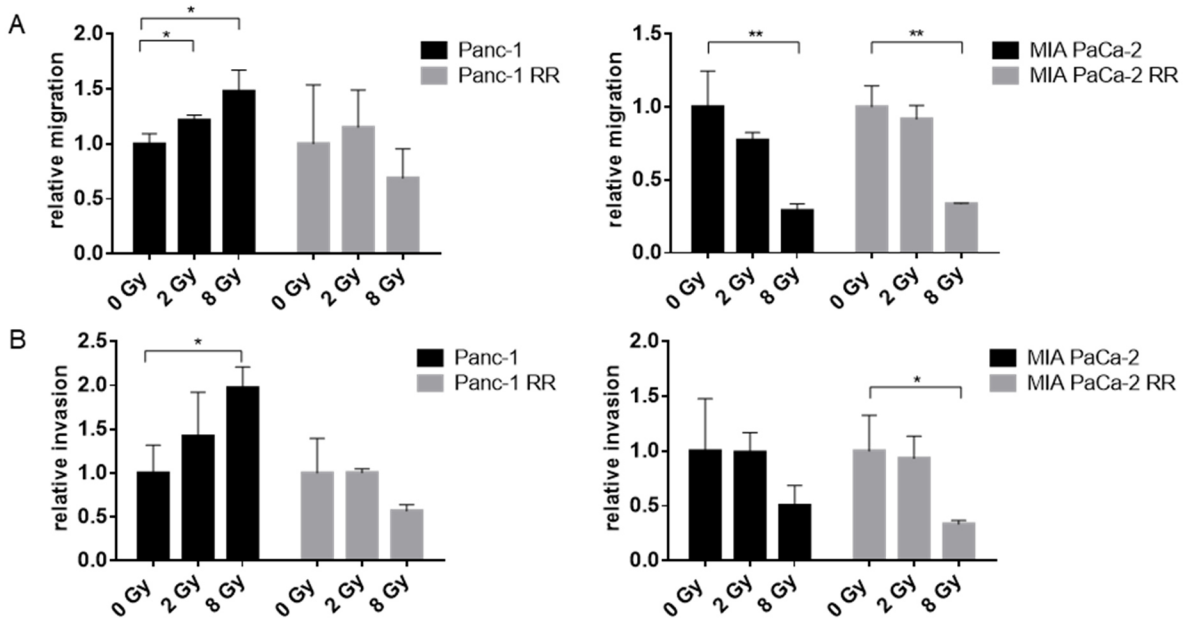

Figure 3.19. Migration and invasion capacity of parental and radioresistant (RR) pancreatic cancer cell lines Panc-1 and MIA PaCa-2 after irradiation. (A) Migration and (B) invasion capacity were measured 24 hours after irradiation using transwell assays. Values were normalized to 0 Gy of the respective cell line. Error bars represent SD (n = 3).*: $p \leq 0.05$; **: $p \leq 0.01$.

3.7 miRNA profile of radioresistant pancreatic cancer cell lines *in vitro* and *in vivo*

3.7.1 miRNA profile of cell lines

miRNA profiles of Panc-1 RR and MIA PaCa-2 RR cells, as well as the parental cell lines, were analyzed by small RNA-Sequencing. When compared to the respective parental cell line, levels of 54 and 41 miRNAs were significantly changed in Panc-1 RR and MIA PaCa-2 RR cells (Figure 3.20A, Appendix 2 and 3). In Panc-1 R cells, 29 miRNAs were downregulated with log2 fold changes smaller than -0.7, while 25 miRNAs were upregulated with log2 fold changes greater than 0.7. For MIA PaCa-2 RR cells, 21 and 20 miRNAs were detected to be up- or downregulated, respectively. Six miRNAs were commonly deregulated in Panc-1 RR and MIA PaCa-2 RR cells; however, only three of these miRNAs (miR-937-3p, miR-126-3p, and miR-335-3p) show the same pattern of either upregulation or downregulation in both RR cells (Figure 3.20B, Table 3.11). Apart from this, both RR cell lines were clearly distinguished from the respective parental cell line by principal component analysis (Figure 3.20C).

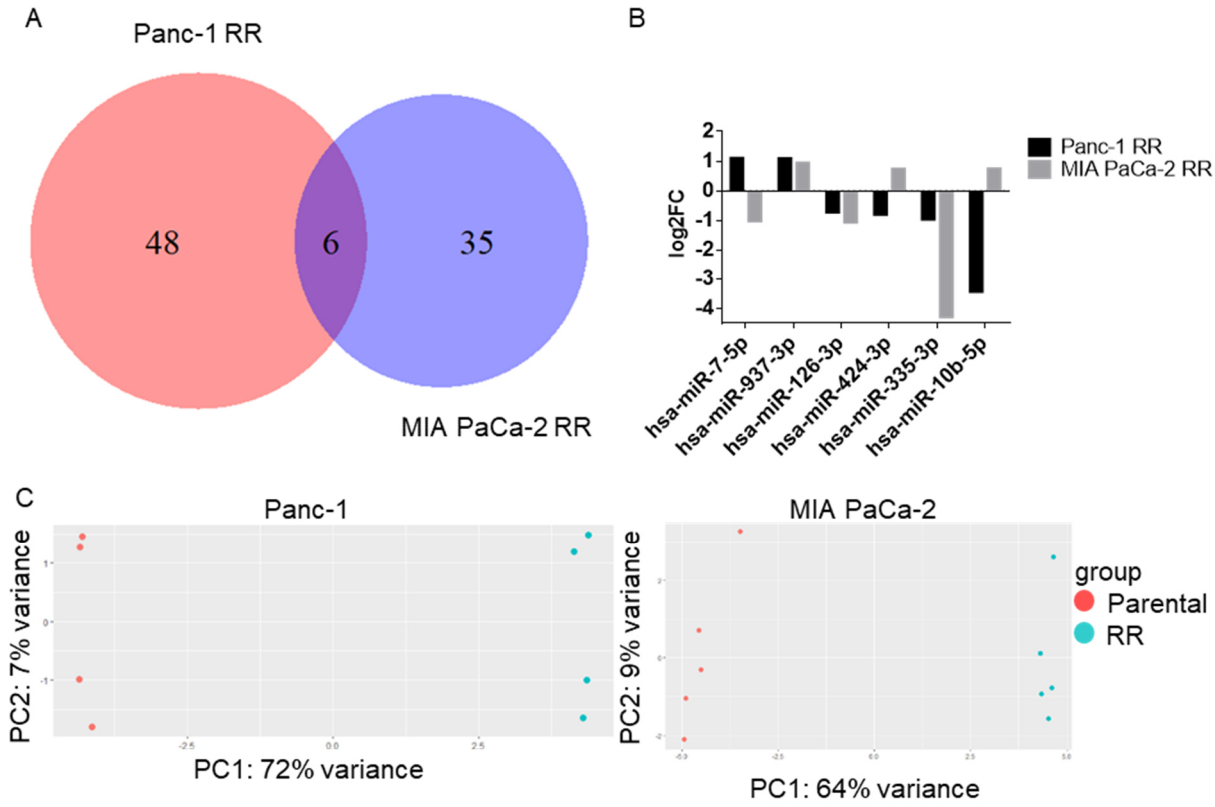

Figure 3.20. miRNA profile of radioresistant (RR) pancreatic cancer cell lines Panc-1 and MIA PaCa-2. (A) Venn diagram of deregulated miRNAs in Panc-1 RR and MIA PaCa-2 RR cells when compared to the respective parental cell lines. (B) Shown are the commonly deregulated miRNAs in Panc-1 RR and MIA PaCa-2 RR cells when compared with the respective parental cell line. Positive log2 fold changes indicate miRNAs upregulated in RR cells compared to parental cells, whereas negative log2 fold changes indicate miRNAs downregulated in RR cells. (C) Principal component analysis of miRNA expression in Panc-1 and MIA PaCa-2 as well as the RR cells. Analysis of all miRNAs in the dataset separated RR from parental cells (PC1) and PC2 represented intra-cell line variability.

Table 3.11. Commonly deregulated miRNAs in radioresistant (RR) cell lines Panc-1 RR and MIA PaCa-2 RR. Positive log2 fold changes indicate miRNAs upregulated in RR cells compared to parental cells, whereas negative log2 fold changes indicate miRNAs downregulated in RR cells.

miRNA	Panc-1 RR		MIA PaCa-2 RR	
	log_2FC	p-adjust	log_2FC	p-adjust
hsa-miR-7-5p	1.10	2.18E-28	-1.01	2.49E-16
hsa-miR-937-3p	1.09	5.05E-05	0.94	9.87E-07
hsa-miR-126-3p	-0.72	2.81E-13	-1.05	1.82E-24
hsa-miR-424-3p	-0.79	3.46E-09	0.73	3.78E-05
hsa-miR-335-3p	-0.96	2.08E-26	-4.29	6.86E-31
hsa-miR-10b-5p	-3.43	8.15E-168	0.74	2.41E-06

3.7.2 miRNA profile of tumor tissue and plasma

Apart from the investigation of whether the acquired radioresistance in MIA PaCa-2 RR cells can be confirmed *in vivo*, the miRNA profile of tumor-bearing mice was examined. Therefore, MIA PaCa-2 and MIA PaCa-2 RR were subcutaneously injected into the right flank of immunodeficient nude mice. Mice were randomly distributed into one of three groups, a control group (0 Gy) and two irradiation groups receiving single fractions of either 5 or 10 Gy. Tumor tissue, as well as plasma samples, were collected 24 hours after irradiation and subsequently analyzed by small RNA sequencing. Mice without a tumor served as an additional control.

First, the miRNA profile from the tumor tissue of control mice (0 Gy) was compared to the previously investigated *in vitro* miRNA profile of MIA PaCa-2 RR cells. For both analyses, MIA PaCa-2 RR cells were compared to parental cells and tumors derived from RR cells compared to parental tumors. In MIA PaCa-2 RR cells, 41 miRNAs were found to be deregulated, while in the tumor tissue 22 miRNAs were changed when compared to the parental cell line and tumors derived from it (Figure 3.21). Only five miRNAs (miR-103a-3p, miR-503-5p, miR-500a-3p, miR-149-5p, and miR-1269b) were deregulated both, *in vitro* in the cells and *in vivo* in the tumor tissue (Table 3.12).

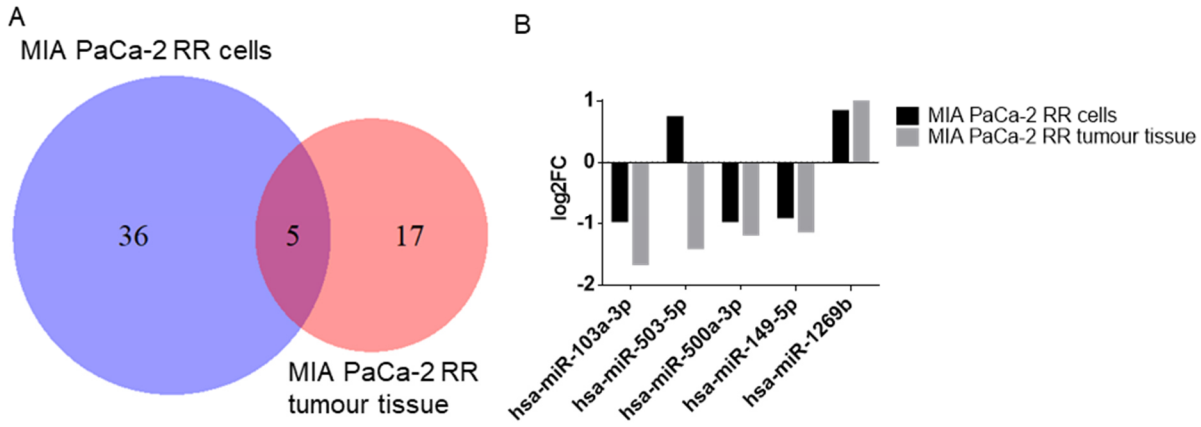

Figure 3.21. Comparison of miRNA profile in radioresistant (RR) MIA PaCa-2 RR cells and tumors derived from MIA PaCa-2 RR. (A) Venn diagram of differential miRNA expression in MIA PaCa-2 RR cells and tumor tissue relative to parental cells and tumor tissue, respectively. (B) Shown are the commonly deregulated miRNAs in MIA PaCa-2 RR cells and tumor tissue when compared with the parental cell line. Positive log2 fold changes indicate miRNAs upregulated in RR cells compared to parental cells.

Table 3.12. Commonly deregulated miRNAs in radioresistant (RR) Mia PaCa-2 RR cells and tumor tissue. Positive log2 fold changes indicate miRNAs upregulated in RR cells or tumor tissue compared to parental cells or tumor tissue, whereas negative log2 fold changes indicate miRNAs downregulated in RR cells or tumor tissue.

	MIA PaCa-2 RR cells		MIA PaCa-2 RR tumor tissue	
miRNA	log2FC	p-adjust	log2FC	p-adjust
hsa-miR-103a-3p	-0.96	1.46E-15	-1.66	2.96E-08
hsa-miR-503-5p	0.73	3.56E-09	-1.40	6.04E-06
hsa-miR-500a-3p	-0.96	2.08E-09	-1.18	9.22E-05
hsa-miR-149-5p	-0.90	5.35E-17	-1.13	2.11E-05
hsa-miR-1269b	0.83	1.80E-14	1.09	6.23E-06

miRNA expression in tumors derived from MIA PaCa-2 RR and parental cells suggested a separation of RR from parental tumors in all treatment groups (0, 5, and 10 Gy) by principal component analysis (Figure 3.22). Deregulated miRNAs are derived from the comparison of MIA PaCa-2 RR tumors with MIA PaCa-2 parental tumors from the respective treatment group. As shown in table 3.13, a total of 22, 30, and 18 miRNAs were found to be significantly deregulated in mice receiving no irradiation, 5 Gy or 10 Gy, respectively (Appendix 4 – 6).

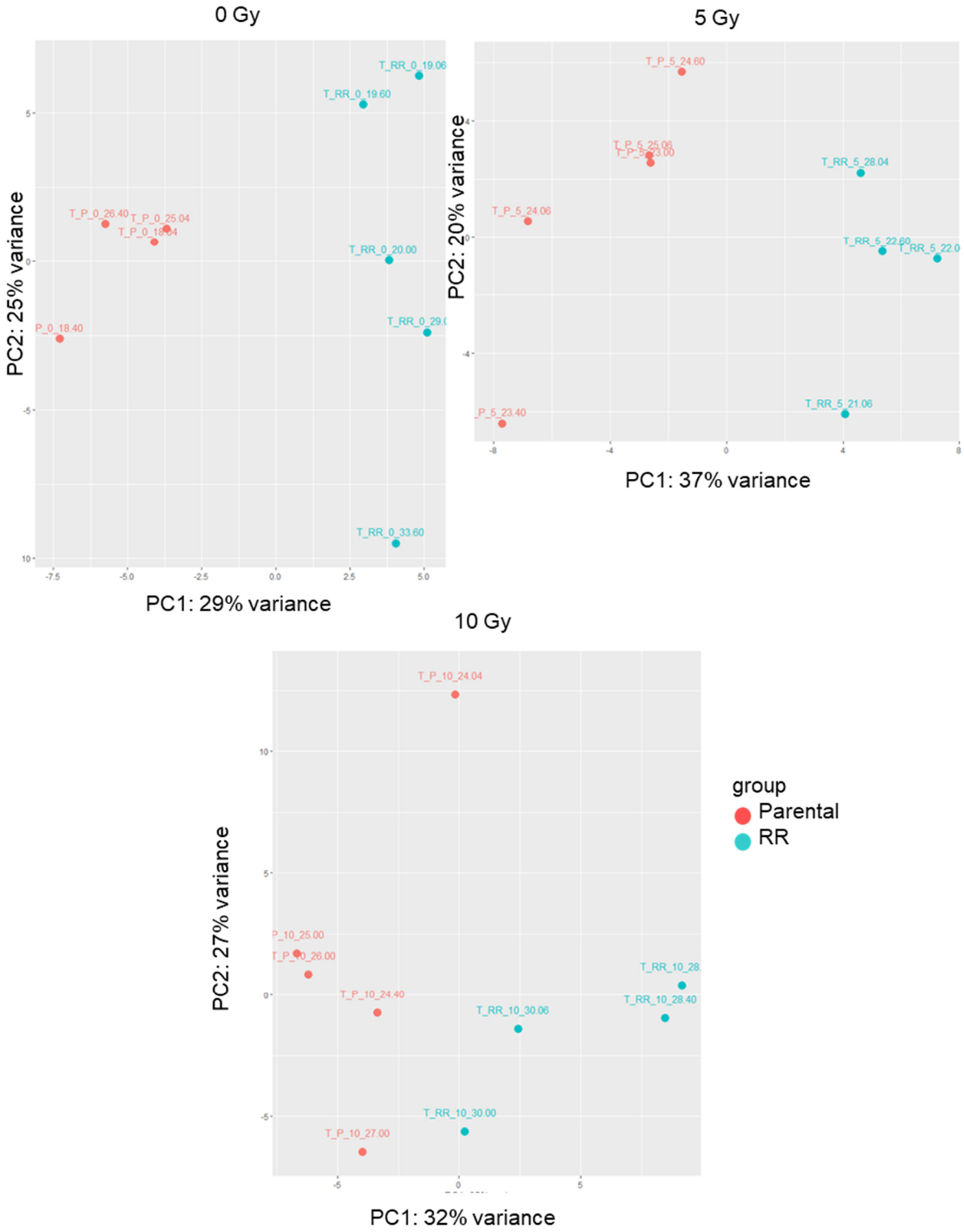

Figure 3.22. Principal component analysis of miRNA expression in tumors derived from MIA PaCa-2 and MIA PaCa-2 RR. Shown are the analyses for the different treatment groups: 0, 5, and 10 Gy. Analysis of all miRNAs in the dataset separated tumors derived from RR or parental cells (PC1) and PC2 showed intra-tumor tissue variability.

Table 3.13. The number of miRNAs significantly deregulated in tumor tissue derived from the radioresistant (RR) cell line Mia PaCa-2 RR.

Dose	upregulated in MIA PaCa-2 RR	downregulated in MIA PaCa-2 RR
0 Gy	12	10
5 Gy	14	16
10 Gy	11	7

In total, nine miRNAs were simultaneously deregulated in all treatment groups, four upregulated and five downregulated (Figure 3.23 and Table 3.14). Interestingly, miR-103a-3p and miR-149-5p were not only downregulated in all treatment groups but also in MIA PaCa-2 RR cells. While miR-503-5p was downregulated in MIA PaCa-2 RR tumor tissue, it was upregulated in the cells.

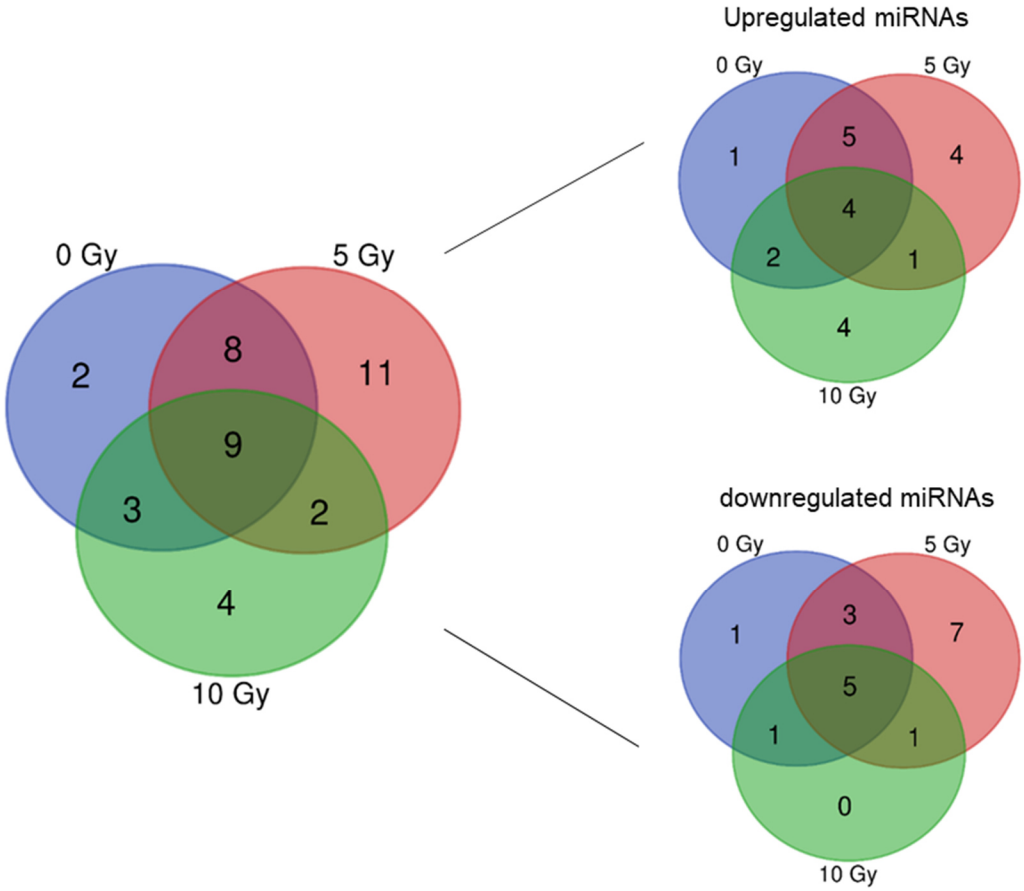

Figure 3.23. miRNA profile of tumors derived from parental and radioresistant (RR) MIA PaCa-2 and MIA PaCa-2 RR cells. Venn diagrams show deregulated miRNAs in MIA PaCa-2 RR tumors compared to the parental cells.

Table 3.14. Commonly deregulated miRNAs in tumor tissue derived from radioresistant (RR) MIA PaCa-2-RR cells after 0, 5, and 10 Gy irradiation. Positive log2 fold changes indicate miRNAs upregulated in RR tumor tissues compared to parental tumors, whereas negative log2 fold changes indicate miRNAs downregulated in RR tumor tissue.

	0 Gy		5 Gy		10 Gy	
miRNA	log_2FC	p-adjust	log_2FC	p-adjust	log_2FC	p-adjust
miR-103a-3p	-1.66	2.96E-08	-1.28	4.26E-07	-1.37	5.23E-06
miR-503-5p	-1.40	6.04E-06	-1.28	2.24E-05	-1.22	1.13E-02
miR-660-5p	-1.39	9.22E-05	-1.20	5.91E-03	-1.20	1.19E-03
miR-107	-1.31	3.01E-03	-1.15	4.57E-03	-1.19	4.30E-04
miR-149-5p	-1.13	2.11E-05	-1.14	2.21E-10	-1.10	2.36E-06
miR-576-3p	1.26	1.65E-05	1.50	1.37E-05	1.80	9.86E-07
mir-576-5p	1.57	4.70E-05	1.85	1.52E-08	1.86	2.79E-11
miR-222-3p	1.79	1.80E-07	1.87	2.46E-35	1.10	3.27E-02
miR-625-3p	3.03	9.32E-10	3.27	2.08E-18	2.8	2.79E-11

Next, it was assessed whether it was possible to detect circulating human miRNAs in the plasma of tumor-bearing mice. The miRNAs profile of plasma samples from mice with unirradiated MIA PaCa-2 or MIA PaCa-2 RR tumors was compared to control mice, i.e., mice without a tumor. Principal component analysis revealed the clustering of control mice and a clear separation from MIA PaCa-2 (Figure 3.23A) or MIA PaCa-2 RR (Figure 3.24B) tumor-bearing mice.

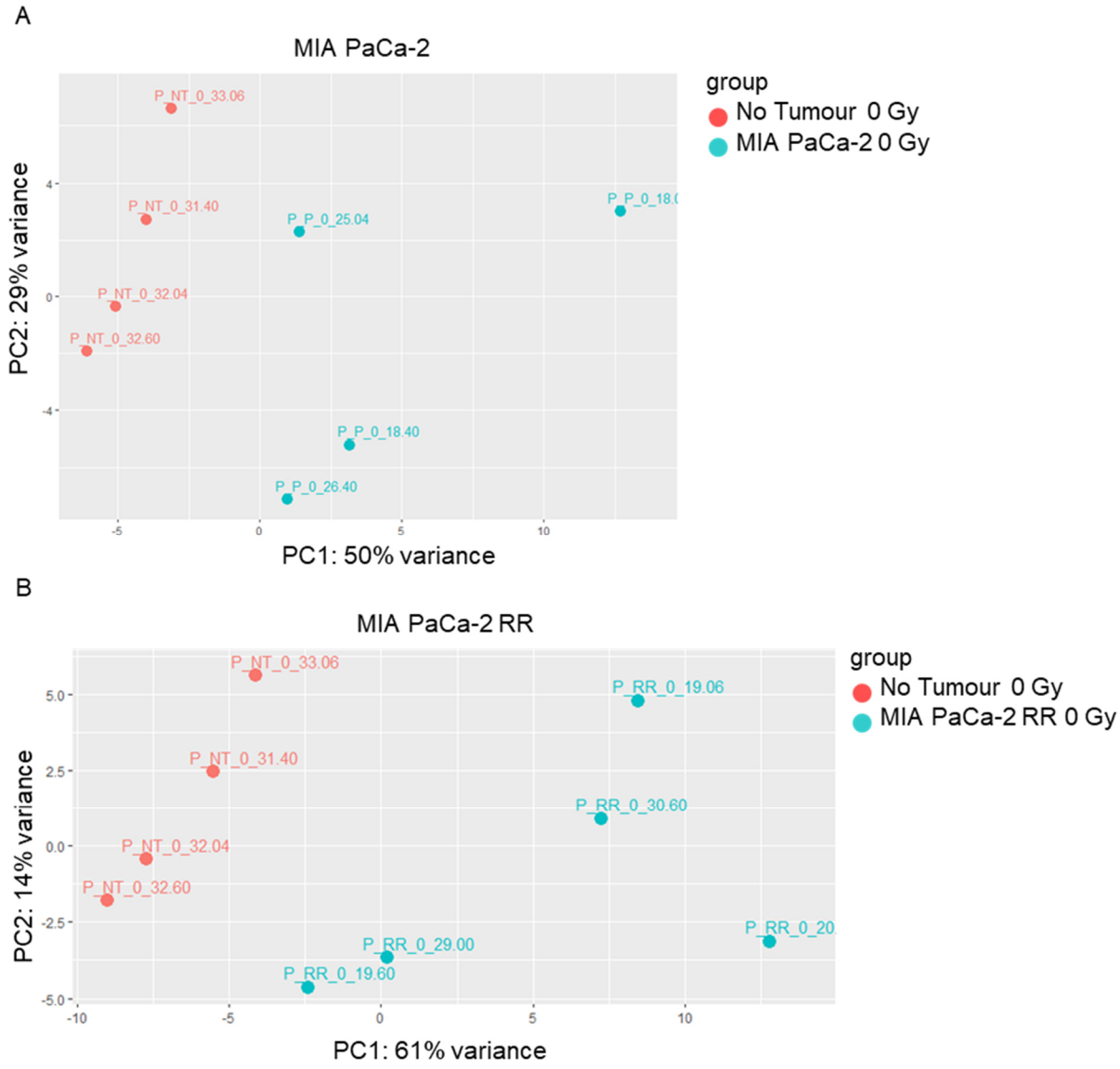

Figure 3.24. Principal component analysis of miRNA expression of plasma samples from mice with unirradiated tumors derived from parental MIA PaCa-2 (A) and radioresistant (RR) MIA PaCa-2 RR (B). Analysis of all miRNAs in the dataset separated plasma samples derived from control mice (no tumor) to tumor-bearing mice (PC1) and PC2 showed intra-plasma sample variability.

Finally, it was determined whether the miRNA profiles of MIA PaCa-2 and MIA PaCa-2 RR plasma samples differ. First, plasma samples from unirradiated mice with tumors derived from MIA PaCa-2 and MIA PaCa-2 RR were compared. Then the plasma of mice with tumors derived from the different cell lines receiving either 5 or 10 Gy were compared in each irradiation, respectively. Principal component analysis showed no clear separation for the groups (Figure 3.25). Only one miRNA was differentially regulated in the plasma of unirradiated MIA PaCa-2 RR tumor-bearing mice when compared to the parental tumor-bearing mice (Table 3.15).

miR-625-3p was significantly upregulated in plasma samples of MIA PaCa-2 RR tumor-bearing mice, with a log2 fold change of 4.38. It is worth noting that this miRNA was also upregulated in MIA PaCa-2 RR tumor tissue. After 5 Gy irradiation, eight miRNAs, two upregulated, and six downregulated, were found to be deregulated (Table 3.16). miR-221-3p was simultaneously upregulated in plasma samples (log2 fold change 1.02) and tumor tissues (log2 fold change 1.88) of MIA PaCa-2 RR bearing mice after 5 Gy irradiation. miRNA profiles of plasma samples from MIA PaCa-2 and MIA PaCa-2 RR tumor-bearing mice receiving 10 Gy irradiation showed no significantly deregulated miRNAs.

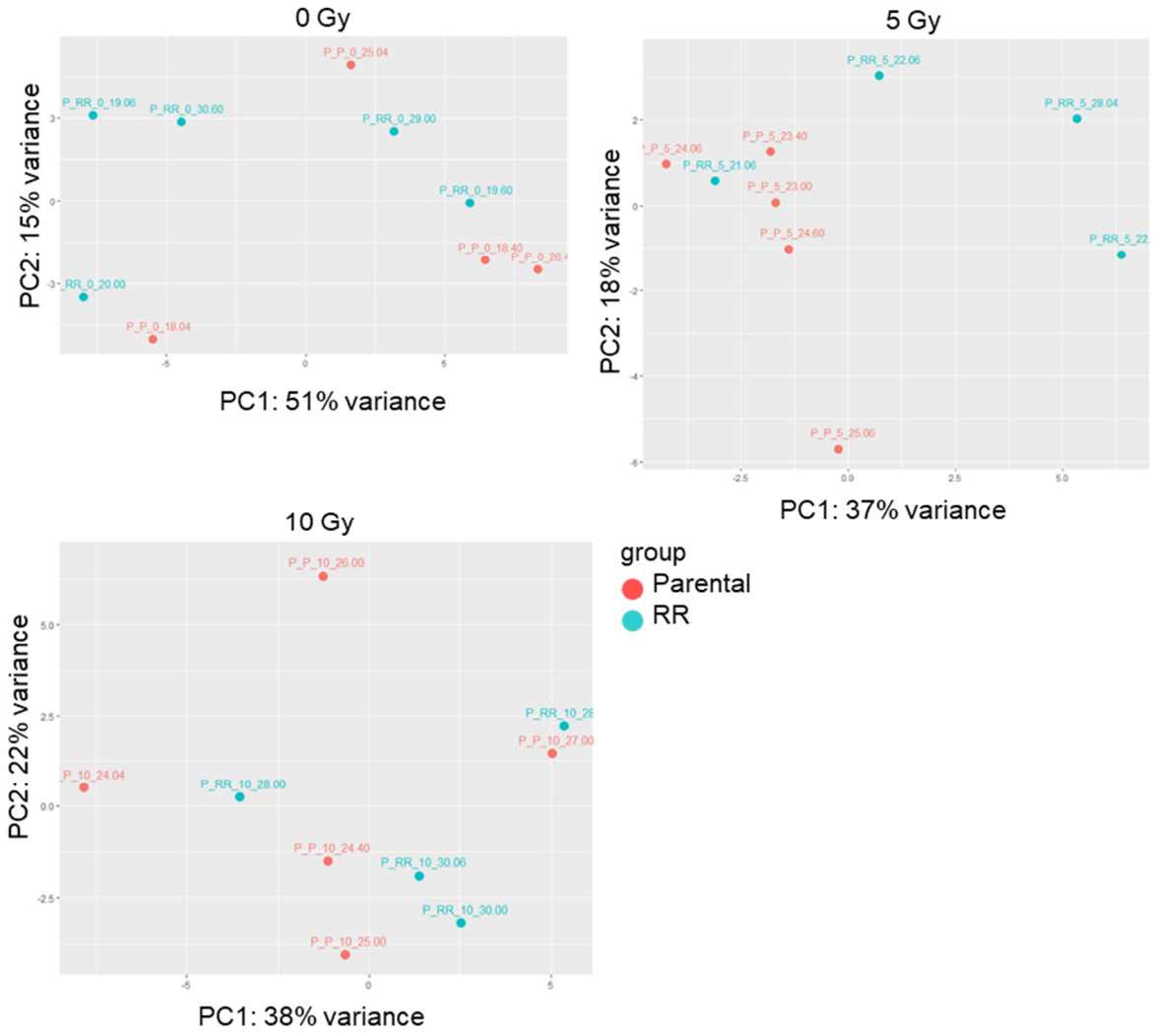

Figure 3.25. Comparison of miRNA profiles from plasma samples of tumor-bearing mice. Principal component analysis of miRNA expression in plasma samples derived from parental MIA PaCa-2 and radioresistant (RR) MIA PaCa-2 RR tumor-bearing mice. Shown are the analyses for the different treatment groups: 0, 5, and 10 Gy.

Table 3.15: Deregulated miRNA in plasma from tumor-bearing MIA PaCa-2 RR mice without irradiation. Positive log2 fold changes indicate miRNAs upregulated in plasma of mice with RR tumors compared to the plasma of mice with parental tumors.

miRNA	log2FC	p-adjust
hsa-miR-625-3p	4.38	4.48E-02

Table 3.16: Deregulated miRNA in plasma from tumor-bearing MIA PaCa-2 RR mice after 5 Gy irradiation. Positive log2 fold changes indicate miRNAs upregulated in plasma of mice with RR tumors compared to the plasma of mice with parental tumors, whereas negative log2 fold changes indicate miRNAs downregulated in plasma of mice with RR tumors.

miRNA	log2FC	p-adjust
hsa-miR-1246	-1.83	1.09E-04
hsa-miR-941	-1.70	2.67E-03
hsa-miR-122-5p	-1.43	4.41E-02
hsa-miR-1307-3p	-1.32	1.26E-02
hsa-miR-193a-5p	-1.31	1.84E-03
hsa-miR-1180-3p	-1.21	2.74E-02
hsa-miR-221-3p	1.02	2.67E-03
hsa-miR-451a	1.15	7.94E-03

4. Discussion

Despite extensive research efforts, surgical resection remains the only potentially curative option for pancreatic cancer patients. However, at the time of diagnosis, only 20-25 % of all patients are eligible for surgery, while the remaining either present distant metastasis or locally advanced unresectable tumors. For these patients, neoadjuvant therapy in terms of chemotherapy in combination with radiotherapy offers an opportunity to downstage borderline resectable and locally advanced tumors and hence, improve not only resection rates but also overall survival [35]. Studies have shown that local radiotherapy in combination with chemotherapy can lead to effective downstaging and in about 30 % of these patients, secondary resectability can be achieved and thereby the overall survival rate is improved [23, 36, 108, 109]. Nonetheless, about 70 % of patients receiving radiation treatment show a treatment failure and no benefit overall. The underlying mechanisms for this cancer's inherent radioresistance remain mostly unknown. In order to improve the poor treatment outcome in pancreatic cancer, it is necessary to understand the biological mechanisms contributing to the radioresistance and to identify and validate novel molecular targets.

4.1 Generation of radioresistant cell lines

The first part of this project compromised the generation of radioresistant pancreatic cancer cell lines by subjection to multiple fractions of irradiation. Therefore, different established pancreatic cancer cell lines were screened for their radiosensitivity. Panc-1 and MIA PaCa-2 were the most radiosensitive cell lines. This finding is in accordance with Souchek et al., who showed in their screening of different pancreatic cancer cell lines that Panc-1 is a more radiosensitive one [92].

The selection of radioresistant subpopulations through repeated exposure to irradiation has been previously reported in several entities of cancer: lung [110-113], esophageal [114-116], laryngeal [117], hepatic [118], prostate [119], breast [113, 120, 121], neuroblastoma [122], head and neck [123] and pancreatic cancer [86, 92]. Many different irradiation treatment protocols regarding the cumulative dose, overall treatment time, and recovery time have been applied to produce radioresistant cell lines [124]. During this project, two distinct approaches were pursued. The first method consisted of ten fractions of two Gy during a time span of two weeks, with a cumulative dose of 20 Gy and was previously described by Souchek et al. [92]. In the second procedure that was modified after Wang et al. [86], cells were subjected to a higher cumulative dose (80 Gy) for several months. In both techniques, the RR cells were not clonally derived in order to obtain a heterogeneous population and thereby reflecting the heterogeneity of pancreatic cancer seen in the clinic [43, 125]. Cells that were exposed to a cumulative dose of 80 Gy for several months exhibited higher radioresistance when compared with the respective parental cell line. However, cells receiving a total of 20 Gy showed fewer differences regarding the radioresistance. Although Souchek et al. were able to generate a radioresistant Panc-1 cell line, the irradiation protocol with ten fractions of 2 Gy did not affect the second cell line, BxPC-3, investigated in their studies. However, with a cumulative dose of 80 Gy, it was possible to generate a radioresistant BxPC-3 cell line [86]. These results suggest that irradiation with a higher total dose over a longer period result in more radioresistant cell lines. This is further reflected in the results of other groups, where the average total radiation dose ranged between 40 and 60 Gy for the successful generation of radioresistant subclones [124]. Therefore, solely the cells receiving a cumulative dose of 80 Gy, termed as Panc-1 RR and MIA PaCa-2 RR, were further investigated in these studies.

The acquired radioresistance was further validated in a subcutaneous xenograft mouse model. The results confirmed that the RR cells maintain the radioresistant properties *in vivo*. In line with other reports [126, 127], it was shown that tumors derived from MIA PaCa-2 RR cells showed significantly reduced tumor growth delay than tumors from the parental cell line after irradiation. Furthermore, not only did the RR cells show a lower radioresponse, but they also demonstrated a faster growth

than tumors from the parental cells. Two methods were used to measure tumor size, digital caliper and ultrasound device. However, only the measurements with the digital caliper revealed significant results. One reason could be the higher number of mice measured with the digital caliper.

Summarizing, radioresistant pancreatic cancer cell lines were generated through repeated exposure to ionizing irradiation. This radioresistance was not only observed *in vitro* but furthermore also demonstrated *in vivo*.

4.2 Mechanisms leading to radioresistance

In order to elucidate the molecular mechanisms underlying radioresistance, the RR cell lines were characterized in terms of proliferation, cell cycle distribution, radiation-induced apoptosis, DNA damage repair, and reactive oxygen species generation. Furthermore, mRNA sequencing of Panc-1 RR and MIA PaCa-2 RR cells and the respective parental cell lines was performed.

4.2.1 Radioresistant cells show an accumulation in G2/M phase

In terms of proliferation, the generated RR cells demonstrated comparable growth rates to the respective parental cells. The finding that the acquired radioresistance did not affect cell proliferation was also reported in another study [115].

Cell cycle distribution is an important aspect of radiosensitivity [128]. While cells in the S phase are the most radioresistant, cells in the G2/M phase are the least radioresistant. Interestingly, cell cycle analysis revealed that both RR cell lines exhibited an accumulation in the G2/M phase. These surprising findings were also seen in another model of a radioresistant cell line [115]. Besides the aforementioned cell cycle phases, cell cycle checkpoints are further determinants for the radio-responsiveness [128]. DNA damage caused by irradiation leads to the subsequent activation of the G1/S and G2/M cell cycle checkpoints. The G1/S

checkpoint is mainly mediated by p53 and p21. As these are often mutated in cancer cell lines, the G1/S checkpoint is generally inactivated [42]. Of more interest is the activation of the G2/M checkpoint after irradiation during which DNA damage repair is promoted. In this study, it was observed that all cell lines exhibited a G2/M arrest after irradiation. While MIA PaCa-2 RR cells showed no difference in the G2/M arrest after irradiation in comparison to parental cells, Panc-1 RR cells exhibited a lower G2/M arrest. This shorter delay in the G2/M phase might be due to reduced DNA damage and, therefore, a potential reason for the acquired radioresistance.

4.2.2 Parental and radioresistant cell lines show no difference in radiation-induced apoptosis

In order to improve therapeutic efficacy, the approach to increase apoptotic cell death has been widely investigated as cell death is induced in part by the activation of apoptotic signaling pathways [42]. For this, either pro-apoptotic molecules/pathways are activated, or anti-apoptotic molecules/pathways are inhibited. During this study, it was observed that the induction of apoptosis after irradiation was comparable in both RR cells and the respective parental cell lines. In line with other reports, it is unlikely that alterations in apoptosis are the main contributor to the radioresistance [115, 124]. Additionally, the deregulation and evasion of apoptosis is already a well-known characteristic of pancreatic cancer [129]. Many clinical studies have investigated whether proteins regulating apoptosis can predict the treatment response, including radiotherapy, but so far, most results were inconsistent [42, 130]. This is mainly due to the fact that apoptosis is not the only cell death pathway induced by radiotherapy, but rather cell killing can occur in several ways following DNA damage, e.g., necrosis, mitotic catastrophe, and autophagy [130].

4.2.3 X-Ray-induced DNA damage is reduced in radioresistant cell lines

Irradiation can cause different types of DNA damage, including the most lethal one, DNA DSBs. DNA damage can lead to the aforementioned variety of cell deaths; therefore, the DNA damage response and furthermore DNA repair mechanisms are

crucial for cell survival. The balance of DNA damage and DNA repair is essential for the success of radiotherapy, either the damage is too severe, and cells undergo cell death, or it can be repaired, and cells survive [42]. After the occurrence of DNA DSBs due to, e.g., irradiation, Ataxia-telangiectasia mutated (ATM), ataxia-telangiectasia, and Rad3-related (ATR) and DNA-dependent protein kinase catalytic subunit (DNA-PKcs) is activated [59]. As a cellular response, these kinases phosphorylate histone H2AX, termed then γH2AX, at the site of DNA lesions to induce DNA repair. This γH2AX formation acts as an initiation signal for the recruitment of DNA repair proteins [131]. γH2AX foci remain until the DBSs are repaired. Therefore, measuring γH2AX is indicative of a cell's ability to repair DNA lesions and a sensitive method for the measurement of DNA DSBs due to the consistent number of breaks with the γH2AX foci formed after irradiation [132, 133]. Schwartz and colleagues screened 12 human tumor cell lines for their radiosensitivity and observed that some of the more radioresistant ones show less initial DNA damage, i.e., the immediate damage after exposure to radiation [134].

Furthermore, radioresistant cell lines revealed a faster repair of DNA damage, mostly within an hour, whereas the sensitive cell lines required more time to repair the lesions [134]. In other models of radioresistant cell lines, derived from repeated exposure to radiation, RR cell lines showed an increased ability to repair the DNA damage [115, 119, 135]. In line with these findings, it was shown that the RR cell lines have less initial DNA damage than the respective parental cell lines.

Moreover, residual γH2AX foci 24 hours after irradiation were analyzed and a lower number of unrepaired foci in Panc-1 RR and MIA PaCa-2 RR cells in comparison to the respective parental cell lines was observed, suggesting a greater efficiency to repair DNA DSBs in the RR cell lines. Additionally, mRNA sequencing of RR cells revealed the upregulation of *aryl hydrocarbon receptor (AHR)*. This is in line with the recent implication for AHR in the repair of DNA DSBs. AHR is part of the γH2AX foci and therefore plays a role in the repair of radiation-induced DNA damage [136].

Currently, many DNA damage response inhibitors are evaluated not only in preclinical but also in clinical studies, including checkpoint kinase 1 (Chk1) inhibitors [137]. DNA damage leads to Chk1 activation and subsequently to cell cycle arrest and the promotion of homologous recombination repair [138]. It was shown that Chk1

inhibitors can sensitize MIA PaCa-2 cells and tumors to chemoradiation *in vitro* and *in vivo* [138, 139]. These findings suggest that inhibiting Chk1 leads to the impairment of DNA damage repair, thereby representing an important molecular target to sensitize tumor cells to irradiation.

4.2.4 Radioresistant cell lines show reduced oxidative stress after irradiation

Reactive oxygen species (ROS) are important for cell signaling and homeostasis; therefore, free radicals are continuously generated in a cell's environment. However, when a cell's antioxidant capacity and the level of ROS production are out of equilibrium, oxidative stress develops, and subsequently, the DNA is damaged by radicals [140]. Many types of cancer exhibit a deregulated metabolism and consequently increased generation of ROS. In order to manage this additional stress, cancer cells adapted through the development of an enhanced antioxidant system, rendering them resistant to exogenous stress [57]. Part of this cellular antioxidant response are antioxidant enzymes (e.g., superoxide dismutases, catalases, and peroxidases), radical scavengers (e.g., cellular thiols (glutathione) and thioredoxin), the monitoring and the repair of DNA, and the initiation of apoptosis [140].

As cells are mainly composed of water, the radiolysis of water and hence the production of ROS play an important role in radiotherapy. Hydroxyl radicals, the most prominent and reactive ones, cause damage to structural and functional molecules, including carbohydrates, proteins, lipids, and nucleic acids [140]. Besides the direct effect of irradiation on the DNA, 60 – 70 % of the DNA damage is produced by free radicals [53, 54]. Therefore, the intracellular ROS levels in Panc-1 RR and MIA PaCa-2 RR cells in comparison to the parental cell lines were investigated. Already without irradiation, RR cells exhibited lower basal ROS levels. Furthermore, after irradiation, the induction of ROS was lower in the RR cells than in the parental cells. The reduced production of ROS after irradiation observed in the RR cells, suggests an enhanced antioxidant system. In line with these findings, RR cells showed lower DNA damage shortly after irradiation.

Following these results, an mRNA profiler screening for genes involved in the oxidative

stress pathway was applied. Panc-1 RR and MIA PaCa-2 RR cells showed an increase of *CCL5* and *MB* and a downregulation of *SOD3*. CCL5 is regulated by the transcription factor NF-κB, which is activated through ROS [141]. In tumor-bearing mice, it was shown that radiotherapy increases the production of CCL5 and using an antagonist against its receptor CCR5 could increase the radioresponse, however only in tumors with inherent sensitivity to irradiation [142]. For the radioresistance of pancreatic cancer, another chemokine seems to play an important role, CCL2. Irradiation stimulates the production of CCL2, which then recruits monocytes to stimulate tumor proliferation and neovascularization [143]. Tumor-bearing mice receiving anti-CCL2 antibody had a greater tumor growth delay after irradiation, suggesting that CCL2 mediates the radioresistance [143]. Besides the upregulation of *CCL5* mRNA in both RR cells, mRNA levels of *MB* were elevated. MB acted as a scavenger of nitric oxide and ROS and was shown to be enhanced in a radioresistant esophageal cell line [144, 145].

Superoxide dismutases are important antioxidant enzymes. However, *SOD3* was downregulated in both RR cells, and *SOD2* was only upregulated in Panc-1 RR cells. This upregulation on the mRNA level was further confirmed on the protein expression level. These results suggest that the upregulation of SOD2 in Panc-1 RR cells could be contributing to the acquired radioresistance. In line with this, another group observed the upregulation of SOD2 in a radioresistant nasopharyngeal cancer line and, consequently, the function in radioresistant [146]. Nonetheless, there are many inconsistent findings regarding the role of superoxide dismutases as either radioprotectors or sensitizers [147].

MIA PaCa-2 RR cells showed upregulation of *glutamate-cysteine ligase catalytic subunit* (*GCLC*), *Scavenger Receptor Class A Member 3* (*SCARA3*), and *Thioredoxin reductase 1* (*TXNRD*), suggesting an elevated antioxidant environment.

Moreover, in Panc-1 RR cells upregulation of NRF2, p-NRF2 and TRX were observed. The cellular antioxidant response is mainly regulated by the transcription factor NRF2 [148]. After its activation, the expression of several other anti-oxidative genes, including *SOD2* and *GCLC*, is enhanced [149]. This could be the reason for the increased level of SOD2 in Panc-1 RR cells as NRF2 levels were found to be elevated. NRF2 is regulated by two mechanisms, a KEAP1 dependent and independent

pathway [149-151]. The binding of NRF2 to KEAP1, its suppressor, leads to proteasomal degradation. But when NRF2 is phosphorylated, leading to the dissociation of NRF2 and KEAP1, p-NRF2 translocates into the nucleus and activates the expression of antioxidant proteins. An elevated level of p-NRF2 in Panc-1 RR cells was also observed, suggesting an enhanced antioxidative response.

The redox homeostasis is preserved by TRX, as TRX reduces ROS. *In vitro* experiments in human breast and pancreatic cancer cell lines (Panc-1) with a combined inhibition of the glutathione and TRX metabolism showed an enhanced response to irradiation [152]. These results were confirmed *in vivo* for the breast cancer cell lines. Furthermore, in non-small cell lung cancer, the overexpression of TRX is associated with an aggressive tumor phenotype and bad prognostic features [153].

As ROS are an important part of the generation of DNA damage, ROS-modulating therapeutic approaches in cancer have gained attention [154]. Targeting TXNRD, which is crucial for the biosynthesis of TRX, showed a radiosensitizing effect in cells and tumor bearing mice [155]. Besides, Edaravone, a free radical scavenger, was shown to exhibit radioprotective effects *in vitro* and *in vivo* [156, 157].

In summary, the results suggest that the acquired radioresistance in Panc-1 RR and MIA PaCa-2 RR cells is mainly due to increased DNA repair capacity and reduced oxidative stress. The lower oxidative stress could be indicative of the reduced DNA damage in the RR cells. mRNA and protein expression levels of Panc-1 RR cells indicated an elevated antioxidant response mechanism through the upregulation of antioxidant enzymes and free radical scavengers. MIA PaCa-2 RR cells also exhibited lower oxidative stress, however this was only observed on the mRNA level but not on the protein levels. Further experiments are necessary to elucidate the mechanisms in this cell line.

4.2.5 Altered gene expression and pathway analysis

To investigate the underlying molecular basis of the radioresistant phenotype, mRNA sequencing was conducted. Souchek and colleagues performed similar experiments

[92]. They generated a radioresistant Panc-1 RR cell line (see above) and compared the gene expression level of the RR cell line to the parental cell line measured via microarray. Their results implicated a role for the cholesterol synthesis pathway in the radioresistance of pancreatic cancer cell lines. However, this was not confirmed during this project. This may have several reasons. Although Panc-1 RR cells were generated, those cells generated after the irradiation protocol by Souchek et al. were not used, but rather the ones who received a higher cumulative dose. These cells demonstrated higher radioresistance and were therefore used for all subsequent experiments. Additionally, a second RR cell line, MIA PaCa-2 RR, was used. For the analysis of the mRNA sequencing, the focus was on the 121 genes commonly deregulated in Panc-1 RR and MIA PaCa-2 RR cells. These genes were considered to be important for the acquired radioresistance and were therefore further investigated. The network-based analysis program, IPA, predicted enhanced cell viability in RR cell lines based on several upregulated genes including *AHR, homeodomain interacting protein kinase 2 (HIPK2), leukemia inhibitory factor (LIF), sonic hedgehog signaling molecule (SHH)* and *ATP binding cassette subfamily C member 3 (ABCC3)*.

AHR, known as a transcription factor, mainly regulates genes involved in cell survival, proliferation, growth, and differentiation [158]. Recently, another function of AHR was discovered. Dittmann et al. are the first ones to demonstrate a role for AHR in the repair of radiation-induced DNA double-strand breaks (DSBs) [136]. Repression of AHR results in the inhibition of DSBs repair and furthermore radiosensitizes cells. Consistently, *AHR* was found to be upregulated in the RR cells.

Although HIPK2 is a well-known tumor suppressor, an upregulation in both RR cell lines was observed. However, it was demonstrated that HIPK2 is a target of NRF2 and can, under certain circumstances, promote cell survival instead of apoptosis [159]. In this study, NRF2 protein levels were elevated in Panc-1 RR cells when compared to the parental cell line. This could explain the upregulation of *HIPK2* in the RR cells.

LIF is a member of the IL-6-type cytokine family. High levels of LIF in nasopharyngeal cancer patients showed a correlation with tumor recurrence. Moreover, *in vitro* and *in vivo* studies demonstrated that LIF modulates the DNA damage response activated

by irradiation and increases the radioresistance [160]. Consistent with these findings, *LIF* was observed to be increased in the RR cells during these studies.
The inhibition of SHH, the namesake of the corresponding pathway, was shown to have a radiosensitizing effect *in vitro* and *in vivo* [161]. The treatment with SHH ligand in combination with radiation showed a radioresistant effect on cancer cells [161] and could explain for the observed increase of *SHH* in the RR cells from this study.
Recently, it was demonstrated that ABCC3 could be a potential therapeutic target in pancreatic cancer. ABCC3 plays a role in the progression of pancreatic cancer, the downregulation on a cellular level and in tumor-bearing mice resulted in a decreased cell proliferation [162]. Interestingly, *ABCC3* was upregulated in both RR cell lines suggesting a further investigation of its therapeutic potential.

In summary, some of the deregulated genes in the cell lines Panc-1 RR and MIA PaCa-2 RR are playing a role in the response to radiation. Furthermore, many of these commonly deregulated genes, including *AHR, HIPK2, SHH, and ABCC3,* in RR cells are implicated in apoptosis, DNA damage repair, and reactive oxygen species generation [136, 163-165]. Therefore, these results further suggest the role of DNA damage repair and oxidative stress in the acquired radioresistance.

4.3 Radioresistant cells show different migration and invasion properties

Characteristic of pancreatic cancer is the rapid progression to metastatic disease, a stage in which the only possible cure, surgery, is no longer feasible. This may explain the high mortality rate of pancreatic cancer; it is assumed that 90 % of all pancreatic cancer deaths are attributed to metastases [16, 17]. Further understanding of the mechanisms leading to metastasis is, therefore, of clinical significance.
To enable tumor cells to leave the primary tumor, invade the surrounding tissue and form a metastasis, migration and invasion is indispensable. During invasion, the microenvironment is altered, mainly by the activation of extracellular proteases.

Radiation therapy aims to control the primary tumor and thus may improve overall survival. However, several studies have shown that ionizing radiation could promote migration and invasion in those cells that are resistant to treatment, thus reducing the effectiveness of radiotherapy [166, 167].

During this investigation of the mRNA profile of the parental and RR cells, IPA predicted changes concerning the migration and invasion properties. The predicted enhanced migratory and invasive capacity of Panc-1 RR cells was validated with transwell assays. In contrast, as predicted by IPA, MIA PaCa-2 RR cells exhibited less migration and invasion. Irradiation increased the migratory and invasive capacity in the parental Panc-1 cells, whereas Panc-1 RR cells showed no changes. MIA PaCa-2 and MIA PaCa-2 RR cells showed reduced migration and invasion after irradiation. The literature on this subject reveals contradictory results. While it was shown, that the migration and invasion of Panc-1 cells is not affected by radiation, MIA PaCa-2 cells demonstrated an increase after irradiation, however after 8 Gy radiation the invasion capacity of MIA PaCa-2 cells were reduced [168], similar to the results shown in this study. Another publication showed that Panc-1 cells only show an increase in invasion, not in migration after irradiation. Other pancreatic carcinoma cell lines did not show any difference after irradiation [169]. These contradictory results could be due to the varying doses used and the different methods applied to measure the migratory and invasive capacity.

The observed enhanced migratory and invasive capacity in Panc-1 RR cells is in line with other reports, where the RR cells exhibited the same characteristics [119, 121, 126]. As far as known, this work shows for the first time a reduced migration and invasion capability in radioresistant cell lines.

Based on IPA, these contrasting phenomena are mainly due to the different expression of the following genes: *Annexin A1 (ANXA1), Bcl-2-like 1 (BCL2L1),* and *N-Myc Downstream Regulated 1 (NDRG1).*

High expression of ANXA1 is associated with higher invasiveness and poorer survival in a variety of cancer patients [170-172], including pancreatic cancer patients [173, 174]. Furthermore, it was shown that ANXA1 knockdown in MIA PaCa-2 and Panc-1 cells leads to a decrease in migration and invasion, and even to lower liver metastasis in mice [175, 176]. In line with this, it was shown that while Panc-1 RR cells

demonstrated an upregulation of *ANXA1* and an increase in migration and invasion, MIA PaCa-2 RR cells showed reduced migration and invasion properties and reduced expression of *ANXA1*.

Although the proteins of the Bcl-2 family are known to be key regulators of apoptosis, they may also contribute to the invasion and metastasis [177]. Overexpression of BCL2L1 was demonstrated to increase migration and invasion in melanoma and glioblastoma cells [178]. In accordance with the literature, *BCL2L1* was found to be upregulated in Panc-1 RR cells and downregulated in MIA PaCa-2 RR cells.

In line with the findings from this study, that high NDRG1 expression is associated with a decrease in migration and invasion, it was published that the overexpression of NDRG1 in pancreatic cancer cell lines leads to a decreased invasion capacity and furthermore the low expression in pancreatic cancer patients is correlated with a poor prognosis [179, 180]. Further studies in other cancer entities confirm this association. Overexpression of NDRG1 not only results in a reduced invasion *in vitro* but also in a lower incidence of metastasis *in vivo* [181, 182].

In summary, the acquired radioresistance in the cell lines Panc-1 RR and MIA PaCa-2 RR led to contrasting migration and invasion characteristics, which might be explained by the reverse expression of several genes.

4.4 miRNA as potential biomarkers predicting the radioresponse in pancreatic cancer

The interest in miRNA research has been growing due to their role in post-transcriptional regulation of gene expression via RNA interference. miRNAs and their potential predictive value for tumor radiation response seem to be of particular interest in the field of biomarkers, thus allowing the stratification of patients in radioresistant and radioresponsive groups for an individualized radiotherapy [183, 184]. For the investigation of common features between the radioresistant cell lines, Panc-1 RR and MIA PaCa-2 RR, small RNA sequencing was performed to analyze the

miRNA profile for potential biomarkers of radioresistance. When compared to the respective parental cell line, 54 and 41 miRNAs were deregulated in Panc-1 RR and MIA PaCa-2 RR cells, respectively. Six miRNAs were commonly deregulated in both RR cell lines; however, only three showed the same pattern of up- or downregulation, miR-937-3p, miR-126-3p, and miR-335-3p.

As far as known, there is yet no evidence of miR-937-3p in the context of therapy resistance in cancer. However, in accordance with this research, several other studies have shown that the other two mentioned miRNAs are involved in chemo- or radioresistance.

Both RR cell lines exhibited lower expression of miR-126-3p when compared to the parental cell lines. It was shown in different cancer cell lines that the low expression of miR-126 is associated with drug resistance, while the overexpression can enhance the sensitivity to various drugs [185-189]. Moreover, this miRNA was also demonstrated to be significantly downregulated in esophageal carcinoma patients belonging to the non-responder group to chemoradiation [190].

Additionally, miR-335-3p was downregulated in both RR cell lines. It was reported that drug-resistant lung cancer cell lines also showed downregulation of miR-335 and the overexpression could increase the response to chemoradiotherapy [191].

Other research groups have also investigated miRNAs in radioresistant pancreatic cancer cell lines. For example, Wang et al., whose protocol was used in a modified version to generate the RR cell lines in this study, showed that miR-23b was found to be downregulated in both generated RR cell lines, Panc-1 RR and BxPC-3 RR. The associated radioresistance with miR-23b was mainly due to the regulation of autophagy [86]. However, in the RR cell lines from this study, the downregulation of miR-23b was not observed. This could be due to several reasons. First, the RR cells were not clonally derived in order to represent a heterogenous population often associated with pancreatic cancer, while Wang et al. selected clones from each cell line. Second, although one cell line is in common (Panc-1), the second cell line differs from the two studies. This might explain the detection of different miRNAs associated with radioresistance.

In order to further investigate the potential of miRNAs as predictive markers for radioresponse *in vivo*, a subcutaneous xenograft mouse model with MIA PaCa-2 and

MIA PaCa-2 RR cells was used. While *in vitro* MIA PaCa-2 RR cells showed 41 deregulated miRNAs, tumors derived from this cell line revealed 22 miRNAs deregulated when compared to the parental counterpart (cells and tumor, respectively). From these deregulated miRNAs, five miRNAs were commonly deregulated *in vitro* and *in vivo (*miR-103a-3p, miR-500a-3p, miR-149-5p, miR-1269b, miR-503-5p). Interestingly, miR-103a-3p and miR-149-5p were additionally significantly downregulated in the tumor tissue derived from MIA PaCa-2 RR cells after irradiation with 5 and 10 Gy. In line with this study's findings, other reports show that low miR-149 expression is not only correlated with low survival and poor prognosis, but the overexpression can have a radiosensitizing effect *in vitro* and *in vivo* [192, 193].

While miR-503-3p was downregulated in tumor tissue derived from MIA PaCa-2 RR cells, *in vitro* it showed an upregulation. In other publications investigating miR-503 and its role in radioresistance, it was shown that miR-503 is downregulated in radioresistant cells and the overexpression can render the cells radiosensitive [194, 195]. These results indicate the importance of investigating the deregulation of miRNA not only at the cellular level but also *in vivo*.

Due to their minimally invasive nature, liquid biopsies from, e.g., plasma and serum, have gained attention. Therefore, not only tumor tissues derived from MIA PaCa-2 and MIA PaCa-2 RR cells were sequenced, but also plasma samples were analyzed during this project. Mitchell et al. and others demonstrated that miRNAs are not only stable in plasma, but furthermore, they can serve as biomarkers for the detection of cancer [196, 197]. Using the miRNA profile in the plasma, they were able to distinguish tumor-bearing mice from control mice [196, 197]. In line with their findings, this study showed that the miRNA profile of plasma samples from tumor-bearing mice (either derived from MIA PaCa-2 or MIA PaCa-2 RR) showed clear separation from control mice, i.e., mice without a tumor. Comparing the plasma samples from unirradiated MIA PaCa-2 tumor-bearing mice to MIA PaCa-2 RR tumor-bearing mice, only miR-625-3p was significantly upregulated in the RR tumors. Of note, this miRNA was additionally upregulated in MIA PaCa-2 RR tumors. Recent literature results confirm that this miRNA is associated with resistance to oxaliplatin [198, 199]. Colorectal cancer cells showed an oxaliplatin resistance after overexpression with miR-625 and

furthermore, miR-625 is elevated in colorectal cancer patients not responding to the oxaliplatin treatment [198, 199].

In summary, three miRNAs commonly deregulated in Panc-1 RR and MIA Paca-2 RR cells were found. Furthermore, five miRNAs were deregulated *in vitro* and *in vivo* in MIA PaCa-2 RR cells and tumors, respectively. However, these miRNAs were not the same as the miRNAs deregulated in both cell lines. One reason for this could be that only MIA PaCa-2 and MIA PaCa-2 RR cells were investigated *in vivo* during this project. Interestingly, only miR-625-3p was upregulated in the plasma of MIA PaCa-2 RR tumor-bearing mice. In the literature, some of these deregulated miRNAs were shown to play a role in chemo- or radioresistance.

5. Conclusion and outlook

While surgical resection is still the only possible curative treatment for pancreatic cancer, radiotherapy in combination with chemotherapy could be beneficial for those patients in an advanced stage, where surgery is no longer feasible. However, about 70 % of patients receiving radiation treatment show no response and no overall benefit. The underlying mechanisms are still unknown; therefore, understanding the biological mechanisms involved in the radioresistance is crucial and may ultimately improve the poor treatment outcome in the future.

The overall aim of this study was to investigate the underlying mechanisms contributing to radioresistance in pancreatic cancer. Therefore, two radioresistant human pancreatic cancer cell lines were generated through repeated exposure to gradually increasing fractions of irradiation. The radioresistance was not only confirmed *in vitro* but furthermore validated *in vivo*. The data suggest that reduced levels of ROS and improved DNA repair mechanisms might contribute to the acquired radioresistance. These results encourage further investigation, either the use of inhibitors of DNA damage response molecules or ROS-enhancing drugs in combination with radiotherapy, thereby improving the response to radiotherapy and thus the prognosis of pancreatic cancer patients.

Furthermore, particle therapy, i.e., carbon ion radiotherapy, has emerged as an alternative to conventional x-ray radiotherapy due to its physical and biological benefits [200]. Carbon ion radiotherapy causes more clustered and complex DNA damage, which requires prolonged time to repair. Moreover, it is assumed that the DNA damage by carbon ions is primarily induced directly and that the indirect effect through ROS is only of less importance compared to x-rays [200]. In pancreatic cancer cell lines, it was observed that irradiation with carbon ion showed an enhanced cytotoxic effect compared to x-ray irradiation [201, 202] and the combination with chemotherapy was superior to the combined treatment with x-ray [203]. In clinical studies with locally advanced pancreatic cancer patients treated with carbon ion radiotherapy, the outcome has so far been favorable with limited toxicities [204, 205],

and further clinical studies are in design [206]. The secondary role of ROS for the induction of DNA damage in carbon ion radiotherapy could potentially be beneficial for the treatment of radioresistant tumors, as this study showed that one mechanism leading to radioresistance in pancreatic cancer is the reduced oxidative stress in the radioresistant cell lines and therefore the overall diminishing effect of radiation-induced DNA damage.

Apart from the lower levels of ROS and higher DNA repair capacity in the radioresistant cell lines, migration and invasion capability were differently affected. Whereas one radioresistant cell line showed a decrease in migration and invasion, the other radioresistant cell line exhibited a more aggressive phenotype with enhanced migratory and invasive characteristics. At the time of diagnosis, many pancreatic cancer patients present with metastasis, and therefore have an overall poor prognosis. Further investigations of the mechanisms leading to these opposing characteristics in the radioresistant cell lines might provide newer insights into the progression of pancreatic cancer to metastatic disease.

Furthermore, several differentially expressed miRNAs may play a role in the acquired radioresistance. Investigating the pathways regulated by these miRNAs might offer more insights about radioresistance. In addition, these results warrant further studies of miRNAs as potential biomarkers predicting response to radiotherapy.

The findings of this study constitute a substantial foundation for further investigations leading to a patient-specific biomarker that differentiates radiosensitive from radioresistant tumors and may allow the selective application of radiotherapy in pancreatic cancer patients. Through this strategy the actual benefits of local radiotherapy can be effectively leveraged while simultaneously avoiding overtreatment in patients with radioresistant tumors.

References

[1] The global, regional, and national burden of pancreatic cancer and its attributable risk factors in 195 countries and territories, 1990-2017: a systematic analysis for the Global Burden of Disease Study 2017, Lancet Gastroenterol Hepatol, 4 (2019) 934-947.

[2] M.C.S. Wong, J.Y. Jiang, M. Liang, Y. Fang, M.S. Yeung, J.J.Y. Sung, Global temporal patterns of pancreatic cancer and association with socioeconomic development, Sci Rep, 7 (2017) 3165.

[3] A. McGuigan, P. Kelly, R.C. Turkington, C. Jones, H.G. Coleman, R.S. McCain, Pancreatic cancer: A review of clinical diagnosis, epidemiology, treatment and outcomes, World J Gastroenterol, 24 (2018) 4846-4861.

[4] F. Bray, J. Ferlay, I. Soerjomataram, R.L. Siegel, L.A. Torre, A. Jemal, Global cancer statistics 2018: GLOBOCAN estimates of incidence and mortality worldwide for 36 cancers in 185 countries, CA: a cancer journal for clinicians, 68 (2018) 394-424.

[5] P. Rawla, T. Sunkara, V. Gaduputi, Epidemiology of Pancreatic Cancer: Global Trends, Etiology and Risk Factors, World J Oncol, 10 (2019) 10-27.

[6] L. Rahib, B.D. Smith, R. Aizenberg, A.B. Rosenzweig, J.M. Fleshman, L.M. Matrisian, Projecting cancer incidence and deaths to 2030: the unexpected burden of thyroid, liver, and pancreas cancers in the United States, Cancer Res, 74 (2014) 2913-2921.

[7] A.S. Quante, C. Ming, M. Rottmann, J. Engel, S. Boeck, V. Heinemann, C.B. Westphalen, K. Strauch, Projections of cancer incidence and cancer-related deaths in Germany by 2020 and 2030, Cancer medicine, 5 (2016) 2649-2656.

[8] M. Ilic, I. Ilic, Epidemiology of pancreatic cancer, World J Gastroenterol, 22 (2016) 9694-9705.

[9] M. Korc, C.Y. Jeon, M. Edderkaoui, S.J. Pandol, M.S. Petrov, Tobacco and alcohol as risk factors for pancreatic cancer, Best Pract Res Clin Gastroenterol, 31 (2017) 529-536.

[10] N. Bardeesy, R.A. DePinho, Pancreatic cancer biology and genetics, Nat Rev Cancer, 2 (2002) 897-909.

[11] L. Haeberle, I. Esposito, Pathology of pancreatic cancer, Transl Gastroenterol Hepatol, 4 (2019) 50.

[12] M. Hidalgo, Pancreatic cancer, N Engl J Med, 362 (2010) 1605-1617.

[13] M. Korc, Driver mutations: a roadmap for getting close and personal in pancreatic cancer, Cancer Biol Ther, 10 (2010) 588-591.

[14] J.P.t. Morris, S.C. Wang, M. Hebrok, KRAS, Hedgehog, Wnt and the twisted developmental biology of pancreatic ductal adenocarcinoma, Nat Rev Cancer, 10 (2010) 683-695.

[15] N. Gaianigo, D. Melisi, C. Carbone, EMT and Treatment Resistance in Pancreatic Cancer, Cancers (Basel), 9 (2017).

[16] E.P. DiMagno, H.A. Reber, M.A. Tempero, AGA technical review on the epidemiology, diagnosis, and treatment of pancreatic ductal adenocarcinoma. American Gastroenterological Association, Gastroenterology, 117 (1999) 1464-1484.

[17] S. Keleg, P. Buchler, R. Ludwig, M.W. Buchler, H. Friess, Invasion and metastasis in pancreatic cancer, Mol Cancer, 2 (2003) 14.

[18] B.J. Kenner, Early Detection of Pancreatic Cancer: The Role of Depression and Anxiety as a Precursor for Disease, Pancreas, 47 (2018) 363-367.

[19] A. Vincent, J. Herman, R. Schulick, R.H. Hruban, M. Goggins, Pancreatic cancer, Lancet, 378 (2011) 607-620.

[20] S. Kaur, M.J. Baine, M. Jain, A.R. Sasson, S.K. Batra, Early diagnosis of pancreatic cancer: challenges and new developments, Biomark Med, 6 (2012) 597-612.

[21] E. Dabizzi, M.S. Assef, M. Raimondo, Diagnostic management of pancreatic cancer, Cancers (Basel), 3 (2011) 494-509.

[22] A.S. Takhar, P. Palaniappan, R. Dhingsa, D.N. Lobo, Recent developments in diagnosis of pancreatic cancer, Bmj, 329 (2004) 668-673.

[23] S.E. Combs, D. Habermehl, K.A. Kessel, F. Bergmann, J. Werner, P. Naumann, D. Jager, M.W. Buchler, J. Debus, Prognostic impact of CA 19-9 on outcome after neoadjuvant chemoradiation in patients with locally advanced pancreatic cancer, Ann Surg Oncol, 21 (2014) 2801-2807.

[24] S. Gillen, T. Schuster, C. Meyer Zum Buschenfelde, H. Friess, J. Kleeff, Preoperative/neoadjuvant therapy in pancreatic cancer: a systematic review and meta-analysis of response and resection percentages, PLoS medicine, 7 (2010) e1000267.

[25] M. Brunner, Z. Wu, C. Krautz, C. Pilarsky, R. Grutzmann, G.F. Weber, Current Clinical Strategies of Pancreatic Cancer Treatment and Open Molecular Questions, Int J Mol Sci, 20 (2019).

[26] D.A. Kooby, T.W. Gillespie, Y. Liu, J. Byrd-Sellers, J. Landry, J. Bian, J. Lipscomb, Impact of adjuvant radiotherapy on survival after pancreatic cancer resection: an appraisal of data from the national cancer data base, Ann Surg Oncol, 20 (2013) 3634-3642.

[27] A.G. Morganti, M. Falconi, R.G. van Stiphout, G.C. Mattiucci, S. Alfieri, F.A. Calvo, J.B. Dubois, G. Fastner, J.M. Herman, B.W. Maidment, 3rd, R.C. Miller, W.F. Regine, M. Reni, N.K. Sharma, E. Ippolito, V. Valentini, Multi-institutional pooled analysis on adjuvant chemoradiation in pancreatic cancer, Int J Radiat Oncol Biol Phys, 90 (2014) 911-917.

[28] C.E. Rutter, H.S. Park, C.D. Corso, N.H. Lester-Coll, B.R. Mancini, D.N. Yeboa, K.L. Johung, Addition of radiotherapy to adjuvant chemotherapy is associated with improved overall survival in resected pancreatic adenocarcinoma: An analysis of the National Cancer Data Base, Cancer, 121 (2015) 4141-4149.

[29] A. Sugawara, E. Kunieda, Effect of adjuvant radiotherapy on survival in resected pancreatic cancer: a propensity score surveillance, epidemiology, and end results database analysis, J Surg Oncol, 110 (2014) 960-966.

[30] J.P. Neoptolemos, P. Baker, H. Beger, K. Link, P. Pederzoli, C. Bassi, C. Dervenis, H. Friess, M. Buchler, Progress report. A randomized multicenter European study comparing adjuvant radiotherapy, 6-mo chemotherapy, and combination therapy vs no-adjuvant treatment in resectable pancreatic cancer (ESPAC-1), Int J Pancreatol, 21 (1997) 97-104.

[31] W.C. Liao, K.L. Chien, Y.L. Lin, M.S. Wu, J.T. Lin, H.P. Wang, Y.K. Tu, Adjuvant treatments for resected pancreatic adenocarcinoma: a systematic review and network meta-analysis, The Lancet. Oncology, 14 (2013) 1095-1103.

[32] A. Lambert, L. Schwarz, I. Borbath, A. Henry, J.L. Van Laethem, D. Malka, M. Ducreux, T. Conroy, An update on treatment options for pancreatic adenocarcinoma, Ther Adv Med Oncol, 11 (2019) 1758835919875568.

[33] A.K. Saluja, V. Dudeja, S. Banerjee, Evolution of novel therapeutic options for pancreatic cancer, Curr Opin Gastroenterol, 32 (2016) 401-407.

[34] M.K. Diener, S.E. Combs, M.W. Buchler, Chemoradiotherapy for locally advanced pancreatic cancer, The Lancet. Oncology, 14 (2013) 269-270.

[35] J. Werner, S.E. Combs, C. Springfeld, W. Hartwig, T. Hackert, M.W. Buchler, Advanced-stage pancreatic cancer: therapy options, Nat Rev Clin Oncol, 10 (2013) 323-333.

[36] D. Habermehl, K. Kessel, T. Welzel, H. Hof, A. Abdollahi, F. Bergmann, S. Rieken, J. Weitz, J. Werner, P. Schirmacher, M.W. Buchler, J. Debus, S.E. Combs, Neoadjuvant chemoradiation with Gemcitabine for locally advanced pancreatic cancer, Radiat Oncol, 7 (2012) 28.

[37] S.E. Combs, Individualized radiotherapy (iRT) concepts for locally advanced pancreatic cancer (LAPC): indications and prognostic factors, Langenbecks Arch Surg, 400 (2015) 749-756.

[38] D. Habermehl, I.C. Brecht, F. Bergmann, T. Welzel, S. Rieken, J. Werner, P. Schirmacher, M.W. Buchler, J. Debus, S.E. Combs, Chemoradiation in patients with isolated recurrent pancreatic cancer - therapeutical efficacy and probability of re-resection, Radiat Oncol, 8 (2013) 27.

[39] P.J. Loehrer, Sr., Y. Feng, H. Cardenes, L. Wagner, J.M. Brell, D. Cella, P. Flynn, R.K. Ramanathan, C.H. Crane, S.R. Alberts, A.B. Benson, 3rd, Gemcitabine alone versus gemcitabine plus radiotherapy in patients with locally advanced pancreatic cancer: an Eastern Cooperative Oncology Group trial, J Clin Oncol, 29 (2011) 4105-4112.

[40] B. Chauffert, F. Mornex, F. Bonnetain, P. Rougier, C. Mariette, O. Bouche, J.F. Bosset, T. Aparicio, L. Mineur, A. Azzedine, P. Hammel, J. Butel, N. Stremsdoerfer, P. Maingon, L. Bedenne, Phase III trial comparing intensive induction chemoradiotherapy (60 Gy, infusional 5-FU and intermittent cisplatin) followed by maintenance gemcitabine with gemcitabine alone for locally advanced unresectable pancreatic cancer. Definitive results of the 2000-01 FFCD/SFRO study, Ann Oncol, 19 (2008) 1592-1599.

[41] P. Hammel, F. Huguet, J.L. van Laethem, D. Goldstein, B. Glimelius, P. Artru, I. Borbath, O. Bouche, J. Shannon, T. Andre, L. Mineur, B. Chibaudel, F. Bonnetain, C. Louvet, Effect of Chemoradiotherapy vs Chemotherapy on Survival in Patients With Locally Advanced Pancreatic Cancer Controlled After 4 Months of Gemcitabine With or Without Erlotinib: The LAP07 Randomized Clinical Trial, Jama, 315 (2016) 1844-1853.

[42] P. Seshacharyulu, M.J. Baine, J.J. Souchek, M. Menning, S. Kaur, Y. Yan, M.M. Ouellette, M. Jain, C. Lin, S.K. Batra, Biological determinants of radioresistance and their remediation in pancreatic cancer, Biochimica et biophysica acta. Reviews on cancer, 1868 (2017) 69-92.

[43] J. Cros, J. Raffenne, A. Couvelard, N. Pote, Tumor Heterogeneity in Pancreatic Adenocarcinoma, Pathobiology : journal of immunopathology, molecular and cellular biology, 85 (2018) 64-71.

[44] H.R. Cardenes, A.M. Moore, C.S. Johnson, M. Yu, P. Helft, E.G. Chiorean, J. Vinson, T.J. Howard, A.W. Stephens, D.F. Tai, P.J. Loehrer, Sr., A phase II study of gemcitabine in combination with radiation therapy in patients with localized, unresectable, pancreatic cancer: a Hoosier Oncology Group study, Am J Clin Oncol, 34 (2011) 460-465.

[45] C.J. McGinn, M.M. Zalupski, I. Shureiqi, J.M. Robertson, F.E. Eckhauser, D.C. Smith, D. Brown, G. Hejna, M. Strawderman, D. Normolle, T.S. Lawrence, Phase I trial of radiation dose escalation with concurrent weekly full-dose gemcitabine in patients with advanced pancreatic cancer, J Clin Oncol, 19 (2001) 4202-4208.

[46] J.D. Murphy, S. Adusumilli, K.A. Griffith, M.E. Ray, M.M. Zalupski, T.S. Lawrence, E. Ben-Josef, Full-dose gemcitabine and concurrent radiotherapy for unresectable pancreatic cancer, Int J Radiat Oncol Biol Phys, 68 (2007) 801-808.

[47] R.A. Wolff, D.B. Evans, D.M. Gravel, R. Lenzi, P.W. Pisters, J.E. Lee, N.A. Janjan, C. Charnsangavej, J.L. Abbruzzese, Phase I trial of gemcitabine combined with radiation for the treatment of locally advanced pancreatic adenocarcinoma, Clin Cancer Res, 7 (2001) 2246-2253.

[48] R. Baskar, J. Dai, N. Wenlong, R. Yeo, K.W. Yeoh, Biological response of cancer cells to radiation treatment, Frontiers in molecular biosciences, 1 (2014) 24.

[49] P.P. Connell, S. Hellman, Advances in radiotherapy and implications for the next century: a historical perspective, Cancer Res, 69 (2009) 383-392.

[50] J. Bernier, E.J. Hall, A. Giaccia, Radiation oncology: a century of achievements, Nat Rev Cancer, 4 (2004) 737-747.

[51] G. Delaney, S. Jacob, C. Featherstone, M. Barton, The role of radiotherapy in cancer treatment: estimating optimal utilization from a review of evidence-based clinical guidelines, Cancer, 104 (2005) 1129-1137.

[52] A.C. Begg, F.A. Stewart, C. Vens, Strategies to improve radiotherapy with targeted drugs, Nat Rev Cancer, 11 (2011) 239-253.

[53] S.S. Wallace, Enzymatic processing of radiation-induced free radical damage in DNA, Radiat Res, 150 (1998) S60-79.

[54] J.F. Ward, DNA damage produced by ionizing radiation in mammalian cells: identities, mechanisms of formation, and reparability, Prog Nucleic Acid Res Mol Biol, 35 (1988) 95-125.

[55] W.P. Roos, B. Kaina, DNA damage-induced cell death: from specific DNA lesions to the DNA damage response and apoptosis, Cancer Lett, 332 (2013) 237-248.

[56] L. Chaiswing, H.L. Weiss, R.D. Jayswal, D.K.S. Clair, N. Kyprianou, Profiles of Radioresistance Mechanisms in Prostate Cancer, Crit Rev Oncog, 23 (2018) 39-67.

[57] D. Trachootham, J. Alexandre, P. Huang, Targeting cancer cells by ROS-mediated mechanisms: a radical therapeutic approach?, Nat Rev Drug Discov, 8 (2009) 579-591.

[58] A. Schulz, F. Meyer, A. Dubrovska, K. Borgmann, Cancer Stem Cells and Radioresistance: DNA Repair and Beyond, Cancers (Basel), 11 (2019).

[59] J. Falck, J. Coates, S.P. Jackson, Conserved modes of recruitment of ATM, ATR and DNA-PKcs to sites of DNA damage, Nature, 434 (2005) 605-611.

[60] A.J. Hartlerode, R. Scully, Mechanisms of double-strand break repair in somatic mammalian cells, The Biochemical journal, 423 (2009) 157-168.

[61] G. Borrego-Soto, R. Ortiz-Lopez, A. Rojas-Martinez, Ionizing radiation-induced DNA injury and damage detection in patients with breast cancer, Genet Mol Biol, 38 (2015) 420-432.

[62] E.J. Hall, A.J. Giaccia, Radiobiology for the radiologist, 6th ed., Lippincott Williams & Wilkins, Philadelphia, 2006.

[63] K. Rycaj, D.G. Tang, Cancer stem cells and radioresistance, Int J Radiat Biol, 90 (2014) 615-621.

[64] M. Baumann, M. Krause, R. Hill, Exploring the role of cancer stem cells in radioresistance, Nat Rev Cancer, 8 (2008) 545-554.

[65] S. Das, S.K. Batra, Pancreatic cancer metastasis: are we being pre-EMTed?, Curr Pharm Des, 21 (2015) 1249-1255.

[66] J. Fares, M.Y. Fares, H.H. Khachfe, H.A. Salhab, Y. Fares, Molecular principles of metastasis: a hallmark of cancer revisited, Signal Transduct Target Ther, 5 (2020) 28.

[67] E. Sahai, Illuminating the metastatic process, Nat Rev Cancer, 7 (2007) 737-749.

[68] D. Ansari, H. Friess, M. Bauden, J. Samnegard, R. Andersson, Pancreatic cancer: disease dynamics, tumor biology and the role of the microenvironment, Oncotarget, 9 (2018) 6644-6651.

[69] T. Arumugam, V. Ramachandran, K.F. Fournier, H. Wang, L. Marquis, J.L. Abbruzzese, G.E. Gallick, C.D. Logsdon, D.J. McConkey, W. Choi, Epithelial to mesenchymal transition contributes to drug resistance in pancreatic cancer, Cancer Res, 69 (2009) 5820-5828.

[70] R.C. Lee, R.L. Feinbaum, V. Ambros, The C. elegans heterochronic gene lin-4 encodes small RNAs with antisense complementarity to lin-14, Cell, 75 (1993) 843-854.

[71] A. Esquela-Kerscher, F.J. Slack, Oncomirs - microRNAs with a role in cancer, Nat Rev Cancer, 6 (2006) 259-269.

[72] M. Rawat, K. Kadian, Y. Gupta, A. Kumar, P.S.G. Chain, O. Kovbasnjuk, S. Kumar, G. Parasher, MicroRNA in Pancreatic Cancer: From Biology to Therapeutic Potential, Genes, 10 (2019).

[73] G.A. Calin, C.D. Dumitru, M. Shimizu, R. Bichi, S. Zupo, E. Noch, H. Aldler, S. Rattan, M. Keating, K. Rai, L. Rassenti, T. Kipps, M. Negrini, F. Bullrich, C.M. Croce, Frequent deletions and down-regulation of micro- RNA genes miR15 and miR16 at 13q14 in chronic lymphocytic leukemia, Proc Natl Acad Sci U S A, 99 (2002) 15524-15529.

[74] J.Y. Park, J. Helm, D. Coppola, D. Kim, M. Malafa, S.J. Kim, MicroRNAs in pancreatic ductal adenocarcinoma, World J Gastroenterol, 17 (2011) 817-827.

[75] K. Yonemori, H. Kurahara, K. Maemura, S. Natsugoe, MicroRNA in pancreatic cancer, J Hum Genet, (2016).

[76] C. Vorvis, M. Koutsioumpa, D. Iliopoulos, Developments in miRNA gene signaling pathways in pancreatic cancer, Future Oncol, 12 (2016) 1135-1150.

[77] O. Brunetti, A. Russo, A. Scarpa, D. Santini, M. Reni, A. Bittoni, A. Azzariti, G. Aprile, S. Delcuratolo, M. Signorile, A. Gnoni, L. Palermo, V. Lorusso, S. Cascinu, N. Silvestris, MicroRNA in pancreatic adenocarcinoma: predictive/prognostic biomarkers or therapeutic targets?, Oncotarget, 6 (2015) 23323-23341.

[78] N.A. Schultz, C. Dehlendorff, B.V. Jensen, J.K. Bjerregaard, K.R. Nielsen, S.E. Bojesen, D. Calatayud, S.E. Nielsen, M. Yilmaz, N.H. Hollander, K.K. Andersen, J.S. Johansen, MicroRNA biomarkers in whole blood for detection of pancreatic cancer, Jama, 311 (2014) 392-404.

[79] K. Qu, X. Zhang, T. Lin, T. Liu, Z. Wang, S. Liu, L. Zhou, J. Wei, H. Chang, K. Li, Z. Wang, C. Liu, Z. Wu, Circulating miRNA-21-5p as a diagnostic biomarker for pancreatic cancer: evidence from comprehensive miRNA expression profiling analysis and clinical validation, Sci Rep, 7 (2017) 1692.

[80] J. Liu, J. Gao, Y. Du, Z. Li, Y. Ren, J. Gu, X. Wang, Y. Gong, W. Wang, X. Kong, Combination of plasma microRNAs with serum CA19-9 for early detection of pancreatic cancer, Int J Cancer, 131 (2012) 683-691.

[81] L. Gao, S.B. He, D.C. Li, Effects of miR-16 plus CA19-9 detections on pancreatic cancer diagnostic performance, Clin Lab, 60 (2014) 73-77.

[82] T. Greither, L.F. Grochola, A. Udelnow, C. Lautenschlager, P. Wurl, H. Taubert, Elevated expression of microRNAs 155, 203, 210 and 222 in pancreatic tumors is associated with poorer survival, Int J Cancer, 126 (2010) 73-80.

[83] M. Dillhoff, J. Liu, W. Frankel, C. Croce, M. Bloomston, MicroRNA-21 is overexpressed in pancreatic cancer and a potential predictor of survival, J Gastrointest Surg, 12 (2008) 2171-2176.

[84] M. Bloomston, W.L. Frankel, F. Petrocca, S. Volinia, H. Alder, J.P. Hagan, C.G. Liu, D. Bhatt, C. Taccioli, C.M. Croce, MicroRNA expression patterns to differentiate pancreatic adenocarcinoma from normal pancreas and chronic pancreatitis, JAMA, 297 (2007) 1901-1908.

[85] T. Kawaguchi, S. Komatsu, D. Ichikawa, R. Morimura, M. Tsujiura, H. Konishi, H. Takeshita, H. Nagata, T. Arita, S. Hirajima, A. Shiozaki, H. Ikoma, K. Okamoto, T. Ochiai, H. Taniguchi, E. Otsuji, Clinical impact of circulating miR-221 in plasma of patients with pancreatic cancer, Br J Cancer, 108 (2013) 361-369.

[86] P. Wang, J. Zhang, L. Zhang, Z. Zhu, J. Fan, L. Chen, L. Zhuang, J. Luo, H. Chen, L. Liu, Z. Chen, Z. Meng, MicroRNA 23b regulates autophagy associated with radioresistance of pancreatic cancer cells, Gastroenterology, 145 (2013) 1133-1143 e1112.

[87] S.L. Wang, Y.J. Wang, S.M. Wu, Z. Yuan, H.M. Du, X. Liu, X.K. Zhu, Identification of unique microRNAs associated with pancreatic cancer radioresistance using deep sequencing, Transl Cancer Res, 7 (2018) 828-838.

[88] F. Wei, Y. Liu, Y. Guo, A. Xiang, G. Wang, X. Xue, Z. Lu, miR-99b-targeted mTOR induction contributes to irradiation resistance in pancreatic cancer, Mol Cancer, 12 (2013) 81.

[89] X. Zhang, H. Shi, S. Lin, M. Ba, S. Cui, MicroRNA-216a enhances the radiosensitivity of pancreatic cancer cells by inhibiting beclin-1-mediated autophagy, Oncol Rep, 34 (2015) 1557-1564.

[90] E.L. Deer, J. Gonzalez-Hernandez, J.D. Coursen, J.E. Shea, J. Ngatia, C.L. Scaife, M.A. Firpo, S.J. Mulvihill, Phenotype and genotype of pancreatic cancer cell lines, Pancreas, 39 (2010) 425-435.

[91] P.S. Moore, B. Sipos, S. Orlandini, C. Sorio, F.X. Real, N.R. Lemoine, T. Gress, C. Bassi, G. Kloppel, H. Kalthoff, H. Ungefroren, M. Lohr, A. Scarpa, Genetic profile of 22 pancreatic carcinoma cell lines. Analysis of K-ras, p53, p16 and DPC4/Smad4, Virchows Arch, 439 (2001) 798-802.

[92] J.J. Souchek, M.J. Baine, C. Lin, S. Rachagani, S. Gupta, S. Kaur, K. Lester, D. Zheng, S. Chen, L. Smith, A. Lazenby, S.L. Johansson, M. Jain, S.K. Batra, Unbiased analysis of pancreatic cancer radiation resistance reveals cholesterol biosynthesis as a novel target for radiosensitisation, Br J Cancer, 111 (2014) 1139-1149.

[93] J. Koster, S. Rahmann, Snakemake-a scalable bioinformatics workflow engine, Bioinformatics, 34 (2018) 3600.

[94] A.M. Bolger, M. Lohse, B. Usadel, Trimmomatic: a flexible trimmer for Illumina sequence data, Bioinformatics, 30 (2014) 2114-2120.

[95] A. Dobin, C.A. Davis, F. Schlesinger, J. Drenkow, C. Zaleski, S. Jha, P. Batut, M. Chaisson, T.R. Gingeras, STAR: ultrafast universal RNA-seq aligner, Bioinformatics, 29 (2013) 15-21.

[96] S. Anders, P.T. Pyl, W. Huber, HTSeq--a Python framework to work with high-throughput sequencing data, Bioinformatics, 31 (2015) 166-169.

[97] G.R. Warnes, B. Bolker, L. Bonebakker, R. Gentleman, W.H.A. Liaw, T. Lumley, M. Maechler, A. Magnusson, S. Moeller, M. Schwartz, B. Venables, gplots: Various R Programming Tools for Plotting Data. R package version 3.0.1. https://CRAN.R-project.org/package=gplots, (2016).

[98] R. Gentleman, V. Carey, W. Huber, F. Hahne, genefilter: genefilter: methods for filtering genes from high-throughput experiments. , (2017).

[99] M. Horikoshi, Y. Tang, ggfortify: Data Visualization Tools for Statistical Analysis Results. https://CRAN.R-project.org/package=ggfortify., (2018).

[100] E. Neuwirth, RColorBrewer: ColorBrewer Palettes. R package version 1.1-2. https://CRAN.R-project.org/package=RColorBrewer, (2014).

[101] K. Blighe, S. Rana, M. Lewis, EnhancedVolcano: Publication-ready volcano plots with enhanced colouring and labeling. R package version 1.4.0, https://github.com/kevinblighe/EnhancedVolcano., (2019).

[102] H. Chen, VennDiagram: Generate High-Resolution Venn and Euler Plots. R package version 1.6.20. https://CRAN.R-project.org/package=VennDiagram, (2018).

[103] D. Buschmann, B. Kirchner, S. Hermann, M. Marte, C. Wurmser, F. Brandes, S. Kotschote, M. Bonin, O.K. Steinlein, M.W. Pfaffl, G. Schelling, M. Reithmair, Evaluation of serum extracellular vesicle isolation methods for profiling miRNAs by next-generation sequencing, Journal of extracellular vesicles, 7 (2018) 1481321.

[104] M. Spornraft, B. Kirchner, B. Haase, V. Benes, M.W. Pfaffl, I. Riedmaier, Optimization of extraction of circulating RNAs from plasma--enabling small RNA sequencing, PLoS One, 9 (2014) e107259.

[105] M.I. Love, W. Huber, S. Anders, Moderated estimation of fold change and dispersion for RNA-seq data with DESeq2, Genome biology, 15 (2014) 550.

[106] A. Kramer, J. Green, J. Pollard, Jr., S. Tugendreich, Causal analysis approaches in Ingenuity Pathway Analysis, Bioinformatics, 30 (2014) 523-530.

[107] L. Nguyen, S. Dobiasch, G. Schneider, R.M. Schmid, O. Azimzadeh, K. Kanev, D. Buschmann, M.W. Pfaffl, S. Bartzsch, T.E. Schmid, D. Schilling, S.E. Combs, Impact of DNA repair and reactive oxygen species levels on radioresistance in pancreatic cancer, [submitted], (2020).

[108] S.E. Combs, D. Habermehl, K. Kessel, F. Bergmann, J. Werner, I. Brecht, P. Schirmacher, D. Jager, M.W. Buchler, J. Debus, Intensity modulated radiotherapy as neoadjuvant chemoradiation for the treatment of patients with locally advanced pancreatic cancer. Outcome analysis and comparison with a 3D-treated patient cohort, Strahlentherapie und Onkologie : Organ der Deutschen Rontgengesellschaft ... [et al], 189 (2013) 738-744.

[109] L. Hazard, J.D. Tward, A. Szabo, D.C. Shrieve, Radiation therapy is associated with improved survival in patients with pancreatic adenocarcinoma: results of a study from the Surveillance, Epidemiology, and End Results (SEER) registry data, Cancer, 110 (2007) 2191-2201.

[110] S. Henness, M.W. Davey, R.M. Harvie, J. Banyer, V. Wasinger, G. Corthals, R.A. Davey, Changes in gene expression associated with stable drug and radiation resistance in small cell lung cancer cells are similar to those caused by a single X-ray dose, Radiat Res, 161 (2004) 495-503.

[111] R. Gomez-Casal, M.W. Epperly, H. Wang, D.A. Proia, J.S. Greenberger, V. Levina, Radioresistant human lung adenocarcinoma cells that survived multiple fractions of ionizing radiation are sensitive to HSP90 inhibition, Oncotarget, 6 (2015) 44306-44322.

[112] W. Guo, L. Xie, L. Zhao, Y. Zhao, mRNA and microRNA expression profiles of radioresistant NCI-H520 non-small cell lung cancer cells, Mol Med Rep, 12 (2015) 1857-1867.

[113] J. Mihatsch, M. Toulany, P.M. Bareiss, S. Grimm, C. Lengerke, R. Kehlbach, H.P. Rodemann, Selection of radioresistant tumor cells and presence of ALDH1 activity in vitro, Radiotherapy and oncology : journal of the European Society for Therapeutic Radiology and Oncology, 99 (2011) 300-306.

[114] Z. Jing, L. Gong, C.Y. Xie, L. Zhang, H.F. Su, X. Deng, S.X. Wu, Reverse resistance to radiation in KYSE-150R esophageal carcinoma cell after epidermal growth factor receptor signal pathway inhibition by cetuximab, Radiotherapy and oncology : journal of the European Society for Therapeutic Radiology and Oncology, 93 (2009) 468-473.

[115] N. Lynam-Lennon, J.V. Reynolds, G.P. Pidgeon, J. Lysaght, L. Marignol, S.G. Maher, Alterations in DNA repair efficiency are involved in the radioresistance of esophageal adenocarcinoma, Radiat Res, 174 (2010) 703-711.

[116] J.A. Yang, B.H. Liu, L.M. Shao, Z.T. Guo, Q. Yang, L.Q. Wu, B.W. Ji, X.N. Zhu, S.Q. Zhang, C.J. Li, Q.X. Chen, LRIG1 enhances the radiosensitivity of radioresistant human glioblastoma U251 cells via attenuation of the EGFR/Akt signaling pathway, Int J Clin Exp Pathol, 8 (2015) 3580-3590.

[117] J.S. Kim, J.W. Chang, H.S. Yun, K.M. Yang, E.H. Hong, D.H. Kim, H.D. Um, K.H. Lee, S.J. Lee, S.G. Hwang, Chloride intracellular channel 1 identified using proteomic analysis plays an important role in the radiosensitivity of HEp-2 cells via reactive oxygen species production, Proteomics, 10 (2010) 2589-2604.

[118] Y. Kuwahara, L. Li, T. Baba, H. Nakagawa, T. Shimura, Y. Yamamoto, Y. Ohkubo, M. Fukumoto, Clinically relevant radioresistant cells efficiently repair DNA double-strand breaks induced by X-rays, Cancer Sci, 100 (2009) 747-752.

[119] N. McDermott, A. Meunier, B. Mooney, G. Nortey, C. Hernandez, S. Hurley, N. Lynam-Lennon, S.H. Barsoom, K.J. Bowman, B. Marples, G.D. Jones, L. Marignol, Fractionated radiation exposure amplifies the radioresistant nature of prostate cancer cells, Sci Rep, 6 (2016) 34796.

[120] T. Wang, D. Tamae, T. LeBon, J.E. Shively, Y. Yen, J.J. Li, The role of peroxiredoxin II in radiation-resistant MCF-7 breast cancer cells, Cancer Res, 65 (2005) 10338-10346.

[121] M. Gray, A.K. Turnbull, C. Ward, J. Meehan, C. Martinez-Perez, M. Bonello, L.Y. Pang, S.P. Langdon, I.H. Kunkler, A. Murray, D. Argyle, Development and characterisation of acquired radioresistant breast cancer cell lines, Radiat Oncol, 14 (2019) 64.

[122] J. Russell, T.E. Wheldon, P. Stanton, A radioresistant variant derived from a human neuroblastoma cell line is less prone to radiation-induced apoptosis, Cancer Res, 55 (1995) 4915-4921.

[123] S. Skvortsov, C.R. Jimenez, J.C. Knol, P. Eichberger, B. Schiestl, P. Debbage, I. Skvortsova, P. Lukas, Radioresistant head and neck squamous cell carcinoma cells: intracellular signaling, putative biomarkers for tumor recurrences and possible

therapeutic targets, Radiotherapy and oncology : journal of the European Society for Therapeutic Radiology and Oncology, 101 (2011) 177-182.

[124] N. McDermott, A. Meunier, T.H. Lynch, D. Hollywood, L. Marignol, Isogenic radiation resistant cell lines: development and validation strategies, Int J Radiat Biol, 90 (2014) 115-126.

[125] A. Makohon-Moore, C.A. Iacobuzio-Donahue, Pancreatic cancer biology and genetics from an evolutionary perspective, Nat Rev Cancer, 16 (2016) 553-565.

[126] M. Cojoc, C. Peitzsch, I. Kurth, F. Trautmann, L.A. Kunz-Schughart, G.D. Telegeev, E.A. Stakhovsky, J.R. Walker, K. Simin, S. Lyle, S. Fuessel, K. Erdmann, M.P. Wirth, M. Krause, M. Baumann, A. Dubrovska, Aldehyde Dehydrogenase Is Regulated by beta-Catenin/TCF and Promotes Radioresistance in Prostate Cancer Progenitor Cells, Cancer Res, 75 (2015) 1482-1494.

[127] N. Lynam-Lennon, S. Heavey, G. Sommerville, B.A. Bibby, B. Ffrench, J. Quinn, C. Gasch, J.J. O'Leary, M.F. Gallagher, J.V. Reynolds, S.G. Maher, MicroRNA-17 is downregulated in esophageal adenocarcinoma cancer stem-like cells and promotes a radioresistant phenotype, Oncotarget, 8 (2017) 11400-11413.

[128] T.M. Pawlik, K. Keyomarsi, Role of cell cycle in mediating sensitivity to radiotherapy, Int J Radiat Oncol Biol Phys, 59 (2004) 928-942.

[129] R. Hamacher, R.M. Schmid, D. Saur, G. Schneider, Apoptotic pathways in pancreatic ductal adenocarcinoma, Mol Cancer, 7 (2008) 64.

[130] J.M. Brown, L.D. Attardi, The role of apoptosis in cancer development and treatment response, Nat Rev Cancer, 5 (2005) 231-237.

[131] T.T. Paull, E.P. Rogakou, V. Yamazaki, C.U. Kirchgessner, M. Gellert, W.M. Bonner, A critical role for histone H2AX in recruitment of repair factors to nuclear foci after DNA damage, Curr Biol, 10 (2000) 886-895.

[132] P.L. Olive, J.P. Banath, Phosphorylation of histone H2AX as a measure of radiosensitivity, Int J Radiat Oncol Biol Phys, 58 (2004) 331-335.

[133] E.P. Rogakou, D.R. Pilch, A.H. Orr, V.S. Ivanova, W.M. Bonner, DNA double-stranded breaks induce histone H2AX phosphorylation on serine 139, J Biol Chem, 273 (1998) 5858-5868.

[134] J.L. Schwartz, J. Rotmensch, S. Giovanazzi, M.B. Cohen, R.R. Weichselbaum, Faster repair of DNA double-strand breaks in radioresistant human tumor cells, Int J Radiat Oncol Biol Phys, 15 (1988) 907-912.

[135] L.I. de Llobet, M. Baro, A. Figueras, I. Modolell, M.V. Da Silva, P. Munoz, A. Navarro, R. Mesia, J. Balart, Development and characterization of an isogenic cell line with a radioresistant phenotype, Clinical & translational oncology : official publication of the Federation of Spanish Oncology Societies and of the National Cancer Institute of Mexico, 15 (2013) 189-197.

[136] K.H. Dittmann, M.C. Rothmund, A. Paasch, C. Mayer, B. Fehrenbacher, M. Schaller, K. Frauenstein, E. Fritsche, T. Haarmann-Stemmann, A. Braeuning, H.P. Rodemann, The nuclear aryl hydocarbon receptor is involved in regulation of DNA repair and cell survival following treatment with ionizing radiation, Toxicology letters, 240 (2016) 122-129.

[137] N. Hosoya, K. Miyagawa, Targeting DNA damage response in cancer therapy, Cancer Sci, 105 (2014) 370-388.

[138] M.A. Morgan, L.A. Parsels, L. Zhao, J.D. Parsels, M.A. Davis, M.C. Hassan, S. Arumugarajah, L. Hylander-Gans, D. Morosini, D.M. Simeone, C.E. Canman, D.P. Normolle, S.D. Zabludoff, J. Maybaum, T.S. Lawrence, Mechanism of radiosensitization by the Chk1/2 inhibitor AZD7762 involves abrogation of the G2 checkpoint and inhibition of homologous recombinational DNA repair, Cancer Res, 70 (2010) 4972-4981.

[139] C.G. Engelke, L.A. Parsels, Y. Qian, Q. Zhang, D. Karnak, J.R. Robertson, D.M. Tanska, D. Wei, M.A. Davis, J.D. Parsels, L. Zhao, J.K. Greenson, T.S. Lawrence, J. Maybaum, M.A. Morgan, Sensitization of pancreatic cancer to chemoradiation by the Chk1 inhibitor MK8776, Clin Cancer Res, 19 (2013) 4412-4421.

[140] P.A. Riley, Free radicals in biology: oxidative stress and the effects of ionizing radiation, Int J Radiat Biol, 65 (1994) 27-33.

[141] S. Sozzani, D. Bosisio, A. Mantovani, P. Ghezzi, Linking stress, oxidation and the chemokine system, Eur J Immunol, 35 (2005) 3095-3098.

[142] K.A. Connolly, B.A. Belt, N.M. Figueroa, A. Murthy, A. Patel, M. Kim, E.M. Lord, D.C. Linehan, S.A. Gerber, Increasing the efficacy of radiotherapy by modulating the CCR2/CCR5 chemokine axes, Oncotarget, 7 (2016) 86522-86535.

[143] A. Kalbasi, C. Komar, G.M. Tooker, M. Liu, J.W. Lee, W.L. Gladney, E. Ben-Josef, G.L. Beatty, Tumor-Derived CCL2 Mediates Resistance to Radiotherapy in Pancreatic Ductal Adenocarcinoma, Clin Cancer Res, 23 (2017) 137-148.

[144] D.J. Garry, P.P. Mammen, Molecular insights into the functional role of myoglobin, Adv Exp Med Biol, 618 (2007) 181-193.

[145] H. Wu, J. Yu, D. Kong, Y. Xu, Z. Zhang, J. Shui, Z. Li, H. Luo, K. Wang, Population and singlecell transcriptome analyses reveal diverse transcriptional changes associated with radioresistance in esophageal squamous cell carcinoma, Int J Oncol, 55 (2019) 1237-1248.

[146] X.P. Feng, H. Yi, M.Y. Li, X.H. Li, B. Yi, P.F. Zhang, C. Li, F. Peng, C.E. Tang, J.L. Li, Z.C. Chen, Z.Q. Xiao, Identification of biomarkers for predicting nasopharyngeal carcinoma response to radiotherapy by proteomics, Cancer Res, 70 (2010) 3450-3462.

[147] A.K. Holley, L. Miao, D.K. St Clair, W.H. St Clair, Redox-modulated phenomena and radiation therapy: the central role of superoxide dismutases, Antioxidants & redox signaling, 20 (2014) 1567-1589.

[148] M. Rojo de la Vega, E. Chapman, D.D. Zhang, NRF2 and the Hallmarks of Cancer, Cancer Cell, 34 (2018) 21-43.

[149] P. Basak, P. Sadhukhan, P. Sarkar, P.C. Sil, Perspectives of the Nrf-2 signaling pathway in cancer progression and therapy, Toxicol Rep, 4 (2017) 306-318.

[150] H.K. Bryan, A. Olayanju, C.E. Goldring, B.K. Park, The Nrf2 cell defence pathway: Keap1-dependent and -independent mechanisms of regulation, Biochemical pharmacology, 85 (2013) 705-717.

[151] H.C. Huang, T. Nguyen, C.B. Pickett, Phosphorylation of Nrf2 at Ser-40 by protein kinase C regulates antioxidant response element-mediated transcription, J Biol Chem, 277 (2002) 42769-42774.

[152] S.N. Rodman, J.M. Spence, T.J. Ronnfeldt, Y. Zhu, S.R. Solst, R.A. O'Neill, B.G. Allen, X. Guan, D.R. Spitz, M.A. Fath, Enhancement of Radiation Response in Breast Cancer Stem Cells by Inhibition of Thioredoxin- and Glutathione-Dependent Metabolism, Radiat Res, 186 (2016) 385-395.

[153] S. Kakolyris, A. Giatromanolaki, M. Koukourakis, G. Powis, J. Souglakos, E. Sivridis, V. Georgoulias, K.C. Gatter, A.L. Harris, Thioredoxin expression is associated with lymph node status and prognosis in early operable non-small cell lung cancer, Clin Cancer Res, 7 (2001) 3087-3091.

[154] M.H. Raza, S. Siraj, A. Arshad, U. Waheed, F. Aldakheel, S. Alduraywish, M. Arshad, ROS-modulated therapeutic approaches in cancer treatment, Journal of cancer research and clinical oncology, 143 (2017) 1789-1809.

[155] H. Wang, S. Bouzakoura, S. de Mey, H. Jiang, K. Law, I. Dufait, C. Corbet, V. Verovski, T. Gevaert, O. Feron, D. Van den Berge, G. Storme, M. De Ridder, Auranofin radiosensitizes tumor cells through targeting thioredoxin reductase and resulting overproduction of reactive oxygen species, Oncotarget, 8 (2017) 35728-35742.

[156] N. Sasano, A. Enomoto, Y. Hosoi, Y. Katsumura, Y. Matsumoto, K. Shiraishi, K. Miyagawa, H. Igaki, K. Nakagawa, Free radical scavenger edaravone suppresses x-ray-induced apoptosis through p53 inhibition in MOLT-4 cells, J Radiat Res, 48 (2007) 495-503.

[157] K. Anzai, M. Furuse, A. Yoshida, A. Matsuyama, T. Moritake, K. Tsuboi, N. Ikota, In vivo radioprotection of mice by 3-methyl-1-phenyl-2-pyrazolin-5-one (edaravone; Radicut), a clinical drug, J Radiat Res, 45 (2004) 319-323.

[158] J. Abel, T. Haarmann-Stemmann, An introduction to the molecular basics of aryl hydrocarbon receptor biology, Biol Chem, 391 (2010) 1235-1248.

[159] L. Torrente, C. Sanchez, R. Moreno, S. Chowdhry, P. Cabello, K. Isono, H. Koseki, T. Honda, J.D. Hayes, A.T. Dinkova-Kostova, L. de la Vega, Crosstalk between NRF2 and HIPK2 shapes cytoprotective responses, Oncogene, 36 (2017) 6204-6212.

[160] S.C. Liu, N.M. Tsang, W.C. Chiang, K.P. Chang, C. Hsueh, Y. Liang, J.L. Juang, K.P. Chow, Y.S. Chang, Leukemia inhibitory factor promotes nasopharyngeal carcinoma progression and radioresistance, J Clin Invest, 123 (2013) 5269-5283.

[161] C.L. Tsai, F.M. Hsu, K.Y. Tzen, W.L. Liu, A.L. Cheng, J.C. Cheng, Sonic Hedgehog inhibition as a strategy to augment radiosensitivity of hepatocellular carcinoma, J Gastroenterol Hepatol, 30 (2015) 1317-1324.

[162] A. Adamska, R. Ferro, R. Lattanzio, E. Capone, A. Domenichini, V. Damiani, G. Chiorino, B.G. Akkaya, K.J. Linton, V. De Laurenzi, G. Sala, M. Falasca, ABCC3 is a novel target for the treatment of pancreatic cancer, Adv Biol Regul, 73 (2019) 100634.

[163] Y. Feng, L. Zhou, X. Sun, Q. Li, Homeodomain-interacting protein kinase 2 (HIPK2): a promising target for anti-cancer therapies, Oncotarget, 8 (2017) 20452-20461.

[164] Y.J. Chen, C.P. Lin, M.L. Hsu, H.R. Shieh, N.K. Chao, K.S. Chao, Sonic hedgehog signaling protects human hepatocellular carcinoma cells against ionizing radiation in an autocrine manner, Int J Radiat Oncol Biol Phys, 80 (2011) 851-859.

[165] Z. Yu, C. Zhang, H. Wang, J. Xing, H. Gong, E. Yu, W. Zhang, X. Zhang, G. Cao, C. Fu, Multidrug resistance-associated protein 3 confers resistance to chemoradiotherapy for rectal cancer by regulating reactive oxygen species and caspase-3-dependent apoptotic pathway, Cancer Lett, 353 (2014) 182-193.

[166] C.F. von Essen, Radiation enhancement of metastasis: a review, Clinical & experimental metastasis, 9 (1991) 77-104.

[167] C. Moncharmont, A. Levy, J.B. Guy, A.T. Falk, M. Guilbert, J.C. Trone, G. Alphonse, M. Gilormini, D. Ardail, R.A. Toillon, C. Rodriguez-Lafrasse, N. Magne, Radiation-enhanced cell migration/invasion process: a review, Critical reviews in oncology/hematology, 92 (2014) 133-142.

[168] M. Fujita, Y. Otsuka, S. Yamada, M. Iwakawa, T. Imai, X-ray irradiation and Rho-kinase inhibitor additively induce invasiveness of the cells of the pancreatic cancer line, MIAPaCa-2, which exhibits mesenchymal and amoeboid motility, Cancer Sci, 102 (2011) 792-798.

[169] L.W. Qian, K. Mizumoto, T. Urashima, E. Nagai, N. Maehara, N. Sato, M. Nakajima, M. Tanaka, Radiation-induced increase in invasive potential of human pancreatic cancer cells and its blockade by a matrix metalloproteinase inhibitor, CGS27023, Clin Cancer Res, 8 (2002) 1223-1227.

[170] T.Y. Cheng, M.S. Wu, J.T. Lin, M.T. Lin, C.T. Shun, H.Y. Huang, K.T. Hua, M.L. Kuo, Annexin A1 is associated with gastric cancer survival and promotes gastric cancer cell invasiveness through the formyl peptide receptor/extracellular signal-regulated kinase/integrin beta-1-binding protein 1 pathway, Cancer, 118 (2012) 5757-5767.

[171] V. Bizzarro, R. Belvedere, M.R. Milone, B. Pucci, R. Lombardi, F. Bruzzese, A. Popolo, L. Parente, A. Budillon, A. Petrella, Annexin A1 is involved in the acquisition and maintenance of a stem cell-like/aggressive phenotype in prostate cancer cells with acquired resistance to zoledronic acid, Oncotarget, 6 (2015) 25076-25092.

[172] F. Rondepierre, B. Bouchon, J. Papon, M. Bonnet-Duquennoy, R. Kintossou, N. Moins, J. Maublant, J.C. Madelmont, M. D'Incan, F. Degoul, Proteomic studies of B16 lines: involvement of annexin A1 in melanoma dissemination, Biochim Biophys Acta, 1794 (2009) 61-69.

[173] C.Y. Chen, J.Q. Shen, F. Wang, R. Wan, X.P. Wang, Prognostic significance of annexin A1 expression in pancreatic ductal adenocarcinoma, Asian Pac J Cancer Prev, 13 (2012) 4707-4712.

[174] X.F. Bai, X.G. Ni, P. Zhao, S.M. Liu, H.X. Wang, B. Guo, L.P. Zhou, F. Liu, J.S. Zhang, K. Wang, Y.Q. Xie, Y.F. Shao, X.H. Zhao, Overexpression of annexin 1 in pancreatic cancer and its clinical significance, World J Gastroenterol, 10 (2004) 1466-1470.

[175] R. Belvedere, V. Bizzarro, G. Forte, F. Dal Piaz, L. Parente, A. Petrella, Annexin A1 contributes to pancreatic cancer cell phenotype, behaviour and metastatic

potential independently of Formyl Peptide Receptor pathway, Sci Rep, 6 (2016) 29660.

[176] R. Belvedere, V. Bizzarro, A. Popolo, F. Dal Piaz, M. Vasaturo, P. Picardi, L. Parente, A. Petrella, Role of intracellular and extracellular annexin A1 in migration and invasion of human pancreatic carcinoma cells, BMC cancer, 14 (2014) 961.

[177] H.D. Um, Bcl-2 family proteins as regulators of cancer cell invasion and metastasis: a review focusing on mitochondrial respiration and reactive oxygen species, Oncotarget, 7 (2016) 5193-5203.

[178] D. Trisciuoglio, M.G. Tupone, M. Desideri, M. Di Martile, C. Gabellini, S. Buglioni, M. Pallocca, G. Alessandrini, S. D'Aguanno, D. Del Bufalo, BCL-XL overexpression promotes tumor progression-associated properties, Cell Death Dis, 8 (2017) 3216.

[179] Y. Maruyama, M. Ono, A. Kawahara, T. Yokoyama, Y. Basaki, M. Kage, S. Aoyagi, H. Kinoshita, M. Kuwano, Tumor growth suppression in pancreatic cancer by a putative metastasis suppressor gene Cap43/NDRG1/Drg-1 through modulation of angiogenesis, Cancer Res, 66 (2006) 6233-6242.

[180] G. Cen, K. Zhang, J. Cao, Z. Qiu, Downregulation of the N-myc downstream regulated gene 1 is related to enhanced proliferation, invasion and migration of pancreatic cancer, Oncol Rep, 37 (2017) 1189-1195.

[181] R.J. Guan, H.L. Ford, Y. Fu, Y. Li, L.M. Shaw, A.B. Pardee, Drg-1 as a differentiation-related, putative metastatic suppressor gene in human colon cancer, Cancer Res, 60 (2000) 749-755.

[182] S. Bandyopadhyay, S.K. Pai, S.C. Gross, S. Hirota, S. Hosobe, K. Miura, K. Saito, T. Commes, S. Hayashi, M. Watabe, K. Watabe, The Drg-1 gene suppresses tumor metastasis in prostate cancer, Cancer Res, 63 (2003) 1731-1736.

[183] E. Korpela, D. Vesprini, S.K. Liu, MicroRNA in radiotherapy: miRage or miRador?, Br J Cancer, 112 (2015) 777-782.

[184] P. Gandellini, T. Rancati, R. Valdagni, N. Zaffaroni, miRNAs in tumor radiation response: bystanders or participants?, Trends Mol Med, 20 (2014) 529-539.

[185] P. Wang, Z. Li, H. Liu, D. Zhou, A. Fu, E. Zhang, MicroRNA-126 increases chemosensitivity in drug-resistant gastric cancer cells by targeting EZH2, Biochem Biophys Res Commun, 479 (2016) 91-96.

[186] X. Zhu, H. Li, L. Long, L. Hui, H. Chen, X. Wang, H. Shen, W. Xu, miR-126 enhances the sensitivity of non-small cell lung cancer cells to anticancer agents by targeting vascular endothelial growth factor A, Acta Biochim Biophys Sin (Shanghai), 44 (2012) 519-526.

[187] F. Baldassari, C. Zerbinati, M. Galasso, F. Corra, L. Minotti, C. Agnoletto, M. Previati, C.M. Croce, S. Volinia, Screen for MicroRNA and Drug Interactions in Breast Cancer Cell Lines Points to miR-126 as a Modulator of CDK4/6 and PIK3CA Inhibitors, Front Genet, 9 (2018) 174.

[188] W. Luo, D. Yan, Z. Song, X. Zhu, X. Liu, X. Li, S. Zhao, miR-126-3p sensitizes glioblastoma cells to temozolomide by inactivating Wnt/beta-catenin signaling via targeting SOX2, Life Sci, 226 (2019) 98-106.

[189] S. Caporali, A. Amaro, L. Levati, E. Alvino, P.M. Lacal, S. Mastroeni, F. Ruffini, L. Bonmassar, G.C. Antonini Cappellini, N. Felli, A. Care, U. Pfeffer, S. D'Atri, miR-126-3p down-regulation contributes to dabrafenib acquired resistance in melanoma by up-regulating ADAM9 and VEGF-A, Journal of experimental & clinical cancer research : CR, 38 (2019) 272.

[190] J. Slotta-Huspenina, E. Drecoll, M. Feith, D. Habermehl, S. Combs, W. Weichert, M. Bettstetter, K. Becker, R. Langer, MicroRNA expression profiling for the prediction of resistance to neoadjuvant radiochemotherapy in squamous cell carcinoma of the esophagus, Journal of translational medicine, 16 (2018) 109.

[191] Y. Luo, L. Tong, H. Meng, W. Zhu, L. Guo, T. Wei, J. Zhang, MiR-335 regulates the chemo-radioresistance of small cell lung cancer cells by targeting PARP-1, Gene, 600 (2017) 9-15.

[192] L.P. Shi, H.L. Guo, Y.B. Su, Z.H. Zheng, J.R. Liu, S.H. Lai, MicroRNA-149 sensitizes colorectal cancer to radiotherapy by downregulating human epididymis protein 4, Am J Cancer Res, 8 (2018) 30-38.

[193] L. Lin, Y.D. Zhang, Z.Y. Chen, Y. Chen, C.P. Ren, The clinicopathological significance of miR-149 and PARP-2 in hepatocellular carcinoma and their roles in chemo/radiotherapy, Tumour Biol, 37 (2016) 12339-12346.

[194] H. Ma, R. Lian, Z. Wu, X. Li, W. Yu, Y. Shang, X. Guo, MiR-503 enhances the radiosensitivity of laryngeal carcinoma cells via the inhibition of WEE1, Tumour Biol, 39 (2017) 1010428317706224.

[195] J. Bargiela-Iparraguirre, L. Prado-Marchal, M. Fernandez-Fuente, A. Gutierrez-Gonzalez, J. Moreno-Rubio, M. Munoz-Fernandez, M. Sereno, R. Sanchez-Prieto, R. Perona, I. Sanchez-Perez, CHK1 expression in Gastric Cancer is modulated by p53 and RB1/E2F1: implications in chemo/radiotherapy response, Sci Rep, 6 (2016) 21519.

[196] P.S. Mitchell, R.K. Parkin, E.M. Kroh, B.R. Fritz, S.K. Wyman, E.L. Pogosova-Agadjanyan, A. Peterson, J. Noteboom, K.C. O'Briant, A. Allen, D.W. Lin, N. Urban, C.W. Drescher, B.S. Knudsen, D.L. Stirewalt, R. Gentleman, R.L. Vessella, P.S. Nelson, D.B. Martin, M. Tewari, Circulating microRNAs as stable blood-based markers for cancer detection, Proc Natl Acad Sci U S A, 105 (2008) 10513-10518.

[197] A. Greystoke, M. Ayub, D.G. Rothwell, D. Morris, D. Burt, C.L. Hodgkinson, C.J. Morrow, N. Smith, K. Aung, J. Valle, L. Carter, F. Blackhall, C. Dive, G. Brady, Development of a circulating miRNA assay to monitor tumor burden: From mouse to man, Molecular oncology, 10 (2016) 282-291.

[198] M.H. Rasmussen, N.F. Jensen, L.S. Tarpgaard, C. Qvortrup, M.U. Romer, J. Stenvang, T.P. Hansen, L.L. Christensen, J. Lindebjerg, F. Hansen, B.V. Jensen, T.F. Hansen, P. Pfeiffer, N. Brunner, T.F. Orntoft, C.L. Andersen, High expression of microRNA-625-3p is associated with poor response to first-line oxaliplatin based treatment of metastatic colorectal cancer, Molecular oncology, 7 (2013) 637-646.

[199] M.H. Rasmussen, I. Lyskjaer, R.R. Jersie-Christensen, L.S. Tarpgaard, B. Primdal-Bengtson, M.M. Nielsen, J.S. Pedersen, T.P. Hansen, F. Hansen, J.V. Olsen, P. Pfeiffer, T.F. Orntoft, C.L. Andersen, miR-625-3p regulates oxaliplatin resistance

by targeting MAP2K6-p38 signalling in human colorectal adenocarcinoma cells, Nat Commun, 7 (2016) 12436.

[200] O. Mohamad, B.J. Sishc, J. Saha, A. Pompos, A. Rahimi, M.D. Story, A.J. Davis, D.W.N. Kim, Carbon Ion Radiotherapy: A Review of Clinical Experiences and Preclinical Research, with an Emphasis on DNA Damage/Repair, Cancers (Basel), 9 (2017).

[201] R.A. El Shafie, D. Habermehl, S. Rieken, A. Mairani, L. Orschiedt, S. Brons, T. Haberer, K.J. Weber, J. Debus, S.E. Combs, In vitro evaluation of photon and raster-scanned carbon ion radiotherapy in combination with gemcitabine in pancreatic cancer cell lines, J Radiat Res, 54 Suppl 1 (2013) i113-119.

[202] K. Oonishi, X. Cui, H. Hirakawa, A. Fujimori, T. Kamijo, S. Yamada, O. Yokosuka, T. Kamada, Different effects of carbon ion beams and X-rays on clonogenic survival and DNA repair in human pancreatic cancer stem-like cells, Radiotherapy and oncology : journal of the European Society for Therapeutic Radiology and Oncology, 105 (2012) 258-265.

[203] S. Sai, T. Wakai, G. Vares, S. Yamada, T. Kamijo, T. Kamada, T. Shirai, Combination of carbon ion beam and gemcitabine causes irreparable DNA damage and death of radioresistant pancreatic cancer stem-like cells in vitro and in vivo, Oncotarget, 6 (2015) 5517-5535.

[204] T. Okada, T. Kamada, H. Tsuji, J.E. Mizoe, M. Baba, S. Kato, S. Yamada, S. Sugahara, S. Yasuda, N. Yamamoto, R. Imai, A. Hasegawa, H. Imada, H. Kiyohara, K. Jingu, M. Shinoto, H. Tsujii, Carbon ion radiotherapy: clinical experiences at National Institute of Radiological Science (NIRS), J Radiat Res, 51 (2010) 355-364.

[205] S. Kawashiro, S. Yamada, M. Okamoto, T. Ohno, T. Nakano, M. Shinoto, Y. Shioyama, K. Nemoto, Y. Isozaki, H. Tsuji, T. Kamada, Multi-institutional Study of Carbon-ion Radiotherapy for Locally Advanced Pancreatic Cancer: Japan Carbon-ion Radiation Oncology Study Group (J-CROS) Study 1403 Pancreas, Int J Radiat Oncol Biol Phys, 101 (2018) 1212-1221.

[206] A.A. Lazar, R. Schulte, B. Faddegon, E.A. Blakely, M. Roach, 3rd, Clinical trials involving carbon-ion radiation therapy and the path forward, Cancer, 124 (2018) 4467-4476.

List of figures

List of tables

Appendix

Appendix 1.

Table A.1. RT2Profiler PCR Array Dataset in Panc-1 RR and MIA PaCa-2 RR. Fold change (2^(-ΔΔCT)) of normalised gene expression (2^(-ΔCT)) of RR cells to normalised gene expression (2^(-ΔCT)) of parental cells. nd = not detected (Cp > 35)

	Panc-1 RR	MIA PaCa-2 RR
Gene	Fold change	Fold change
ALB	nd	nd
ALOX12	1.56	2.06
AOX1	3.29	nd
APOE	0.20	0.55
ATOX1	1.93	0.74
BNIP3	0.87	0.59
CAT	1.27	1.75
CCL5	84.45	2.58
CCS	1.24	0.74
CYBB	5.03	nd
CYGB	2.75	nd
DHCR24	0.49	1.78
DUOX1	2.55	0.53
DUOX2	nd	0.42
DUSP1	1.83	1.31
EPHX2	0.62	1.66
EPX	3.51	1.42
FOXM1	1.87	1.41
FTH1	1.51	1.77
GCLC	1.97	3.53
GCLM	2.33	1.43
GPX1	1.43	0.90
GPX2	1.39	1.47
GPX3	0.50	1.14
GPX4	1.04	0.86
GPX5	nd	nd
GPX6	nd	nd

GPX7	1.92	nd
GSR	0.60	1.46
GSS	2.19	0.54
GSTP1	1.58	0.84
GSTZ1	2.71	1.10
GTF2I	1.73	0.93
HMOX1	1.65	0.51
HSPA1A	1.68	2.16
KRT1	nd	nd
LPO	nd	nd
MB	11.96	8.11
MBL2	nd	nd
MGST3	1.42	1.21
MPO	2.53	0.96
MPV17	1.73	0.90
MSRA	2.36	0.98
MT3	1.75	1.39
NCF1	0.71	1.22
NCF2	1.34	1.21
NOS2	2.07	1.73
NOX4	nd	nd
NOX5	nd	nd
NQO1	2.55	1.11
NUDT1	1.01	0.70
OXR1	1.54	1.11
OXSR1	2.27	1.15
PDLM1	1.20	0.04
PNKP	2.45	0.84
PRDX1	2.55	1.20
PRDX2	2.27	0.76
PRDX3	1.22	0.91
PRDX4	2.69	1.24
PRDX5	1.17	0.78
PRDX6	1.45	1.08
PREX1	0.97	nd
PRNP	1.42	0.76
PTGS1	nd	nd
PTGS2	nd	nd

PXDN	1.39	0.76
RNF7	1.29	1.01
SCARA3	1.56	4.99
SELS	1.82	1.13
SEPP1	0.79	1.10
SFTPD	0.08	nd
SIRT2	2.22	0.55
SOD1	1.46	0.86
SOD2	2.48	0.98
SOD3	0.24	0.41
SQSTM1	1.59	0.98
SRXN1	0.85	0.96
STK25	0.93	0.53
TPO	1.88	nd
TTN	nd	nd
TXN	2.23	0.81
TXNRD1	1.24	2.23
TXNRD2	1.01	1.06
UCP2	0.96	0.06

Appendix 2.

Table A.2. Deregulated miRNAs in Panc-1 RR cells. Positive log2 fold changes indicate miRNAs upregulated in RR cells compared to parental cells, whereas negative log2 fold changes indicate miRNAs downregulated in RR cells.

miRNA	Panc-1 RR	
	Log2 fold change	p-adjust
hsa-miR-135b-5p	2.62	2.63E-29
hsa-miR-147b	2.33	2.85E-47
hsa-miR-155-5p	1.94	7.64E-45
hsa-miR-146a-5p	1.60	6.53E-52
hsa-miR-34c-5p	1.51	9.04E-38
hsa-miR-33b-3p	1.42	2.03E-10
hsa-miR-574-5p	1.21	2.25E-05
hsa-miR-186-5p	1.19	3.99E-32
hsa-miR-3613-5p	1.15	1.50E-06
hsa-miR-181d-5p	1.12	6.02E-12
hsa-miR-641	1.12	1.33E-21
hsa-miR-7-5p	1.10	2.18E-28
hsa-miR-937-3p	1.09	5.05E-05
hsa-miR-212-5p	1.03	1.15E-07
hsa-miR-330-5p	0.94	3.68E-12
hsa-miR-152-3p	0.93	2.76E-11
hsa-miR-22-3p	0.92	1.15E-26
hsa-miR-99a-5p	0.90	3.25E-14
hsa-miR-222-3p	0.88	4.90E-18
hsa-miR-22-5p	0.81	8.04E-15
hsa-miR-589-5p	0.77	9.64E-09
hsa-miR-4664-3p	0.77	4.94E-04
hsa-miR-181b-5p	0.74	1.25E-10
hsa-miR-221-5p	0.74	5.16E-03
hsa-miR-665	0.73	2.73E-05
hsa-miR-485-5p	-0.72	1.77E-05
hsa-miR-126-3p	-0.72	2.81E-13
hsa-miR-30e-3p	-0.73	9.90E-13
hsa-miR-1303	-0.75	4.39E-13
hsa-miR-425-3p	-0.76	1.06E-05
hsa-miR-556-5p	-0.76	1.26E-02
hsa-miR-128-1-5p	-0.78	7.74E-03

hsa-miR-106b-3p	-0.78	1.07E-26
hsa-miR-424-3p	-0.79	3.46E-09
hsa-miR-361-5p	-0.85	1.51E-06
hsa-miR-15b-3p	-0.87	1.01E-07
hsa-miR-30c-1-3p	-0.88	8.71E-04
hsa-miR-27b-5p	-0.94	8.62E-11
hsa-miR-335-3p	-0.96	2.08E-26
hsa-miR-374b-5p	-1.09	5.76E-20
hsa-miR-374a-5p	-1.10	1.85E-24
hsa-miR-1292-5p	-1.18	6.60E-07
hsa-miR-374b-3p	-1.23	2.26E-05
hsa-miR-16-2-3p	-1.26	6.35E-21
hsa-miR-374a-3p	-1.37	1.02E-26
hsa-miR-1257	-1.38	1.08E-07
hsa-miR-95-3p	-1.39	1.18E-06
hsa-miR-129-5p	-1.47	2.29E-22
hsa-miR-138-5p	-1.72	1.70E-12
hsa-miR-25-5p	-1.73	1.10E-11
hsa-miR-187-3p	-2.10	3.71E-40
hsa-miR-1-3p	-2.22	2.50E-62
hsa-miR-10b-5p	-3.43	8.15E-168
hsa-miR-363-3p	-4.39	6.83E-114

Appendix 3.

Table A.3. Deregulated miRNAs in MIA PaCa-2 RR cells. Positive log2 fold changes indicate miRNAs upregulated in RR cells compared to parental cells, whereas negative log2 fold changes indicate miRNAs downregulated in RR cells.

miRNA	MIA PaCa-2 RR	
	log_2FC	p-adjust
hsa-miR-210-3p	1.93	1.88E-16
hsa-miR-195-3p	1.81	3.41E-15
hsa-miR-542-3p	1.08	1.09E-10
hsa-miR-937-3p	0.94	9.87E-07
hsa-miR-4521	0.90	1.40E-04
hsa-miR-450b-5p	0.90	5.33E-09
hsa-miR-10a-3p	0.89	8.89E-15
hsa-miR-181a-5p	0.86	6.57E-10
hsa-miR-98-5p	0.85	9.34E-22
hsa-miR-148b-3p	0.85	5.01E-19
hsa-miR-450a-5p	0.84	2.19E-06
hsa-miR-1269b	0.83	1.80E-14
hsa-miR-320a	0.83	1.81E-15
hsa-miR-3529-5p	0.77	5.16E-03
hsa-miR-181a-2-3p	0.75	2.86E-12
hsa-miR-320b	0.75	7.60E-11
hsa-miR-10b-5p	0.74	2.41E-06
hsa-miR-361-3p	0.74	2.19E-06
hsa-miR-503-5p	0.73	3.56E-09
hsa-miR-424-3p	0.73	3.78E-05
hsa-miR-10a-5p	0.72	1.46E-15
hsa-miR-532-3p	-0.81	2.50E-03
hsa-miR-3934-5p	-0.81	8.22E-04
hsa-let-7f-1-3p	-0.81	9.33E-08
hsa-miR-941	-0.82	1.11E-10
hsa-miR-1307-5p	-0.83	1.01E-03
hsa-miR-149-5p	-0.90	5.35E-17
hsa-miR-130b-5p	-0.92	3.62E-15
hsa-miR-500a-3p	-0.96	2.08E-09
hsa-miR-103a-3p	-0.96	1.46E-15
hsa-miR-7-5p	-1.01	2.49E-16
hsa-miR-126-3p	-1.05	1.82E-24

hsa-miR-362-5p	-1.09	2.78E-08
hsa-miR-502-3p	-1.25	4.49E-13
hsa-miR-532-5p	-1.31	7.25E-39
hsa-miR-501-3p	-1.40	1.61E-29
hsa-miR-188-5p	-1.58	9.53E-10
hsa-miR-148a-3p	-2.00	3.76E-58
hsa-miR-139-5p	-2.03	4.47E-25
hsa-miR-335-3p	-4.29	6.86E-31
hsa-miR-100-5p	-5.10	2.27E-160

Appendix 4.

Table A.4. Deregulated miRNAs in MIA PaCa-2 RR tumor tissue without irradiation. Positive log2 fold changes indicate miRNAs upregulated in RR tumors compared to parental tumors, whereas negative log2 fold changes indicate miRNAs downregulated in RR tumors.

miRNA	log_2FC	p-adjust
hsa-miR-1269b	1.09	6.23E-06
hsa-miR-486-5p	1.12	2.37E-05
hsa-miR-151a-3p	1.21	4.73E-03
hsa-miR-576-3p	1.26	1.65E-05
hsa-miR-486-3p	1.40	1.92E-02
hsa-miR-221-5p	1.52	5.86E-07
hsa-miR-221-3p	1.55	6.54E-08
hsa-miR-576-5p	1.57	4.70E-05
hsa-miR-6510-3p	1.58	1.34E-03
hsa-miR-222-3p	1.79	1.80E-07
hsa-miR-135b-5p	2.68	8.57E-16
hsa-miR-625-3p	3.03	9.32E-10
hsa-miR-103a-3p	-1.66	2.96E-08
hsa-miR-503-5p	-1.40	6.04E-06
hsa-miR-660-5p	-1.39	9.22E-05
hsa-miR-107	-1.31	3.01E-03
hsa-miR-146a-5p	-1.25	2.22E-03
hsa-miR-500a-3p	-1.18	9.22E-05
hsa-miR-149-5p	-1.13	2.11E-05
hsa-miR-23a-3p	-1.04	4.78E-03
hsa-miR-330-3p	-1.02	3.33E-05
hsa-miR-194-5p	-1.00	3.67E-03

Appendix 5.

Table A.5. Deregulated miRNAs in MIA PaCa-2 RR tumor tissue with 5 Gy irradiation. Positive log2 fold changes indicate miRNAs upregulated in RR tumors compared to parental tumors, whereas negative log2 fold changes indicate miRNAs downregulated in RR tumors.

miRNA	log_2FC	p-adjust
hsa-miR-151a-5p	1.02	4.53E-07
hsa-miR-486-5p	1.11	3.70E-05
hsa-miR-193b-3p	1.12	9.32E-05
hsa-miR-345-5p	1.21	8.03E-07
hsa-miR-3617-5p	1.21	3.42E-04
hsa-miR-486-3p	1.28	1.75E-05
hsa-miR-338-5p	1.32	1.77E-05
hsa-miR-576-3p	1.50	1.37E-05
hsa-miR-221-5p	1.83	1.01E-18
hsa-miR-576-5p	1.85	1.52E-08
hsa-miR-222-3p	1.87	2.46E-35
hsa-miR-221-3p	1.88	3.13E-08
hsa-miR-135b-5p	2.81	2.53E-26
hsa-miR-625-3p	3.27	2.08E-18
hsa-miR-203a-3p	-3.35	3.14E-02
hsa-miR-424-3p	-1.44	1.01E-05
hsa-miR-200a-3p	-1.42	1.25E-02
hsa-miR-146a-5p	-1.40	1.78E-05
hsa-miR-200b-3p	-1.29	2.02E-02
hsa-miR-103a-3p	-1.28	4.26E-07
hsa-miR-503-5p	-1.28	2.24E-05
hsa-miR-27a-5p	-1.27	6.57E-05
hsa-miR-660-5p	-1.20	5.91E-03
hsa-miR-615-3p	-1.19	4.11E-03
hsa-miR-107	-1.15	4.57E-03
hsa-miR-149-5p	-1.14	2.21E-10
hsa-miR-330-3p	-1.13	4.11E-10
hsa-miR-1299	-1.12	1.19E-03
hsa-miR-500a-3p	-1.06	1.66E-06
hsa-miR-181a-2-3p	-1.03	6.11E-03

Appendix 6.

Table A.6. Deregulated miRNAs in MIA PaCa-2 RR tumor tissue with 10 Gy irradiation. Positive log2 fold changes indicate miRNAs upregulated in RR tumors compared to parental tumors, whereas negative log2 fold changes indicate miRNAs downregulated in RR tumors.

miRNA	log_2FC	p-adjust
hsa-miR-222-3p	1.10	3.27E-02
hsa-miR-99a-5p	1.12	1.68E-03
hsa-miR-125b-1-3p	1.34	4.15E-03
hsa-miR-409-3p	1.38	6.76E-03
hsa-miR-338-5p	1.38	1.24E-04
hsa-miR-151a-3p	1.40	8.20E-06
hsa-miR-6510-3p	1.46	3.69E-06
hsa-miR-370-3p	1.48	3.44E-02
hsa-miR-576-3p	1.80	9.86E-07
hsa-miR-576-5p	1.86	2.79E-11
hsa-miR-625-3p	2.80	2.79E-11
hsa-miR-103a-3p	-1.37	5.23E-06
hsa-miR-424-3p	-1.37	8.59E-03
hsa-miR-503-5p	-1.22	1.13E-02
hsa-miR-660-5p	-1.20	1.19E-03
hsa-miR-107	-1.19	4.30E-04
hsa-miR-149-5p	-1.10	2.36E-06
hsa-miR-23a-3p	-1.03	1.31E-05

Scientific contributions

L. Nguyen, S. Dobiasch, G. Schneider, R.M. Schmid, O. Azimzadeh, K. Kanev, D. Buschmann, M.W. Pfaffl, S. Bartzsch, T.E. Schmid, D. Schilling, S.E. Combs, Impact of DNA repair and reactive oxygen species levels on radioresistance in pancreatic cancer, [submitted], (2020).

L. Nguyen, D.Schilling, S. Dobiasch, S. Raulefs, M.S. Franco, D. Buschmann, M.W. Pfaffl, T.E. Schmid, S.E. Combs, The Emerging Role of miRNAs for the Radiation Treatment of Pancreatic Cancer, Cancers (Basel), 12 (2020).

K. Schwarz, S. Dobiasch, **L. Nguyen**, D. Schilling, S.E. Combs, Modification of radiosensitivity by Curcumin in human pancreatic cancer cell lines, Sci Rep, 10 (2020) 3815.

Acknowledgment

I would like to express my gratitude to all the people who have supported me with their expertise, time, or patience during this dissertation.

First and foremost, I would like to thank Prof. Dr. Stephanie E. Combs for giving me this exciting topic and the opportunity to carry out this thesis. I would like to thank you for the great supervision, the constant support and monitoring of the project, and for the many suggestions and ideas throughout the time.

I would also particularly like to thank Prof. Dr. Michael W. Pfaffl for our excellent collaboration and for kindly agreeing to serve on my thesis committee. Thank you for the friendly meetings, helpful ideas, and discussions. Thank you to all the people involved in our collaboration work.

Thank you, Prof. Dr. Thomas E. Schmid, for your support and guidance. I am thankful for your patience and the encouraging words during this project.

Special thanks to Dr. Daniela Schilling for your enthusiasm, inspiration, and many ideas. Thank you for your support with your valuable advice, expertise, and continuous encouragement during this thesis.

I would like to thank all my colleagues for the fun and joyful atmosphere in the lab and office and your support. Thanks to Dr. Sophie Dobiasch for your advice and expertise.

Thank you, PD Dr. Omid Azimzadeh and Dr. Stefan Bartzsch, for your support with the analysis of the data.

Last but not least, I would like to thank my family and my partner, who have lovingly supported me over the past years with great patience, understanding, and countless pieces of advice. Thank you for always being there for me.